Project Number: MQP CBP-LGO2 - 15084

A Major Qualifying Project Report

Submitted to the Faculty

of the

WORCESTER POLYTECHNIC INSTITUTE

in partial fulfillment of the requirements for the

Degree of Bachelor of Science

In Robotics Engineering,

in Mechanical Engineering,

and in Industrial Engineering

by

Joseph D. Gallagher

Dhionis Zhidro

Date: May 2020

Approved:

_____

Prof. Craig Putnam

_____

Prof. Bradley Miller

_____

Prof. Adam Powell

_____

Prof. Joseph Sarkis

Abstract

The Scalable Sort Automation MQP evaluates the effectiveness of a system level design for an automated sortation system that is scalable to high class count and high volume. Subsystems underwent low level design, prototyping, and evaluation of criteria such as cycle time, cost, and volume. The system architecture couples traditional sorting techniques such as linear grating and serialization with novel machine learning technology. The LEGO catalog is used as a base case in testing the subsystems, the catalog carries a high-class count of close to 70,000 with many of the classes being distinct in size, shape, weight and other mechanical properties and features. The system is then evaluated in an economic model centered around conducting LEGO aftermarket sales through bricklink.com.

Acknowledgements

The project team is thankful for its advisors and supporters. Their patience, willingness to work with the team through its problems, both on and off the drawing board, and comments greatly contributed to the success of the team and project. Despite the daunting scope of the project, they sustained their support.

We thank

Professor Craig Putnam

Professor Bradley Miller

Professor Adam Clayton Powell

Professor Joseph Sarkis

The WPI Tinkerbox Committee

The Technocopia Board of Directors

Jerry's Hardware

The Gallagher Family

The Zhidro Family

Executive Summary

Sorting is typically a net non-value-added process for most companies interested in reclaiming value from mixed bulk. The human labor cost typically outweighs the benefit of reclaiming this value. Mechanical sorting methods have been found in many industries across the last century, optical and sensor-based sorting systems have also been in practice for decades. However, new advances in machine learning open the potential of image-based sorting. While machine learning has its hardware constraints, these constraints can be worked around if mechanical and sensor-based sorting methods are also implemented to reduce hardware intensity.

Sorting is an industry ripe for automation. While custom tailored sorting solutions are in existence, a scalable solution can potentially be lucrative and groundbreaking to the industry. The system level design being realized implements all these methods to execute the sorting process in an efficient manner. The system must be able to handle high volume and so it must have low cycle times at each subsystem leading to a low takt time, the ultimate target takt time being 1 second per component. In addition to scalability, this is essential to profitability as each second the component is not being identified or not in storage is non-value-added time. While the system level design was envisioned and established prior to the actual start of the MQP, the individual subsystems had yet to be designed, proven, and evaluated.

The system must also be able handle high and continually increasing variety which is where the machine learning aspect is critical. Being able to continually add classes to the systems catalog is essential to its overall life cycle and longevity. High variety presents not just an informational challenge but also a mechanical handling challenge when it comes to manipulating individual components. Variation in size and geometry lends to different manipulation solutions but each has their limitations and drawbacks. The team had considered different manipulation methods and determined that the most elegant solution would be a universal granular jamming manipulator. This low load manipulation solution is ideal for dealing with the components in the LEGO catalog as it is highly dexterous and can conform to a wide variety of size and geometries without the need for multiple manipulators. It is low cost and made from highly available components and materials; almost everything can be sourced from a local Wal-Mart. The team, despite having experience with a variety of mechanisms, had no experience on this novel

technology. Time was spent in prototyping and understanding the manipulator, its quirks, and limitations.

Throughout the MQP, the subsystems, from the rotating drum grate sorter to the serialization conveyor to the identification cell to the placement gantry were designed, fabricated, and tested with some exceptions due to COVID-19 limitations. Key prototyping principles were kept in mind during the design phase such as designing for manufacturing and assembly to minimize time spent in the production phase and avoid costly human errors. The subsystems were constructed using available, affordable, and easily processable materials. Different manufacturing technologies such as CNC machining and fused deposition manufacturing were acquired and used in the realization of the subsystems. Fabrication cost was further minimized by designing for affordable actuators, sensors, and mechanical components, many of which were already in the team's possession. Furthermore, to fulfill the scalability property, these subsystems were designed with repeatability and modularity in mind.

The system is extensive in terms of hardware and actuators; many repeated mechanisms or entire subsystems were cut back in count to make the project non-cost prohibitive. In addition, external funding was acquired to make the project financially feasible. Funding was acquired through applying to the WPI Tinkerbox committee where $1,500 was allocated to the team's endeavor in realizing the subsystems. The families of the team members, along with the team members themselves, also contributed to funding the project. Organizations like Technocopia and Jerry's Hardware assisted in providing the team the resources it needed to fabricate the subsystems, this including machinery, tooling, and hardware. The project itself was executed in several locations including the former AIM Robotics Lab at WPI's Prescott Street facility, Technocopia, the Gallagher Estate, Jerry's Hardware, and the Washburn Labs and Foisie Innovation Studio at WPI's main campus. The size and intricacy of the system required the space and resources provided by each location. Resourcefulness on the part of the team was essential in realizing the system. Almost every component across the subsystems were produced or sourced across the locations with the subsystems mainly assembled at the Gallagher Estate.

While much of the system has been proven, there are still aspects of it which remain unrealized such as the final storage tower, and handling from placement gantry to final storage tower. Component retrieval and presentation are also left to be desired. Regarding the system as

a piece of capital equipment for the purpose of LEGO aftermarket sales, fulfilling orders would greatly benefit from retrieval. In addition, the software controlling the system could have inventory tracking features implemented along with component projections on likelihood of specific components entering the system to develop probability distributions of future component quantities. The team at this time is set on adding these desirable functions and features to the system to increase its ability to perform in the aftermarket sales industry.

Table of Contents

Table of Figures

Introduction

Sorting has posed unique challenges for different applications since the dawn of the process. The process relies on being able to differentiate details of entities to discern and identify them from mixed bulk, potentially from a large variety of entities. The process also relies on having means to physically handle the entity and store it in an appropriate location which may be restrictive based on selected method for higher volumes.

In commercial application, the process itself is non-value added. Sorting is done to reclaim value that's already present, but because it is non-value added, it lends itself to be overlooked. In addition to being non-value added, often whatever value that can be reclaimed via sorting may fall short of the labor cost to sort. While various industries have designed and implemented sortation systems tailored to a specific category of objects such as fasteners, tools, or packages, more generalized solutions are not as commonplace. These systems rely on mechanical means of identifying components, utilizing sensors that can collect data on components such as weight or length or perhaps even using physical means of separating components based on geometric parameters. Once again, these tailored solutions are not applicable across different domains of sorting and are often unscalable.

Scalability is defined as the effectiveness of the system as these two operational parameters increase, volume and variety. Volume and variety each present their own challenges in developing an effective system architecture and increasing these parameters can cause system parameters to reach undesirable levels. These parameters include takt time, space, sensor and actuator count, and many more. The aim of this MQP is to investigate the challenges presented by high volume, high class count sortation. This form of sorting can be applied to different applications and industries, however, applying it to LEGO carries its own benefits both as a learning experience in understanding these challenges and as the beginning of a commercial endeavor. Developing an effective system level sorting architecture for LEGO is effectively developing an architecture that can handle a massive catalog of components with different mechanical features, properties, and geometry. This potentially has ubiquitous applications which are not only profitable from a patenting standpoint but, depending on execution, is also potentially lucrative in the aftermarket LEGO sales industry. This industry is driven by sorting as

its main process; in this industry, sorting is a value-added process. However, the industry is highly susceptible to non-value-added time as the process is mainly done via human labor. With no commercially available systems, the industry is ripe for automation and the MQP evaluates financial potential of such a system and what attempts have been made at such a system and why they fail at the higher volume and variety levels.

Background

While the aim of the MQP as it stands is to evaluate an approach to an automated scalable sorting system, the true roots of the motivation behind the team's endeavor lies in their childhood. Each team member grew up on LEGO. LEGO is a cultural icon in many industrial states and has permeated through generations of tinkerers; the team is no exception. LEGO inspired creativity for each member in their early childhood and adoration for the modular construction system remains to this day.

One of the team members had amassed an extensive LEGO collection and reached a level of financial constraint that they sought to address their income issue through reselling parts of their collection. The team member then discovered bricklink.com, the enthusiast's choice for buying both new and preowned LEGO components. Bricklink.com attracts a wide variety of customers, from parents replacing missing components in their children's sets to hardcore enthusiasts looking for the exact components at the right quantity they need to complete a sculpture at a LEGO sponsored convention.

Millions of components are sold on bricklink.com on a monthly basis. With over 700,000,000 individual products listed across close to 10,000 stores, it is the central entity of the LEGO aftermarket economy. Many vendors are dedicated to the business as it can be quite lucrative with some operating out of warehouses staffed with employees manually sorting components from bulk. This bulk can either be acquired by the pound or lot on eBay or through more direct secondhand sales such as yard sales or thrift stores. Absurd as it is, people getting rid of the famed LEGO bins sitting in their garage is leading to vendors making millions. This sparked interest in the team member and they began to explore aftermarket LEGO sales. It wasn't long until the repetitive nature of the manual sorting process prompted the team member to explore automating the process.

With the goal of profit in mind, the team member studied the problem at hand. The process, however, is derived from the problem addressed by this project, high class count, high volume sorting. The goal of developing a LEGO sorting system has been approached by LEGO enthusiasts since the inception of the product. The variety of components and the tendency to accumulate large volumes of components results in enthusiasts has envisioning a sorting system.

Over many years, enthusiasts have created sorting systems tailored to LEGO, often made of LEGOs. The team member sought to design a system level architecture to meet the needs of the process. In doing so the team member studied the designs and systems that have been published on the internet, in the forms of blog posts, YouTube videos, and forum threads. The team member found a lack of scalability, many designs that would fail should the volume and variety parameters be pressed any further. Many of these enthusiasts, although good problem solvers and demonstrating proof of fundamental concepts, are not aiming for the scale the team is.

The problem of sorting LEGO bricks is not a previously untouched problem. To the contrary, a quick search turns up dozens of implemented solutions, of varying degrees of sophistication and utility. However, these solutions have generally not actually been applied to the problem in a practical sense, typically only being run in short bursts of time for demonstration purposes, often on small, carefully curated subsets of the variety of parts present in true mixed bulk LEGO, or sorting into broad categories rather than individual parts. In many cases, existing sort machines are built purely as technical demonstration exercises, for the sake of the challenge and fun visual result, rather than with intent to extract actual value out of mixed LEGO. Alternatively, in some cases, the project will be presented along with a nebulous statement that by simply making it larger or spending more time programming the classification system, it could be scaled to a point where it could be practically applied. In this section, we look at some of these systems in depth, and specifically, evaluate whether their designs are scalable to a level where the device could provide practical economic utility

First, we look at a series of machines which can be broadly categorized as limited scope mechanical sorters. These machines use a rudimentary classifier system, sometimes a simple sensor-based setup but more commonly a purely mechanical sort based on the geometry of the part, to reliably classify a small, carefully curated subset of the LEGO part catalog. Some examples of these include the Liftarm sorter by YouTube user Akiyugi, and the pin sorter by Andreas Nilsson. The liftarm sorter operates using a series of openings along a feed mechanism, which progressively increase in size and allow longer and longer parts to pass through, sorting the long, narrow liftarm pieces very precisely. The pin sort design, meanwhile, uses a rudimentary optical sensing system to characterize the color and length of pin components.

These designs are quite simple to build and construct – as shown, both can be made to work solely from LEGO components themselves, and work well on the limited subset of parts that they are designed to handle.

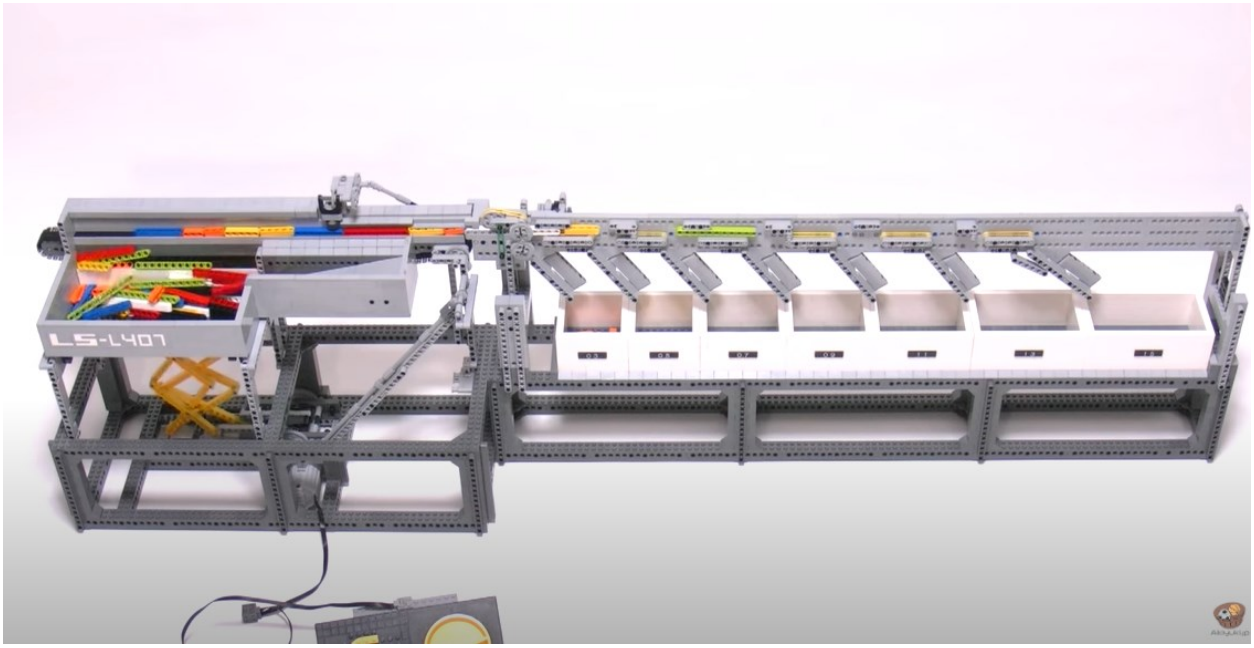

Figure 1: Liftarm Variant 1

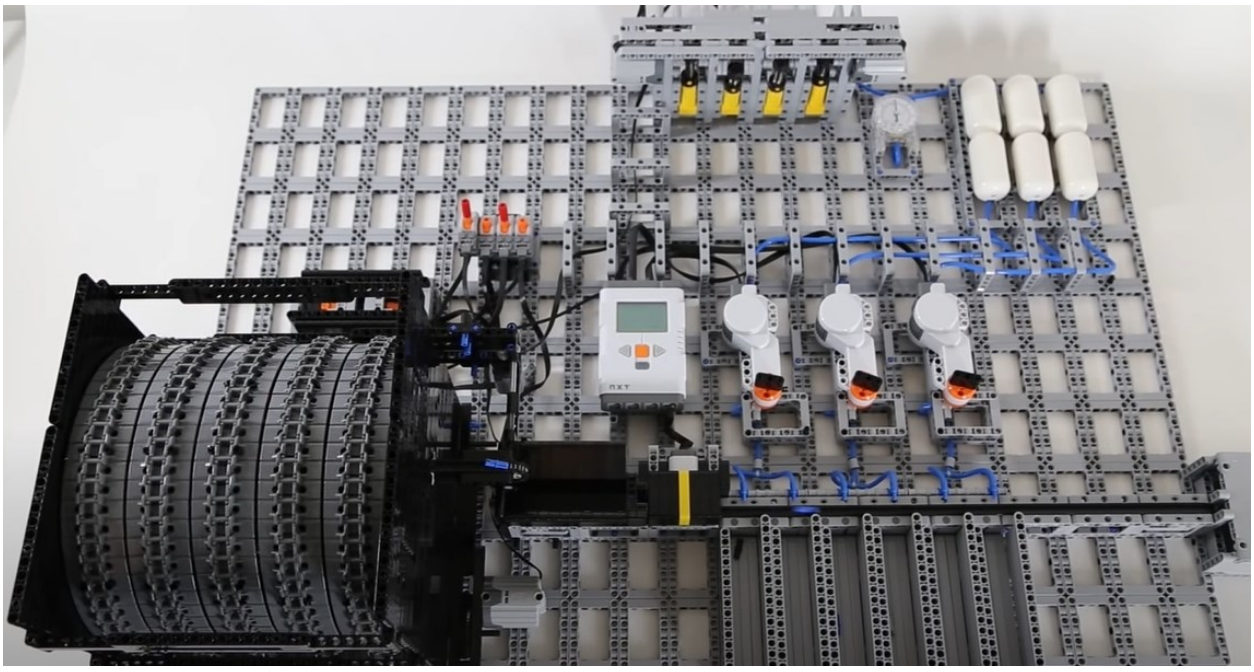

Figure 2: Liftarm Variant 2

The drawback, then, of these designs is that they are extremely restricted in the types of components they can operate on. In both cases, these systems are able to work due to the specially built mechanical feed system, which allows for components to be fed through the classifying components in a very predictable manner and orientation. But introducing non-liftarm or non-pin components into one of these systems would possibly result in a non-sensical classification, such as small parts dropping through the first aperture of the liftarm sorter, or much more likely, a catastrophic jam. The desired outcome would be a "none of the above" option, but this is infeasible as invalid components will not neatly fit with the mechanical systems employed. The input to these types of machines must therefore be very sanitized, consisting only of valid components, which requires a whole extra tier of high-level sorting into broad categories to achieve.

An attempt to perform both low and high level sorting through these kinds of approaches can be found in a machine created by YouTube user Brickformula. This machine uses the same sequentially widening aperture design found on the liftarm sorter, and a wide range of specially designed mechanical devices to sort components at a higher level. The mechanical sprawl and complexity of the machine is immediately apparent, as is the challenge of incrementally building up such a machine's capabilities. In order to create a gate which only allows a single variety of part through, the designer must comprehensively ensure that every other variant passes over, which creates a daunting task in both testing, and in planning the optimal order through which components could be practically filtered through. Small modifications are likely to have wide-reaching unintended effects, making this type of predominantly mechanical design philosophy unsuited for first-order or high-level categorization of parts, only for final classification of a small subset.

Figure 3: Liftarm with Widening Aperture

As discussed in the next section, software-based classifiers which do not need to sequentially physically filter components have much more potential power in performing high level classification. However, as will be discussed in detail, it is much more straightforwards for these kinds of identification solutions to precisely identify components straightaway, than to build a system which only targets broadly classifying components. The machine learning processes which will form the basis of these solution approaches perform much better in cases where there are low levels of intra-class variability.

Therefore, a hypothetical solution which could broadly categorize components to feed to these mechanical sort devices will have already precisely identified them. Even if, as will be discussed, multiple tiers of sort operations are desired, the developmental effort to perform the functionality of these low-level sort approaches will by necessity have been developed in developing high-level categorization capacity, thus rendering any additional developmental effort on these kinds of object-specific approaches redundant.

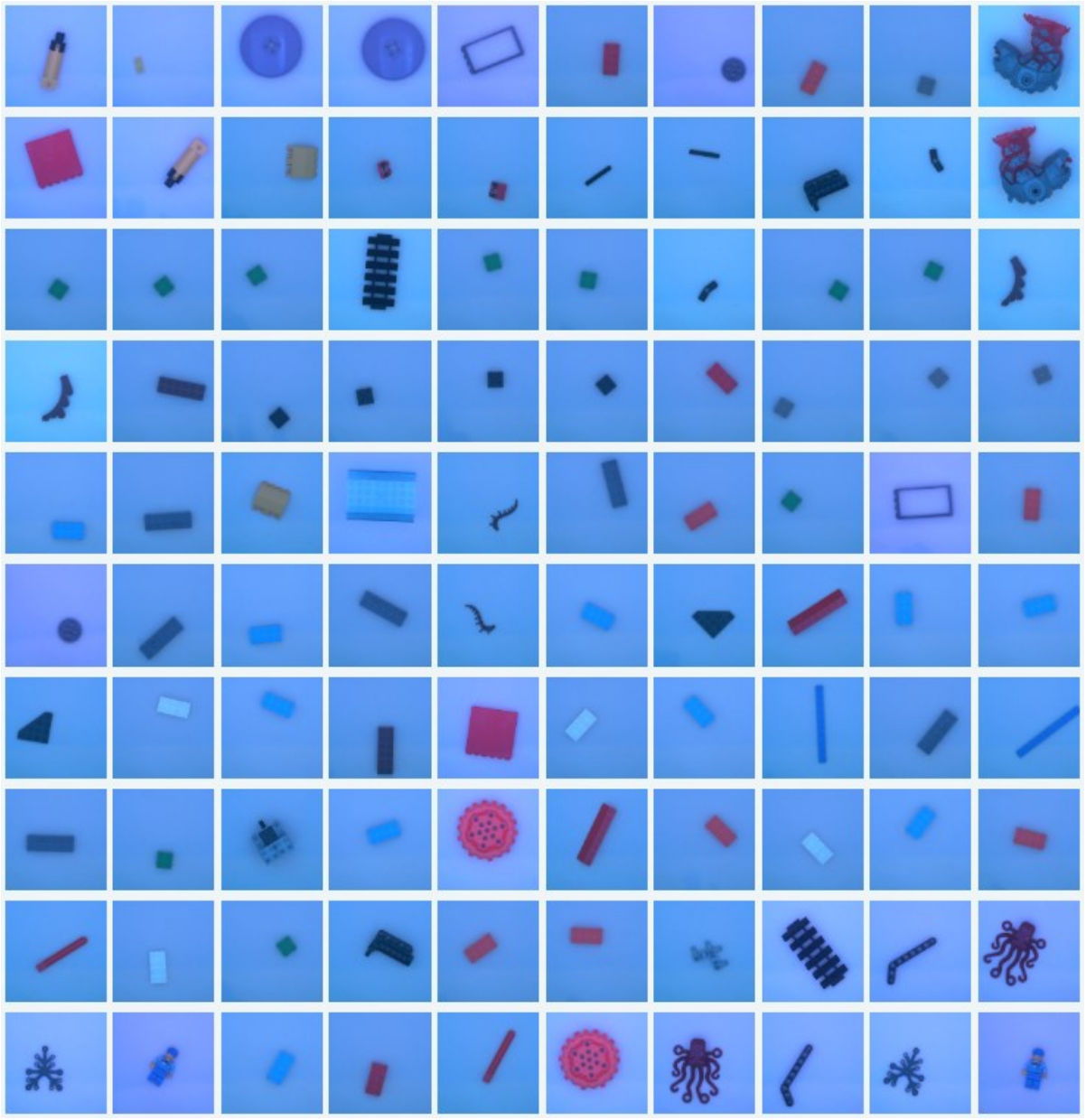

Figure 4: Sample Training Set from Later Vision Prototype

As discussed in the next section, software-based classifiers which do not need to sequentially physically filter components have much more potential power in performing high level classification. However, as will be discussed in detail, it is much more straightforwards for these kinds of identification solutions to precisely identify components straightaway, than to build a system which only targets broadly classifying components. The machine learning processes which will form the basis of these solution approaches perform much better in cases where there are low levels of intra-class variability. Seen in Figure 4, 100 images of parts from

the vision prototype. 50 could be broadly classified as “bricks,” while 10 are “Part 3001, Medium Azure 2x4 Brick.” Building a classifier which picks out the 10 Medium Azure 2x4 bricks is much more straightforwards and useful than one which collects the 50 very diverse brick pieces under one label.

Therefore, a hypothetical solution which could broadly categorize components to feed to these mechanical sort devices will have already precisely identified them. Even if, as will be discussed, multiple tiers of sort operations are desired, the developmental effort to perform the functionality of these low-level sort approaches will by necessity have been developed in developing high-level categorization capacity, thus rendering any additional developmental effort on these kinds of object-specific approaches redundant.

Looking at systems which have been built around software classifiers, again, numerous shortcomings are seen in most designs. In this case, as in the examples shown below by Daniel West and UGCS, despite vision systems which would hypothetically be able to handle any part, the parts which could actually be fed past the camera are dramatically restricted by the physical feed geometry. This can be most easily seen on the UGCS design with a vibratory bowl feeder tuned to feed only a single type of part, with the vision system only distinguishing color. Illustrating limitations enthusiasts have run into.

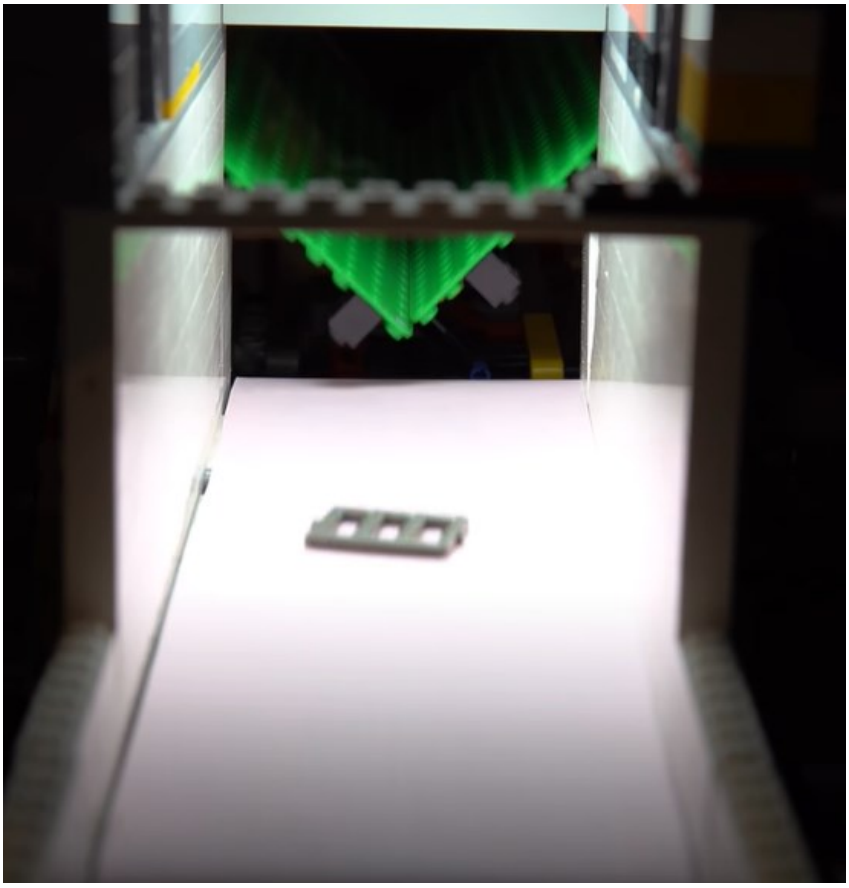

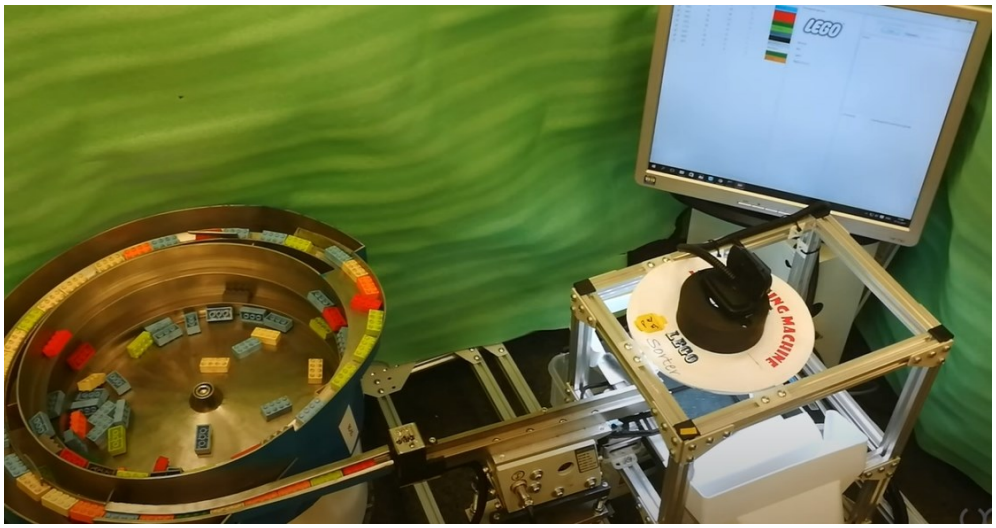

The most practical solutions developed to date are also based on computer vision, but with a much more comprehensive implementation of actual classification software. Examples include the vision guided sorter by Akiyugi, and Jacques Mattheij's universal sorter design. Both use a camera system, in the case of the Akiyugi design, supplemented with mass data. The former's classifier is based around classical computer vision feature recognition, while the latter

is entirely driven by a neural net. Both claim the capability of classifying many thousands of component varieties.

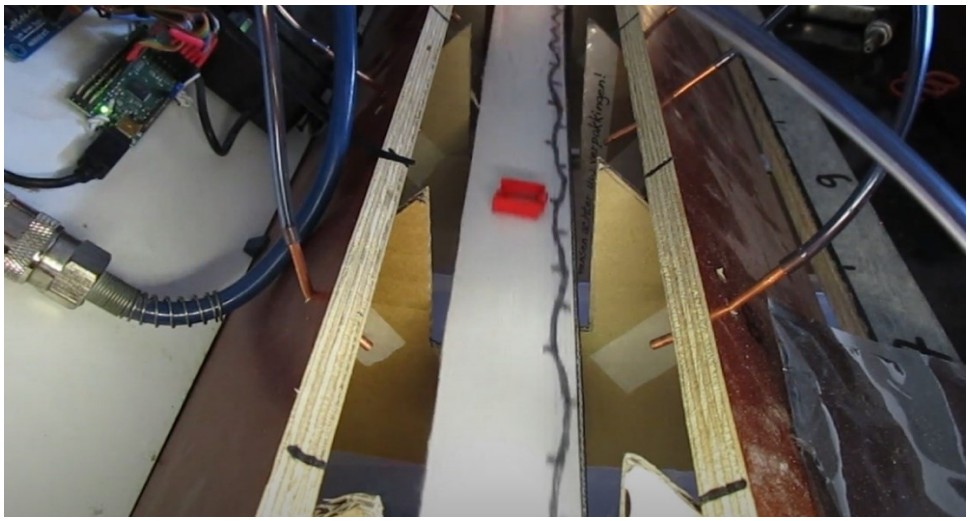

However, their actual output options are extremely limited, with only 8-16 categories into which components can be sorted. Even though components are conclusively identified, they are distributed into broad categories which provide little immediate utility, and require the machine to re-filter components sequentially several times to produce useful results. The distribution

mechanics of these designs are given relatively little consideration compared to the software classifier, and it results in a non-scalable solution. The air nozzle design of the Mattheij's sorter would need to be extended an impractical length to sort thousands of component varieties in a useful manner in one shot. The turntable design, meanwhile, if scaled to a large number of compartments, would increase the cycle time waiting for the correct cup to arrive at the pickup location from seconds to hours if too many parts were added.

This shows how, despite a robust classification system, even the best systems which exist right now do not have an overall hardware architecture which scales effectively to the massive and diverse class count present in the LEGO sort problem, and many other analogous real world solutions. This is therefore the driving goal of our project, to develop a system which does meet this key scalability criteria.

Synthesis & Design

The aim of the project was to evaluate the effectiveness of an initial arrangement of sorting processes and the subsystems required to carry out each sorting process stage. In this section, the initial system level architecture and the design process of its subsystems are discussed.

Initial System Level Architecture

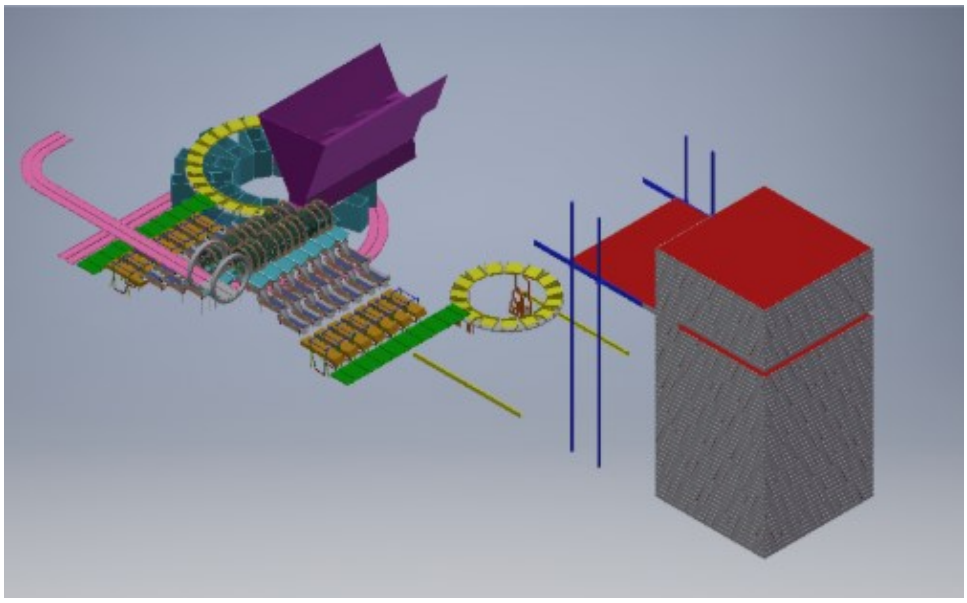

Figure 5: Initial System Level Architecture

In the initial system level architecture seen in Figure 5, there are 3 sorting stages with the 3rd stage being a repeat of the 1st and 2nd stages. Establishing the sorting process itself began with the final subprocess of sorting, storage.

The final key process in the system level architecture is the end placement process, storing. After components have been manipulated and identified through the system, they must be placed in their end storage locations. The end storage arrangement of components is in a 3D-array in the form of a multilevel drawer system, also called the final storage tower. Each drawer would correspond to a position along the Z-Axis of the storage arrangement while the compartments correspond to a position in the XY-Plane. This splits the flow direction of components into 2 stages, as with any drawer system, first the drawer location, Z-Position, is established. The second stage is placing the component in the correct compartment of the

respective drawer, essentially establishing the XY-Position. Having the placement flow broken into 2 different stages poses design questions such as,

-Which of the two placement stages is done first?

-Is placement done in a batch or continuous process?

Flow Analysis

In answering the posed design questions, the system level architecture currently splits the flow first in the Z-Axis and then in the XY-Plane as depicted in Figure 6. Placement in the Z-Axis is done in batches, components are essentially grouped based on destined drawers. Placement in the XY-Plane is done semi-continuously; a given batch of components corresponding to a single drawer in the drawer system is selected and components from the batch are placed, one at a time, in a continuous fashion.

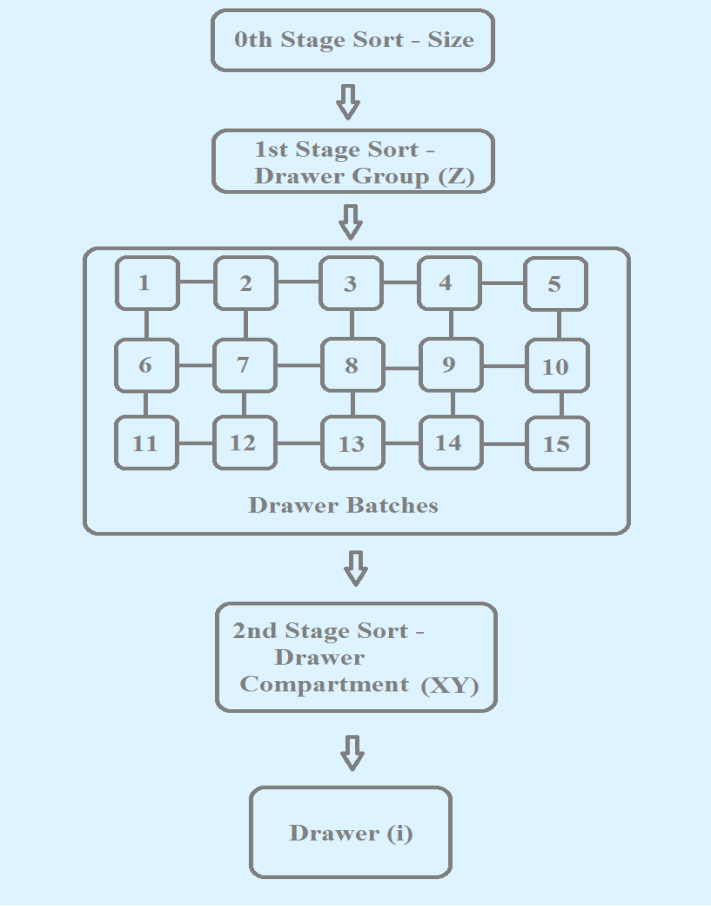

Figure 6: System Flow Splitting

This configuration poses its own design questions such as,

-How is the placement, and by extension the sorting process, physically split?

-How are the continually identified components going to be split into batches?

-How are these batches managed?

The system level design essentially ends up sorting the components twice. The first sorting process groups components into their respective drawers. The second sorting process sorts each group individually on a component by component basis and results in each component getting placed into their own respective compartment. This describes the 1st and 2nd stage sort, the 1st establishes component Z-Position and the 2nd establishes XY-Position. There is no difference in how components are identified in these stages and the subsystems corresponding to the 1st and 2nd stages are nearly identical. The 0th stage enables parallel processing, or multiple concurrent instances, of the 1st and 2nd stages by partitioning components based on their size and allowing each size category to processed simultaneously through repeating subsystems.

With a two stage sort design, it is important to develop an understanding of the fill characteristics of the intermediate stages of the system. If the intermediate bins are made too small, they will overflow, necessitating that the system's first stage cease operation. If they are too large, the first stage, already pushing practicality limits, would be constructed much larger than necessary. A key simplifying assumption, and target objective for the breakdown of components across the 1st tier categories, would be that the bins will fill at the same rate as one another, both in terms of volume filled, and number of parts present in the bin. This allows the quantity of parts across all bins, represented in the equation below as 1, and therefore the time required for the second stage to process each bin, to be considered to represent the parts in each bin equally. The objective is to first verify that the net delta q is less than zero, indicating that overall, parts are exiting the system faster than they are entering it, which in turn shows that if the system is left to run indefinitely, it would never eventually overflow. Second, we want to ensure that q plateaus at a reasonable quantity of parts per bin.

Delta q can be represented by the following equation in Figure 7:

$$\frac{dq}{dt} = R_i - \frac{q/b}{t_{bin}}$$

Figure 7: Differential Equation Expressing Change in Bin Component Count with Respect to Time

Where Ri is the rate at which parts enter the first order storage system via the first order vision cell, b is the number of bins present in the 1st stage, and t_{bin} is the time required for the second stage to process a single bin. t_{bin} can further be written as seen in Figure 8.

$$t_{bin} = \frac{q}{R_o} + C$$

Figure 8: Expression for Bin Processing Time

Where R_o is the processing rate of the second-tier sort, and C is a time constant, representative of the time it would take for the hardware to swap over which 1st stage storage bin is currently being processed by the second stage, here assumed to be equal for all bins. Solving the resultant non-linear differential equation numerically for q yields an asymptotic graph, shown in Figure 9, for all cases where $R_i < R_o$, showing that as long as the second stage operates marginally faster than the first, the first key criteria is met, and the quantity of parts within a bin will eventually plateau. Seen in Figure 10 is the opposite, divergence as the fill rate outpaces the processing rate.

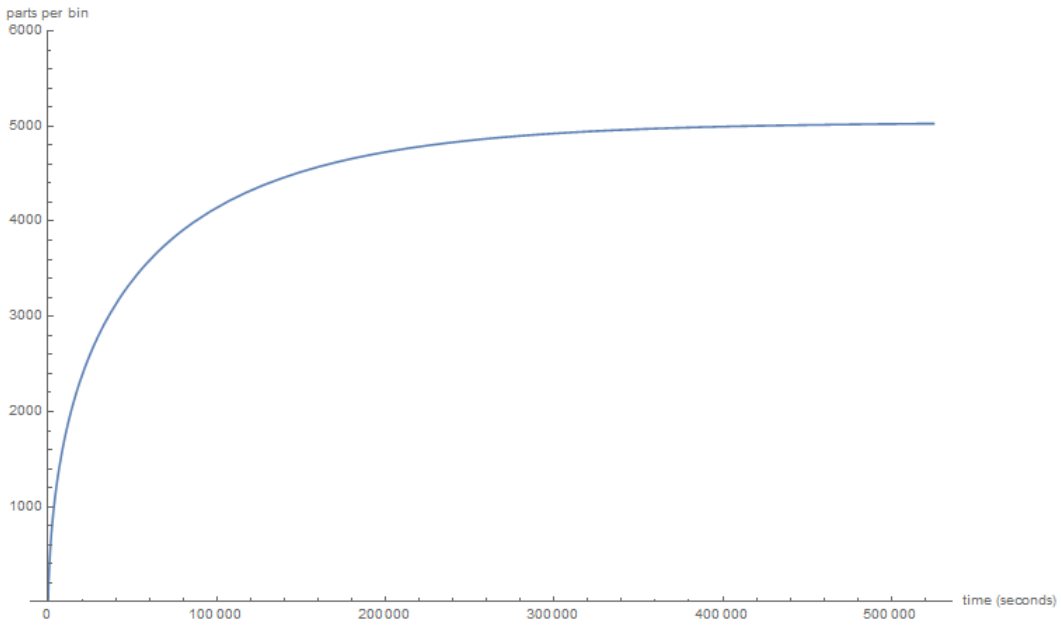

Figure 9: Parts Per Bin as a Function of Processing Time Under $R_i < R_o$ Condition

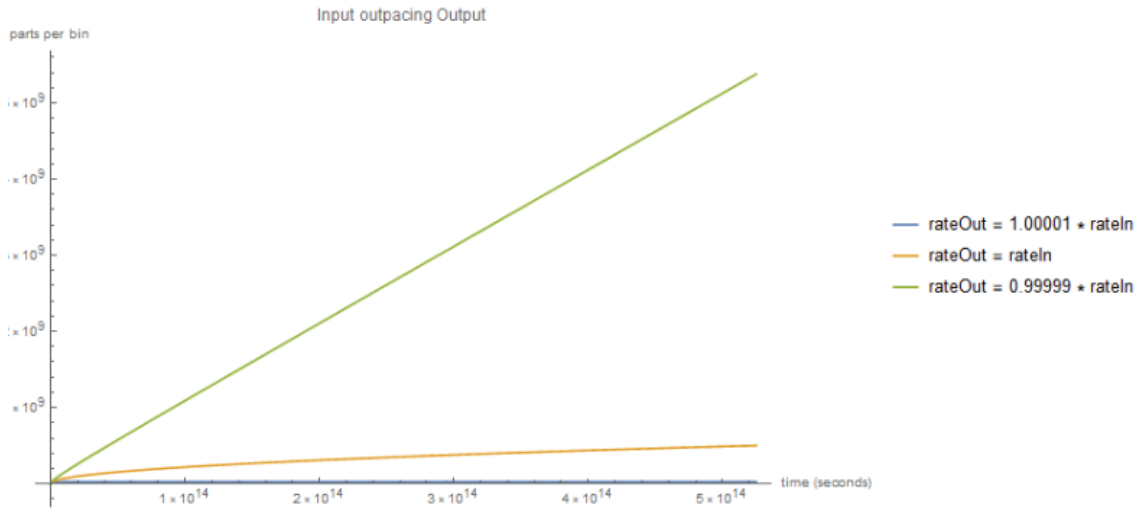

Figure 10; Divergence in Parts Per Bin as a Function of Processing Time Under Ri > Ro Condition

A further helpful quirk of this equation can be shown in Figure 11, which represents the behavior with different assumed initial values for q, or in other words, different initial fills to the bins. If the initial fill is above the steady-state value, the system will asymptotically approach the steady state from above. This robust behavior is observed because as more parts are present in each bin, a smaller percentage of the cycle time is spent on the unchanging bin changeover period, allowing the marginally faster second stage to more fully outpace the second stage and work through any backlog. This is helpful because random variance in part feed will inevitably result in violation of the assumption on which the equation was based, and certain bins filling faster than others. Even when this happens, the system will remain stable.

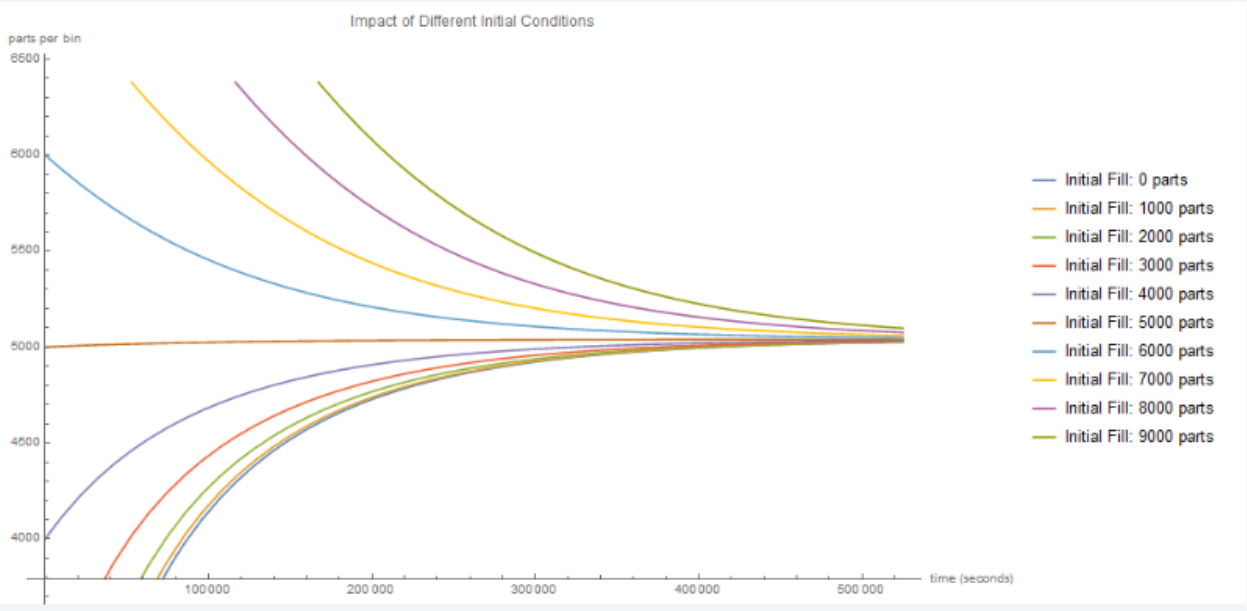

Figure 11: Parts Per Bin as a Function of Processing Time for Different Initial Conditions

Figure 12, Figure 13, and Figure 14 show the effects of altering constant parameters. As expected, seen in Figure 12, reductions in bin changeover time lower the capacity requirement of the system. While creating an automated system for bin changeover was considered out of project scope for the time, this clearly demonstrates that a robust and effective system for this is vital. Figure 13 shows how tweaking the relative speed of the first and second stage changes the plateau, with diminishing returns in effectiveness around a 5% differential. Figure 14 shows that, somewhat counterintuitively, reducing the number of bins actually reduces the number of parts which will need to be stored in each bin, because less time will be spent on changeover. This value could not be reduced to zero because this would force the second stage to handle an impractically large quantity of parts, but should be kept as small as reasonable for the quantities being processed by the machine. For the scope of our project, targeting 2500 unique parts, we determined that a 14 bin 1st stage would be optimal.

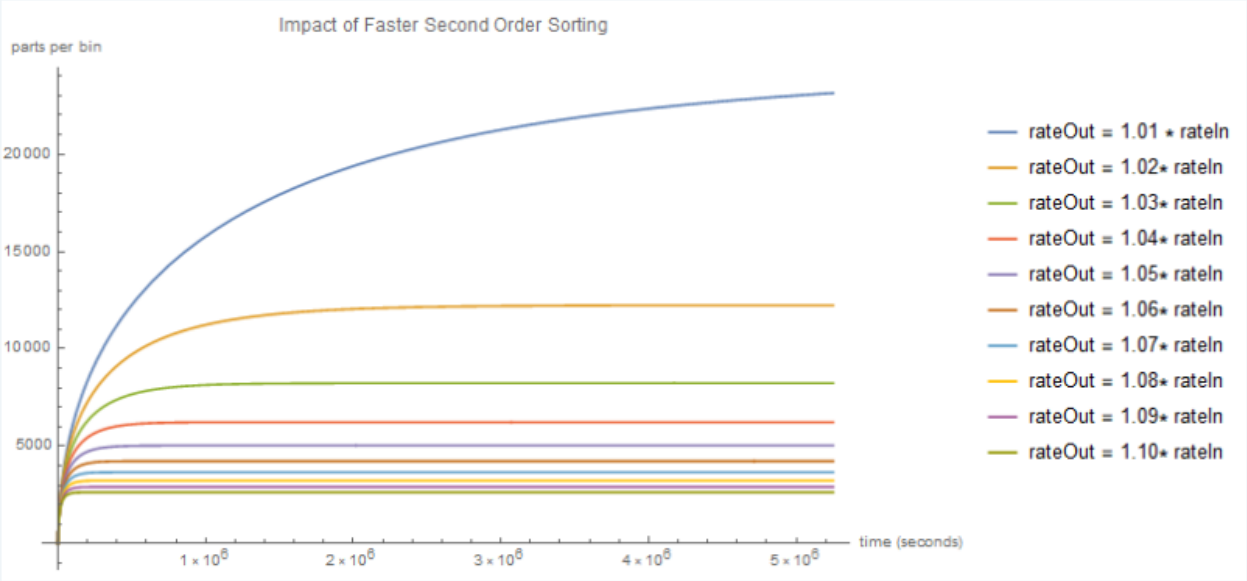

Figure 12: Parts Per Bin as a Function of Processing Time for Different Second Order Sorting Conditions

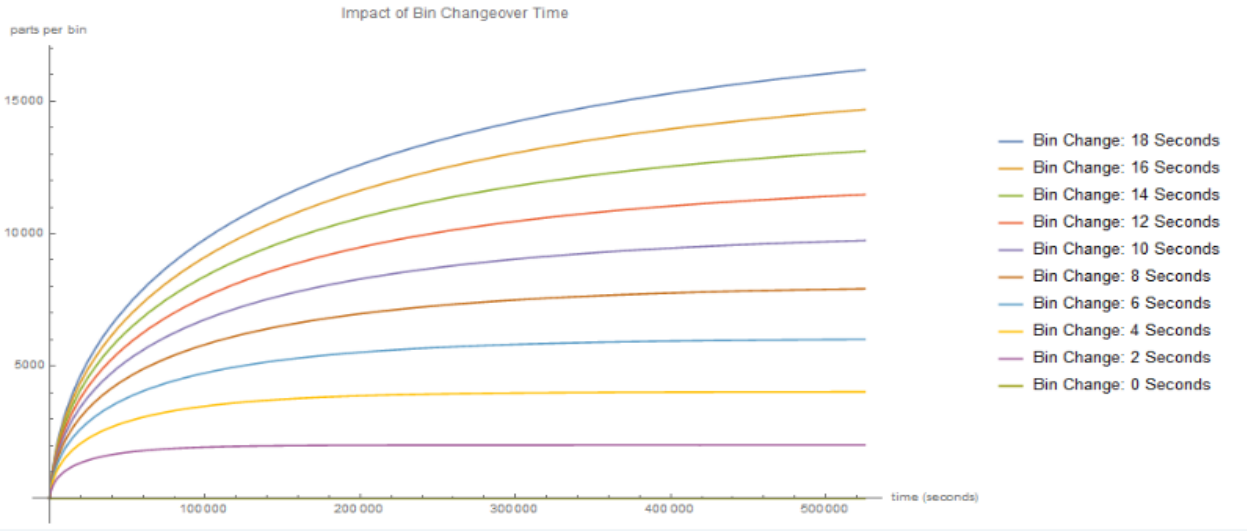

Figure 13: Parts Per Bin as a Function of Processing Time Under Different Bin Changeover Time Conditions

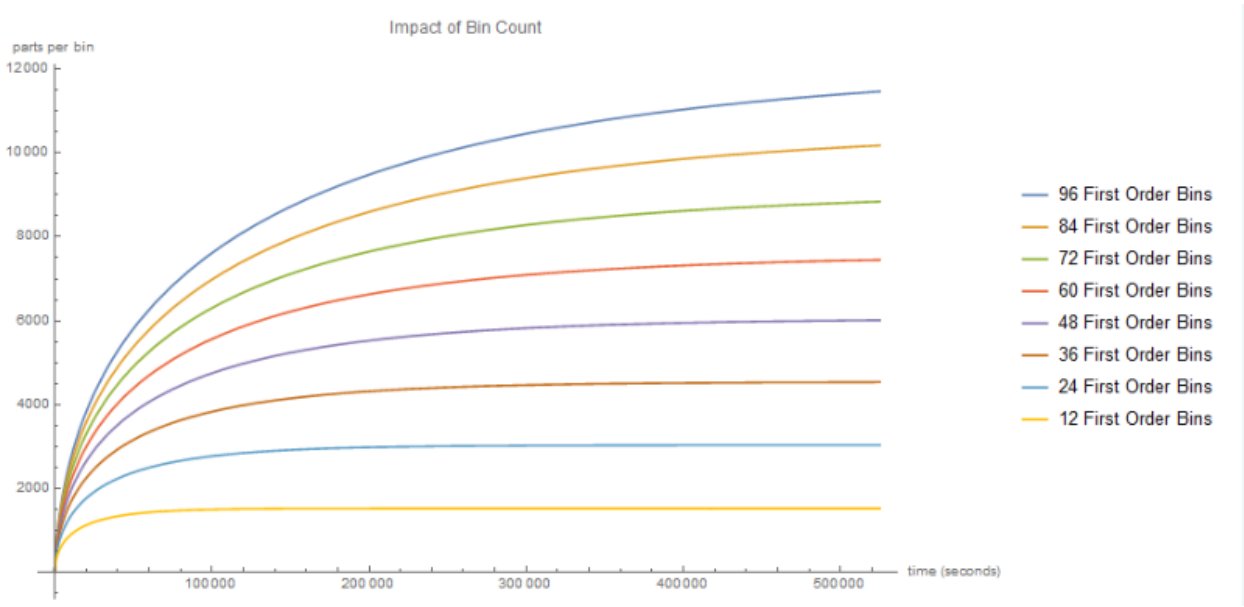

Figure 14: Parts Per Bin as a Function of Processing Time Under Different Bin Count Conditions

Development of Subsystems

0th Stage Sort: Partition by Size, Rotating Grate Drum Sorter

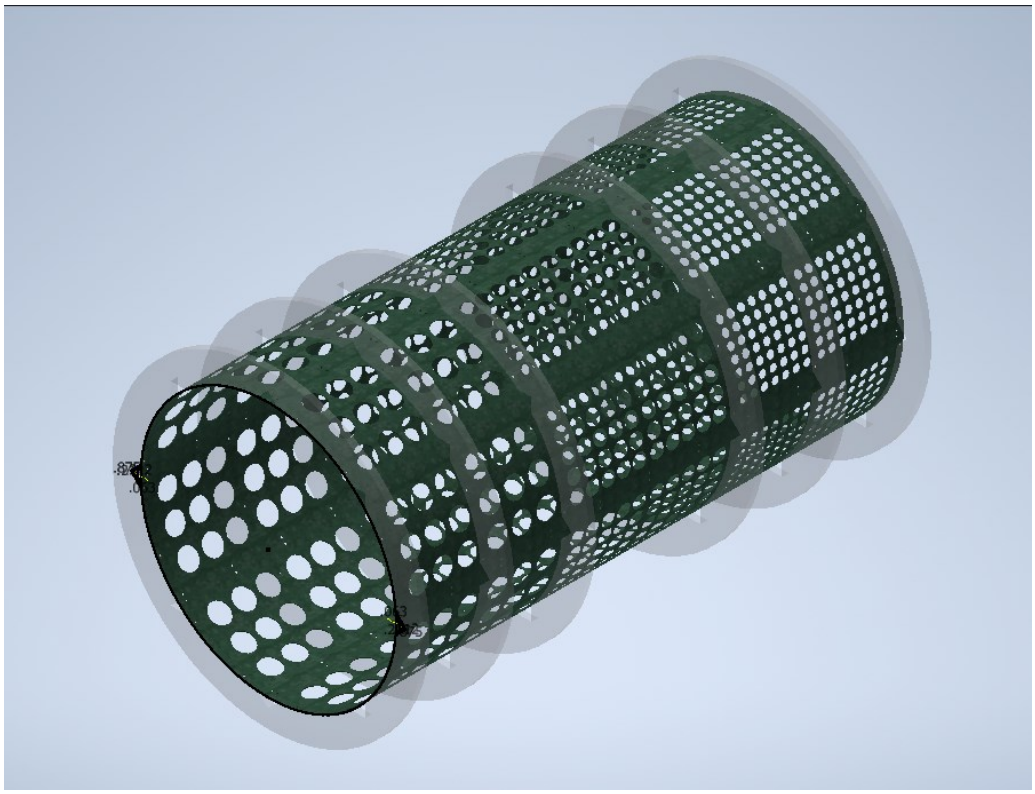

Figure 15: Grate Drum

The intent of the 0th stage was to enable parallel processing within the 1st stage of the sorting process. The 0th stage divides component flow by size categories and each stream is simultaneously processed, the 1st stage sorting subsystems repeat for each stream as seen in Figure 16. Allowing for parallel processing provides multiple benefits such as increasing system capacity, reducing queue length for each identification system, relieving strain on the information processing system for each identification system, and increasing overall system throughput tremendously.

The 0th stage consists of a single subsystem, a Rotating Grate Drum Sorter. As the subsystem rotates, the components gradually slide down the length of the drum's sidewall. The sidewall itself is a cylindrical profile with an array of holes gradually increasing in diameter along its length. The components fall through the side wall as they pass over the holes. They are then shuttled via conveyor belt into the 1st sorting stage.

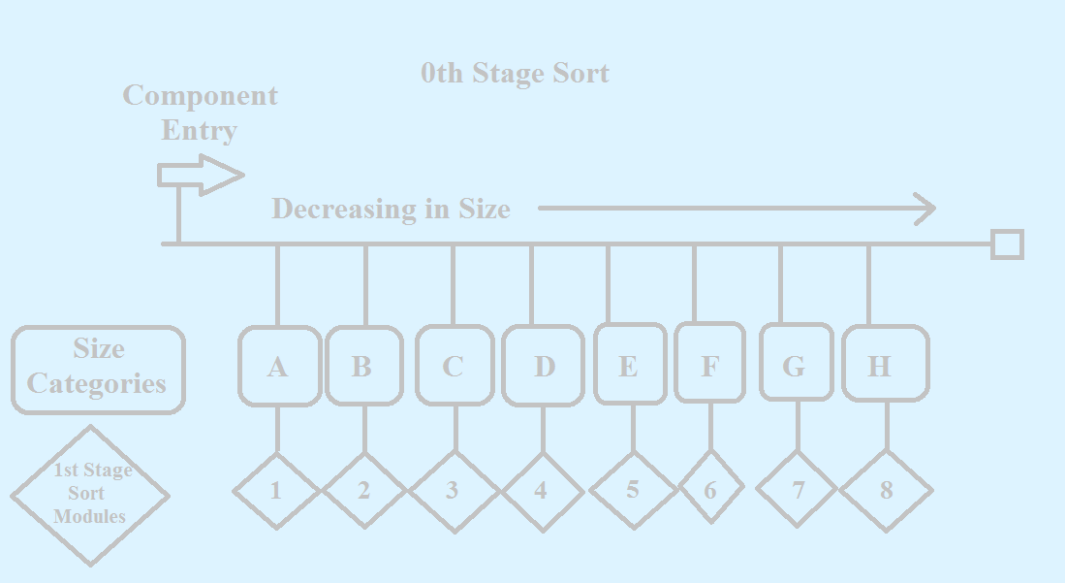

Figure 16: 0th Stage Flow Splitting into Parallel Processing

The low-level design began with the team being posed the following manufacturing challenge, producing a cylinder with hundreds, potentially thousands of holes. Producing the holes manually would have been grossly impractical in all metrics. Producing the holes using CNC equipment would require specialized fixturing and a large working volume which was outside the capacity of available equipment. The team approached the challenge by forming the cylinder by taking a sheet, cutting the hole pattern, and rolling the sheet into a single cylinder held to form by rings. The sheet and its hole patterns could be produced by laser cutting. The rolled sheet and rings can be seen in Figure 17.

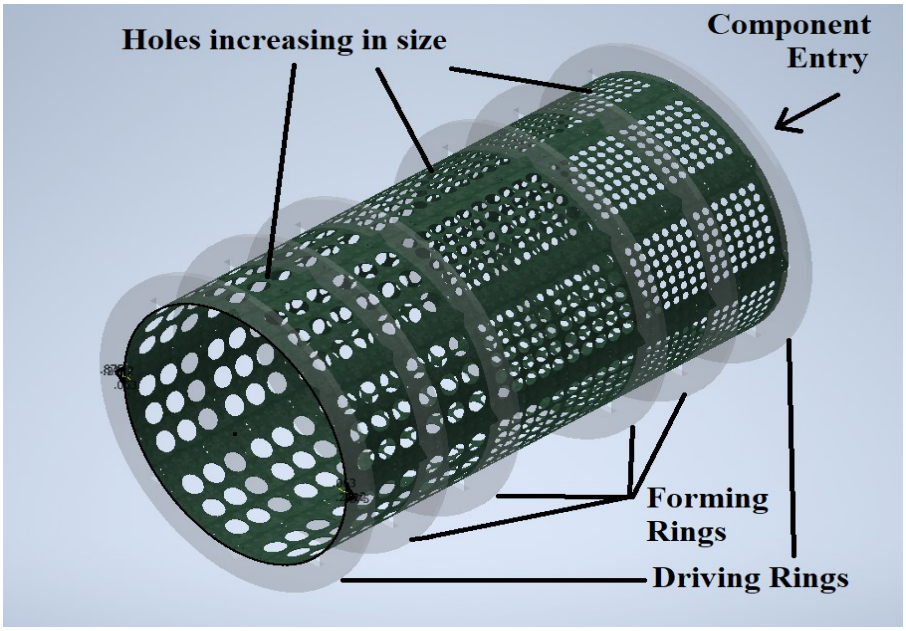

Figure 17: Annotated Grate Drum Features

The next challenge was generating a hole pattern that, when wrapped around a cylinder, would have circular cross-sections. This was modeled by generating a cylinder, projecting the row of circles decreasing in diameter down the length of the cylinder, and then rotationally patterning the row about the center axis of the cylinder. These holes were then cut from the cylinder. From there, utilizing sheet metal wrapping functions, the cylinder was split and then unwrapped to create a rectangular prism with ellipsoidal holes from which the laser tool path geometry could be derived. While exact hole geometry was an area potentially worth exploring regarding impact on subsystem performance, circular cross-sections were selected for design simplicity. The material selected for the sheet was fiberboard, highly available, affordable, has no complications regarding lasering, and can be plastically deformed.

To capture the sheets and form them to a cylindrical shape, outer rings were modeled. The sheets would insert into a set of these forming rings, fasteners driven into the inner surface of the rings would hold the sheet to a cylindrical form. To provide rigidity down the length of the cylinder, contours on the inner forming ring's circumference were cut to fit an extruded angle aluminum profile. Like the sheet itself, the rings were intended to be produced via laser cutting and so additional contour geometry was trivial. Angle aluminum lengths could then be inserted down the length of drum to stiffen the system. These features are annotated in Figure 18.

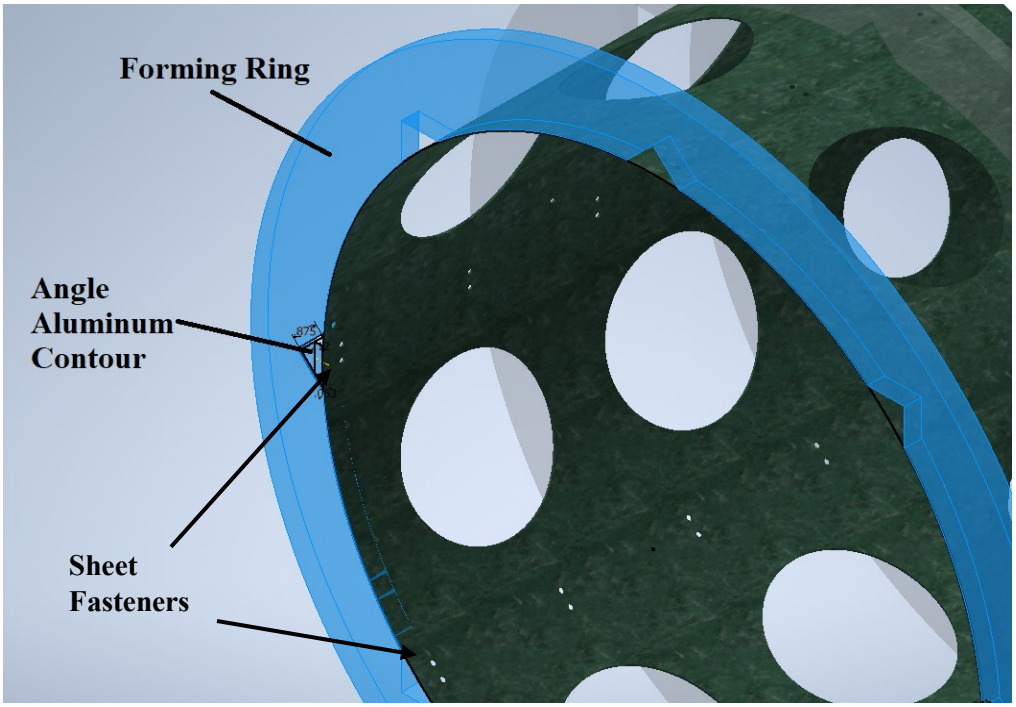

Figure 18: Annotated Forming Ring Features

A coincidental benefit of shaping the sheet using rings is the rings provide a surface to rotate the system. The team recognized this and developed an actuation system that would capture and rotate a ring to rotate the drum. The team proceeded to develop the drive geometry seen in Figure 19.

.

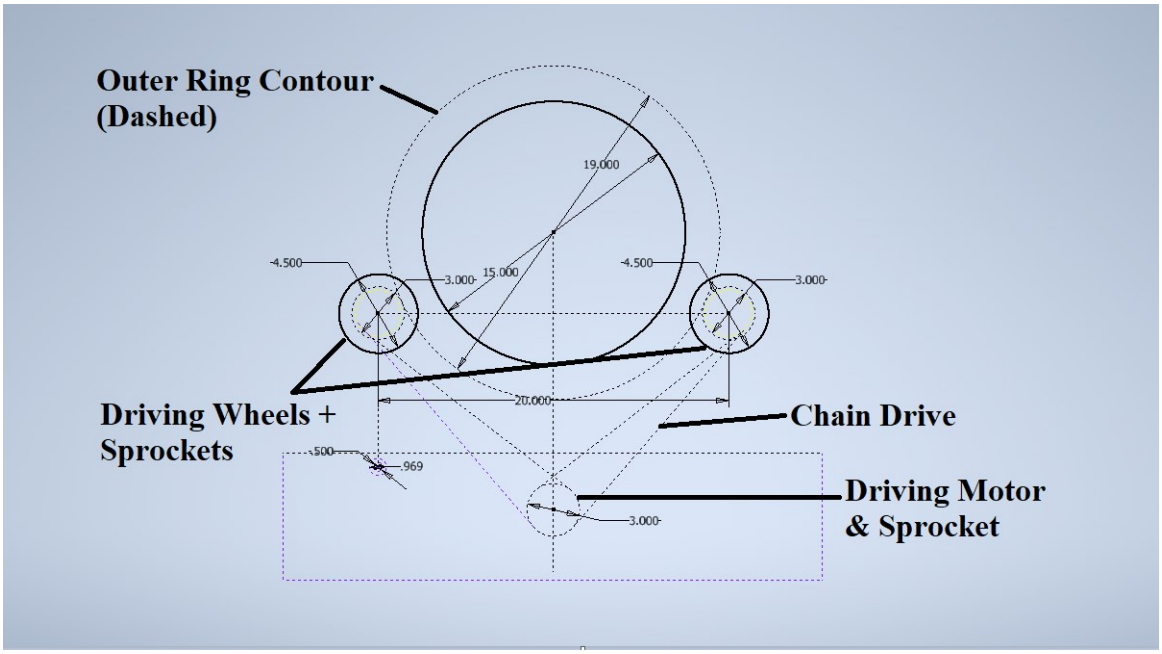

Figure 19: Annotated Drum Sorter Drive System Geometry

The driving wheels are driven by a chain sprocket drive which are in turn driven by a worm gearbox motor. The driving wheels have a slot cut into the outer surface of the wheel which the driven ring can ride on. The inner sides of the slot then capture the ring laterally. This is shown by the two tangential construction circles in Figure 19. The driving wheels were intended to be COTS parts, wheel, hub, and sprocket. To support the drive system, support panels, intended to be produced from laser cut .25" plywood were modeled. Tab and slot support cross braces could nestle in between the two panels, providing rigidity. The kerf of the laser beam was accounted for in the slot dimension to prevent loose fitment of the support cross braces. These features are annotated in Figure 20.

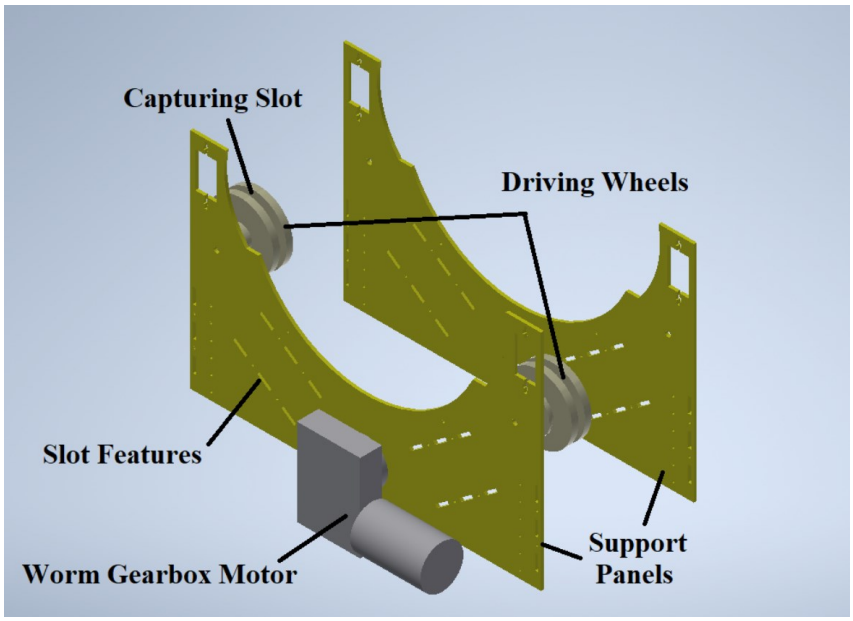

Figure 20: Annotated Drum Sorter Drive System

At one end of the drum would be a powered actuation assembly and at the other would be a non-driven assembly purely to support the weight and rotation of the other end. Because the application of the drum and its drive system was low load, no analysis was necessary and therefore was not conducted.

1st Stage Sort: Serialization, Identification, Distribution

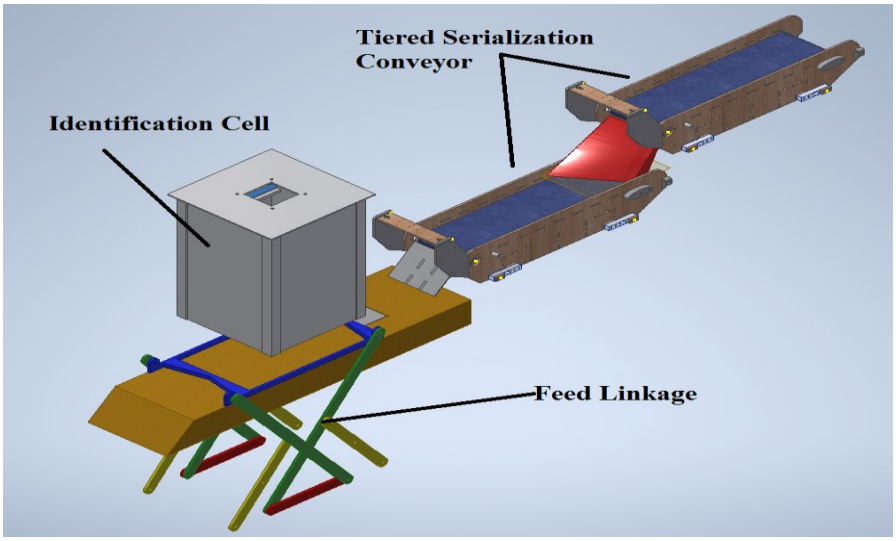

Figure 21: Annotated 1st Stage Sort Single Module

The 1st stage sort serializes the components for each size category and then subsequently identifies each component. Each size category has its own dedicated 1st sort module, allowing the size categories to be processed in parallel, as depicted in Figure 22. The identified components are then distributed into each of their respective final storage drawer groups. There are 3 subsystems operating in the 1st stage sort, a serialization conveyor, an identification cell, and a rotary distribution mechanism.

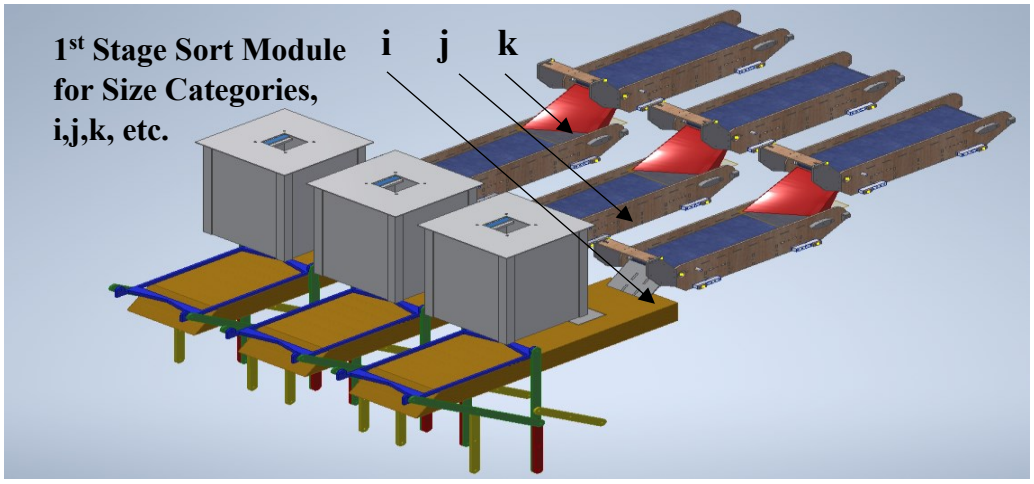

Figure 22: 1st Stage Sort Module Array

Tiered Serialization Conveyor

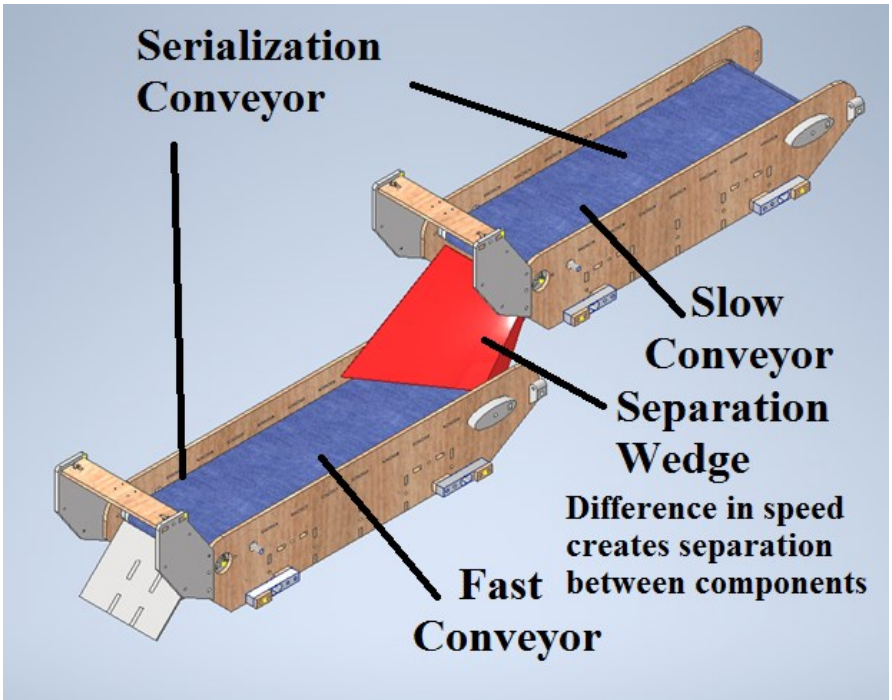

Figure 23: Annotated Tiered Serialization Conveyor

In order to identify a component from mixed bulk, it must be isolated from the bulk. The 0^{th} stage partially isolates components from bulk as it divides the bulk into smaller groups for each identification cell. The intent of the tiered serialization conveyor is two-fold. The primary intent is to serialize the components, to separate the components from each other in a single file line with adequate distance between each component. The secondary intent is to convey the parts up to the feed linkage identification cell.

The serialization conveyor is vertically tiered with each conveyor segment operating at differing speeds as is annotated in Figure 23. The topmost tier operates at a lower speed while each subsequent tier operates at increasing speeds. As components gradually fall from the topmost tier on to the next tier conveyor, the difference in conveyor speeds creates distance between the components. This repeats until sufficient distance is created between the components such that they can be distinctly identified from one another. As it stands currently, only 2 tiers are deemed necessary, however, the modularity of the design permits additional tiers to be added on with little effort.

The rear pulley features a thumbscrew tensioner, allowing separate tensioning of the left and right side, by pushing on the sliding dead axle mounting blocks. This is vital to ensuring that a flat belt tracks straight and doesn't wander off to one side.

The design features a support plate under the entire length of the conveyor surface. This prevents parts from sagging, makes their behavior on the belt more predictable, and ensures that impact shock from falling parts is transmitted directly to the frame, for reliable detection via strain gauges. The support piece was also built with mounting features to enable possible future experimentation with vibratory feed mechanisms built onto the same base conveyor structure

The design uses interchangeable front slope pieces, for testing various geometries. The final stage uses a simple straight ramp, but for intermediate stages we have experimented with more exotic geometries, like the 3d printed lofted profile shown in figure. This profile is meant to encourage part separation as parts leave a slow-moving belt. If two parts exit at the same time, the part on the right side will travel further than the one on the left, ensuring that they're spread out and easily processed one at a time by the next belt in line.

Feed Linkage

Once components are serialized by the tiered conveyors, they are fed through the identification cell by the feed linkage. The identification cell identifies the components using 2 data types, weight data and visual data.

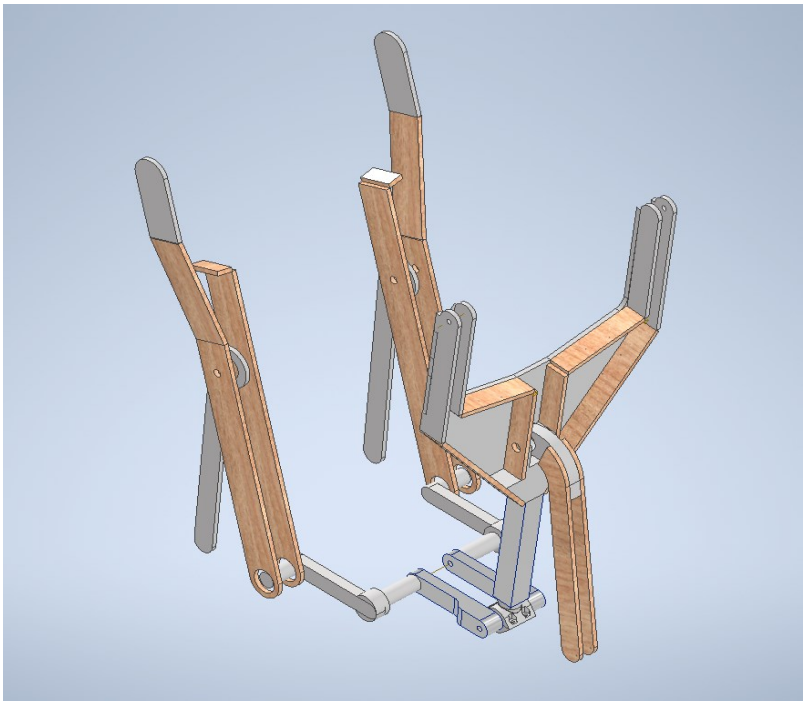

Figure 24: Feed Linkage with Coupler Removed

The feed linkage is a complex planar path generator linkage as seen in Figure 24. The feed linkage is repeated across two planes, synchronously turned by a double journal crankshaft, one journal for each plane of the feed linkage. The top coupler of the linkage glides components across the identification cell as the crankshaft rotates. The linkage is designed such that the coupler is constrained to horizontal motion as it pass components through the identification cell. After reaching the extent of its horizontal motion, the coupler vertically retracts and moves in a concave down curve back to its initial position. The coupler and links are defined such that they cannot contact the part unless the coupler is moving horizontally, no interference is experienced during downward travel. As the coupler passes a newly introduced component through the identification cell, it pushes the previous part out of the identification cell into the distribution carousel.

Identification Cell

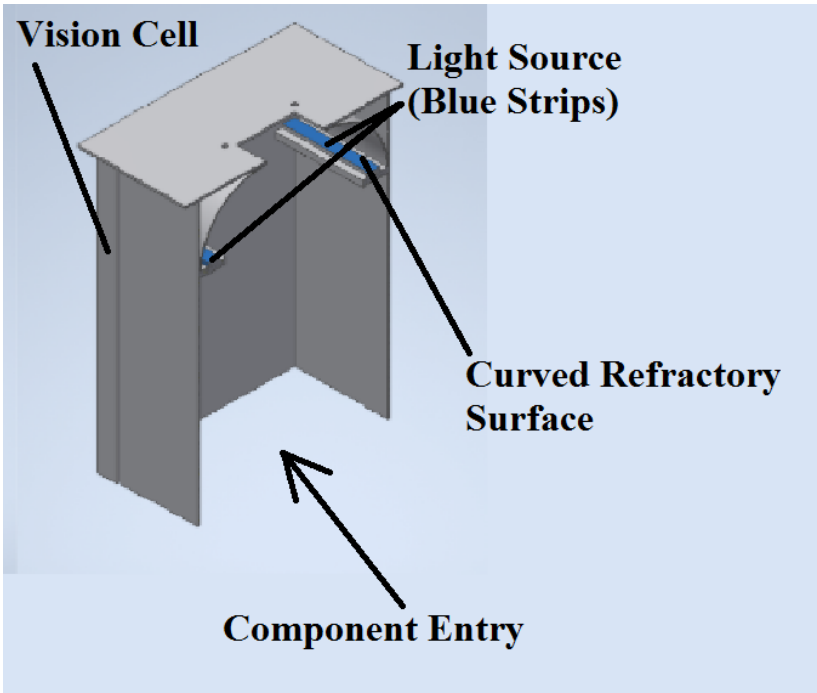

Figure 25: Annotated Identification Cell

The bulk of the information processing in the overall system happens within the identification cell. Identification takes into consideration 3 data types, size, weight, and image. The components arrive at the identification cell already identified in the size category as they were partitioned by size at the 0^{th} stage sort. The weight data is captured using a sensitive jewelry scale. As the feed linkage moves a component through the identification cell, it will pause motion once the component is properly placed on the scale. The feed linkage allows the component enough time to settle onto the scale to prevent noise in the acquired weight data. The gap between the bottom face of the coupler and the top surface of the weight scale is kept minute while preventing contact with the scale surface.

The identification cell, seen in Figure 25, houses a camera which then acquires visual data from the component such as color, patterns, and outline through images taken by the camera. Maintaining adequate illumination within the cell is essential for minimizing noise in the visual data. An excessive amount of illumination distorts image quality and so the identification cell uses refractory illumination to ensure that the images aren't over exposed. A moderate amount of

backlighting through the frosted bottom surface of the identification cell improves contrast along the component outline.

The volume of data involved in identification can be incredibly cumbersome on the computers processing the data. The full class count of LEGO components is close to 70,000 and the cumulative amount of visual data needed for machine learning based identification is colossal. Identification through purely visual means would take supercomputer-tier processing power and memory. The class count must be physically stratified across multiple computers to distribute the computing intensity. The first acquired data type, size, essentially stratifies the classes across the computers of the identification cells and reduces the total class count each computer must identify components from. The second data type, weight, further divides each computer's class count, digitally as opposed to physically, into weight categories. The result of division by size and then by weight results in a decrease in the total class count in which components are identified, from 70,000 classes down to 1,000-10,000 classes per size category and then down to 100-200 classes per weight category. Identification by weight is near instantaneous; vision processing, however, is much more complex computationally and is a function of identification class count. Identifying a component by weight category drastically reduces identification class count and results in a substantial decrease in visual identification cycle time, improving overall system throughput. The 1st identification cells identify a component and instructs the system on which drawer the component belongs in. The next step for the component is placement into its respective drawer group.

Distribution Carousel

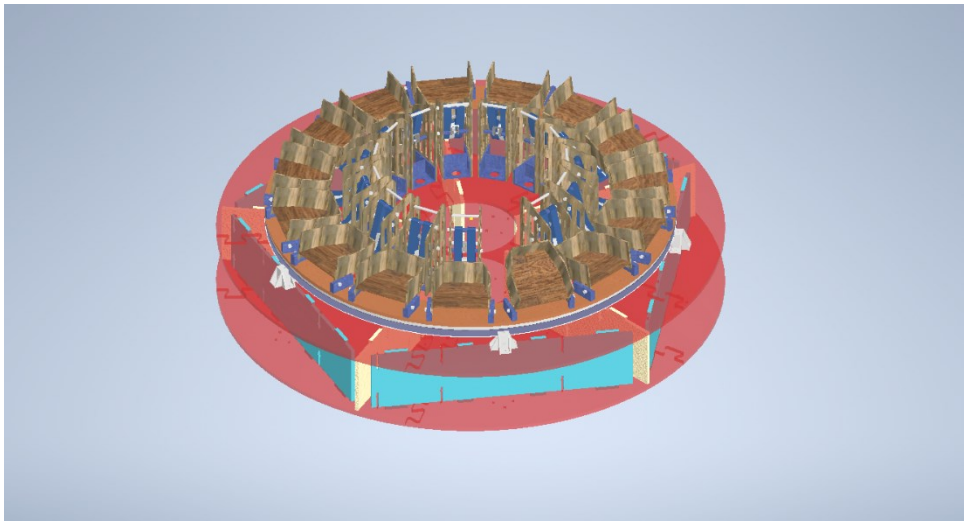

Figure 26: Distribution Carousel

After components have been identified by the identification cell and pushed off the identification cell by the feed linkage, they must be placed with their respective drawer group. This is the function of the distribution carousel. The distribution carousel temporarily stores a component and releases the component into its drawer group where the component will remain until its group is introduced the 2nd stage sort.

When a component exits the identification cell, it then enters the distribution carousel. Each component enters an empty pivot container along the top rotating ring. The ring rotates discretely such that there is always an empty pivot container at the component entry point and only one component populates a pivot container at any given time. When a populated pivot container arrives at the component's corresponding drawer group location, a pneumatic lever will pivot the pivot holder and deposit the component into its respective drawer group. The most apparent drawback of distributing components into groups is the loss of component identity as the component enters the group. This reidentification is done in the 2nd stage sort.

The design of the distribution carousel began with a concept solid model assembly, detailing the key features of the assembly and its design. The initial concept assembly is shown in Figure 27.

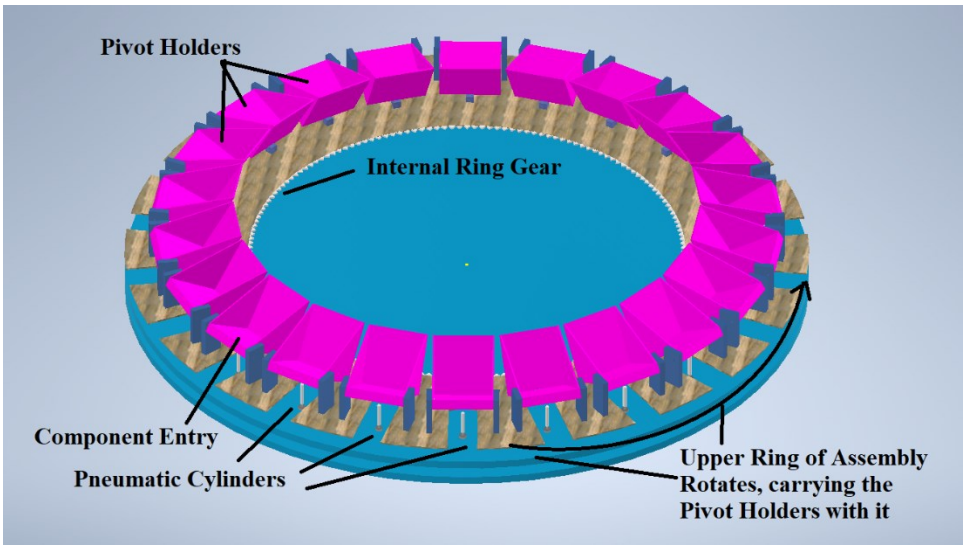

Figure 27: Annotated Distribution Carousel Concept Assembly

For the scope of the MQP, the pivot holders were designed to accept 16x16 stud components. Stud is a standardized unit for LEGO component dimensions, 1 Stud = 8 MM, measured by calipers. Early in the design of the pivot holder, it was established that the pivot holders would not experience high loads. This prompted the team to design the pivot holders with the intent of producing them from laser cut plywood.

The pivot holders were designed with the reference component in 2 configurations. The first configuration has the component square with the reference frame. The second configuration is the first configuration rotated 90 degrees about its center and translated down such that the bottom vertex of the second configuration is coincident with the bottom edge of the first configuration. The two configurations are shown in Figure 28.

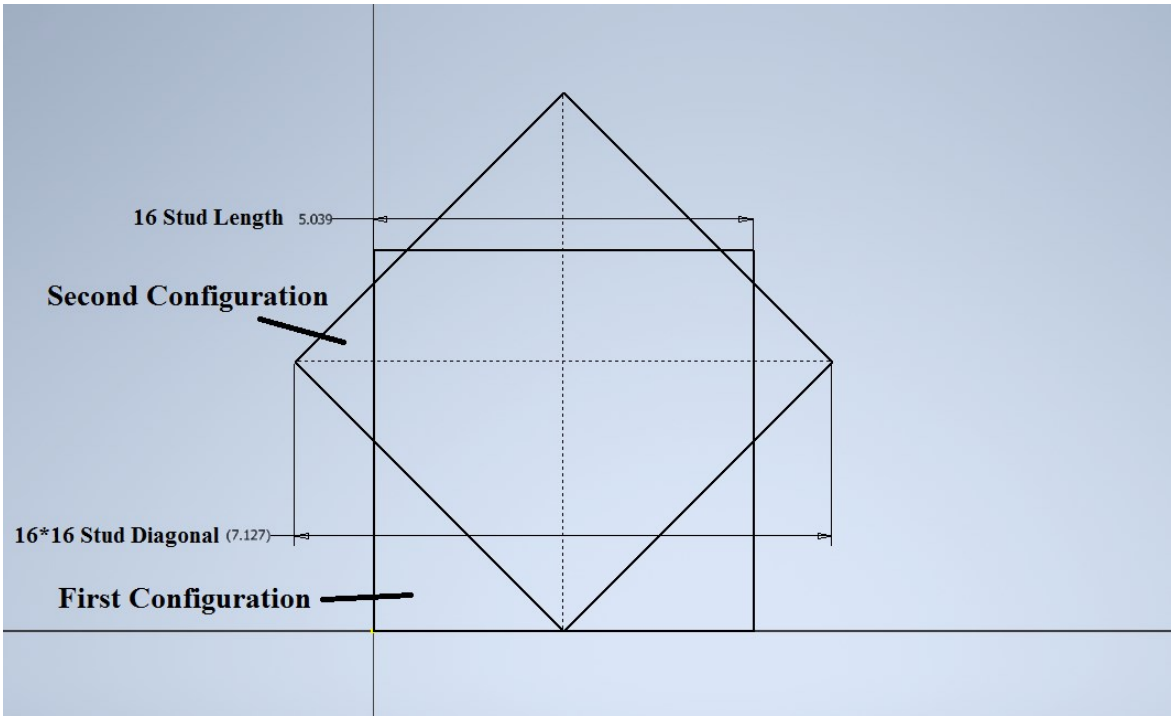

Figure 28: Annotated Reference Component Landing Configurations

Drawing the component in its 2 extreme configurations allowed the team to establish the holder footprint. The footprint had to accommodate components entering the pivot holders in their second configuration. The footprint therefore needed a length equivalent to the diagonal of the reference component. At the entry point of the holder, the width of the footprint also needed to be equivalent to the diagonal of the reference component. At the rear-most point of the pivot holder, the width could be shortened to the width of the reference component, resulting in less material usage. The pivot holder footprint is shown in Figure 29.

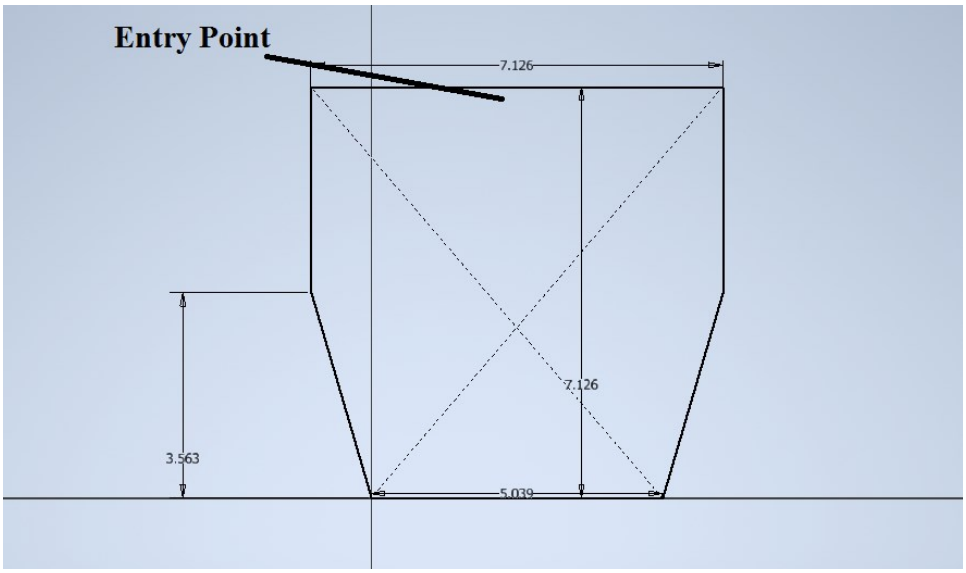

Figure 29: Pivot Holder Geometry Sketch

From there, the bottom face of the pivot holder was extruded. As previously mentioned, the team intended to produce the pivot holders from laser cut plywood, the tabs along the perimeter of the extruded bottom face are used in mating the laser cut components together. These tabs are used in mating the sidewalls of the pivot holders to the bottom face. The bottom panel can be seen in Figure 30.

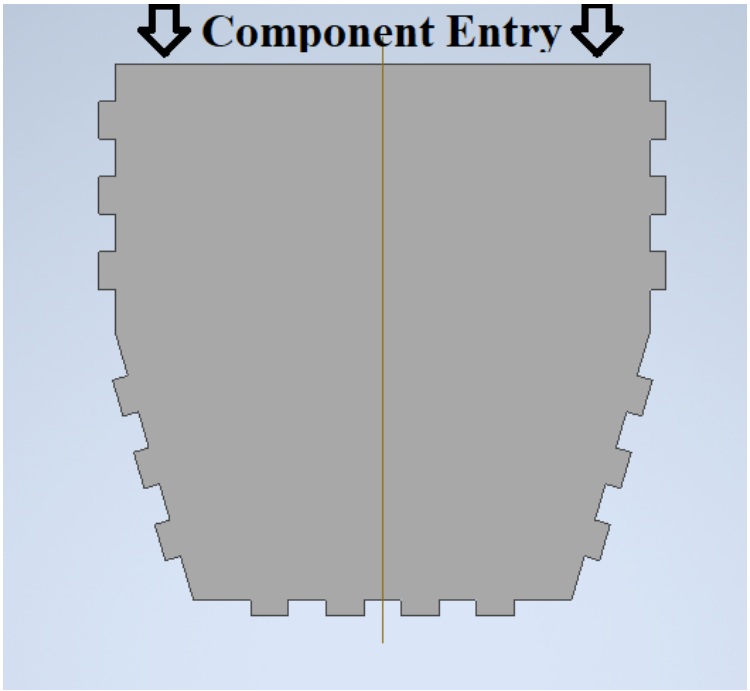

Figure 30: Pivot Holder Bottom Panel

From the model of the bottom panel of the pivot holder, the corresponding sidewalls were extruded. The height of these sidewalls was arbitrarily chosen to be 3 inches, with the intent of being conservative on material usage and volume envelope. Likewise, location of the pivot holes in the sidewalls was arbitrarily chosen with the intent of keeping the pivot points close to the bottom panel with same intents as the height choice. The sidewalls of the pivot holders are shown in Figure 31, the segmented nature of the pivot holder footprint requires 5 separate sidewalls per bottom panel. Below Figure 31 is Figure 32, the completed assembly of the pivot holder.

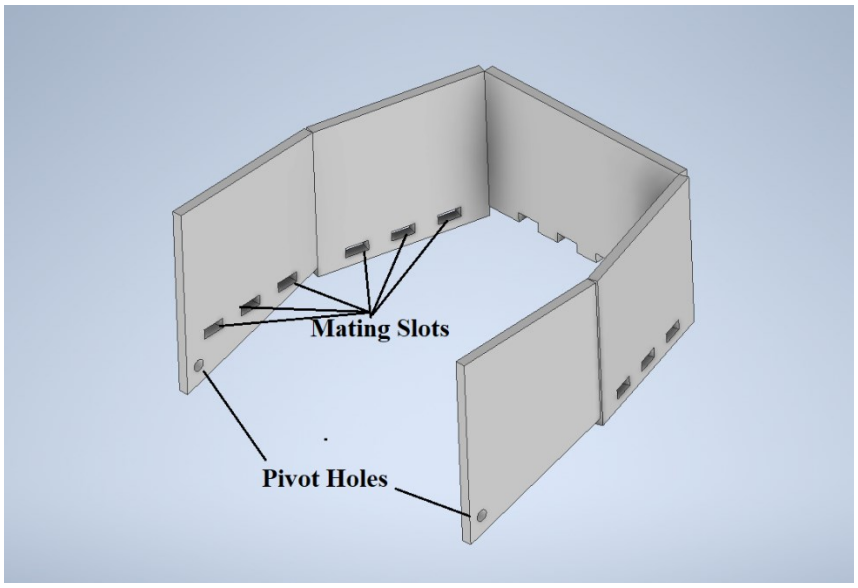

Figure 31: Annotated Pivot Holder Side Walls

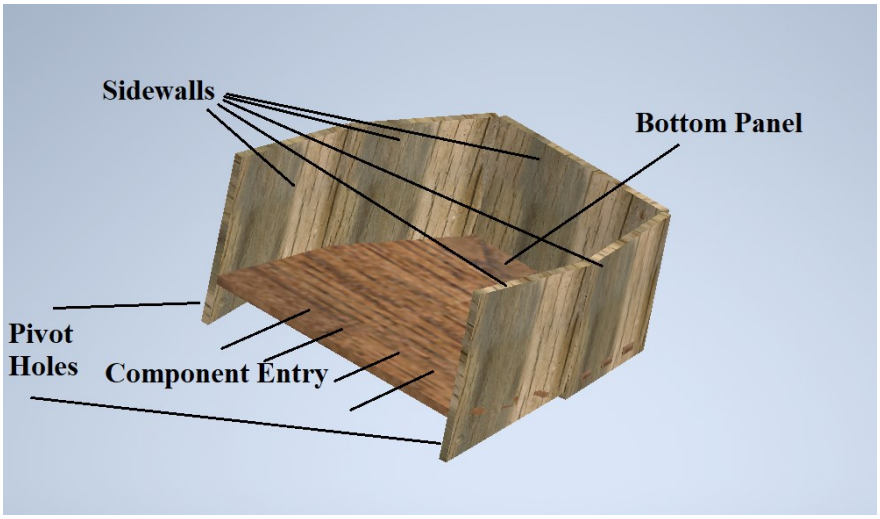

Figure 32: Annotated Pivot Holder Assembly

With design of the pivot holders complete, the team moved on to designing a method of actuating the pivot holders, making them pivot. Initially, multiple actuation methods were considered; different forms of motorized actuation and different forms of pneumatic actuation were all viable.

Determining the optimal actuation method was based on control. From a control perspective, pneumatic actuation was ideal, the system only had two states, loading or unloading. This binary nature suggested pneumatic actuation as pneumatic cylinders also have a binary nature, extended or retracted. This binary nature negates the need for a sophisticated control system. In addition, to achieve maximum throughput, the actuation system needs to operate to maximum speed. The speed with which a pneumatic cylinder actuates can be directly adjusted using a needle valve, motorized approaches require a more sophisticated control system to adjust actuation speed.

With the usage of pneumatic cylinders established, the team selected a pneumatic cylinder. Selection of the pneumatic cylinders was predicated on cost, since the actuation method would be repeated throughout the distribution carousel assembly, a low-cost actuator would result in high savings. Research into pneumatic cylinders uncovered that the cost of a cylinder is a function of its bore and its length. In selection based on cost, the team was inclined to select a narrow bore, short stroke cylinder. The team ultimately selected the NITRA A07015SN Pneumatic Cylinder. This cylinder had a relatively low cost and would serve the design's needs.

The team proceeded to develop a geometric sketch of the pivot holder's bottom panel in its two states, loading and unloading. In the loading state, the angle of the bottom panel relative to the X-Axis is –15°, the team determined this angle would be shallow enough to minimize volume envelope while providing enough of a decline for loaded components to settle. In the unloading state, that angle changes to +60°, the team determined this angle would be satisfactory for unloading the component via gravity. While experimentation to ascertain the minimal angle necessary to break static friction was not executed, values for coefficient of friction of hard and soft plastics on wood are provided by the University of Florida's Mechanical Engineering Department. Analysis for the angle based on the tabulated coefficients of friction was then conducted. Given the classic physics problem of a weight on an incline as seen in Figure 33.

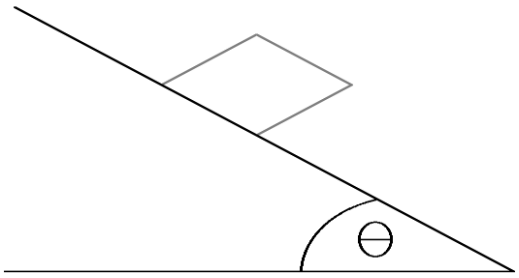

Figure 33: Mass on an Incline

It is known from elementary mechanics that the tangent of the angle that the weight begins to move is the static coefficient of friction as seen in Figure 34.

$$\tan(\theta) = \mu$$

Figure 34: Expression for Coefficient of Friction as a Function of Incline Angle

By taking the arctangent of each side of the equation above.

$$\theta = \tan^{-1}(\mu)$$

The results for angle based on the provided coefficients of friction are seen below in Figure 35.

For hard plastics on wood $\mu = .4, \arctan(.4) = 21.8\ degrees$

For soft plastics on wood $\mu = .7, \arctan(.7) = 34.99\ degrees$

Figure 35: Incline Angle Analysis

One can observe from the calculations that the angle of 60° is ample for breaking static friction between the component and bottom panel. Although the values used are ambiguous regarding specific materials, ABS plastic on Baltic birch plywood, the team felt the angle was in fact sufficient. The later evaluation of the prototype confirmed this belief.

The bottom panel in its two states is shown in Figure 36.

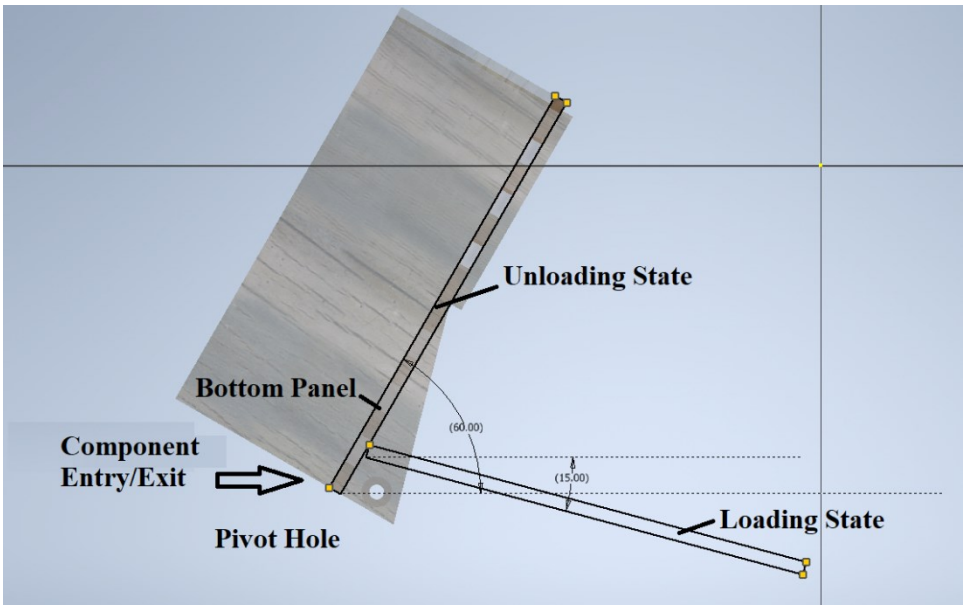

Figure 36: Annotated Pivot Holder Bottom Panel in Loading and Unloading States

This geometry sketch was used to make further design decisions such as location of the pneumatic cylinder relative to the rest of the assembly. In the initial concept assembly shown in Figure 27, the pneumatic cylinders sit directly below the pivot holders. This was a simple and direct approach to actuating the pivot holders, however, it carried a potentially detrimental risk. Should the top ring rotate while a pivot holder is still contacting the tip of the rod of a pneumatic cylinder, the pivot holder could exert a side load, through normal and frictional forces, on the tip. This carries the risk of bending the pneumatic cylinder's rod and thus ruining or hindering the performance of the actuator. This led to the team establishing need for an intermediary linkage for the pneumatic to actuate, which would in turn actuate the pivot holder.

Building from the previous geometry sketch, the team projected in the geometry of the selected pneumatic cylinder in its extended and retracted states per the manufacturer's specifications. Friction along the bottom panel of the pivot holders was a concern, the team decided to implement a sealed ball bearing to run against the bottom surface of the panel. A .5" ball bearing was arbitrarily selected and then drawn in the sketch, for both the extended and retracted states. An initial lever arm was also drawn in with its pivot arbitrarily selected. The pneumatic cylinder also had an arbitrarily selected pivot location. The selected pneumatic cylinder was a nose-mount cylinder; it had no mechanical pivot feature and so the team was free

to design in their own. This pivot was kept close to the profile of the pneumatic cylinder itself to minimize the system's volume envelope. The resulting geometry is seen in Figure 37.

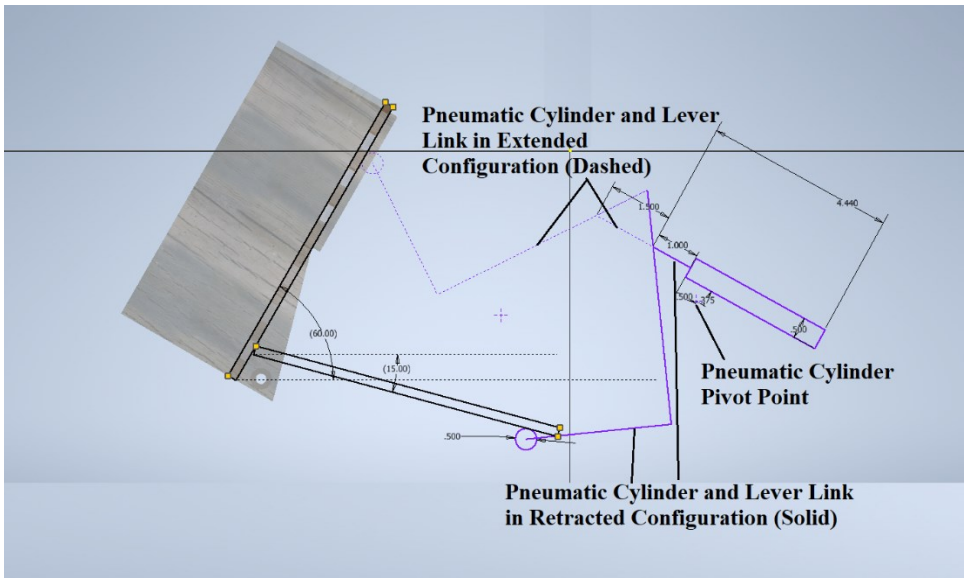

Figure 37: Annotated Pivot Holder Actuation Lever Link Geometry Sketch

It was clear from the geometry sketch that the design here could be optimized to reduce volume envelope. By adjusting the lever link pivot point, the length and geometry of the lever link, the location of the pneumatic cylinder and where it connects to the lever link, the volume envelope of the system could be reduced. The result of adjusting these parameters is shown in Figure 37.

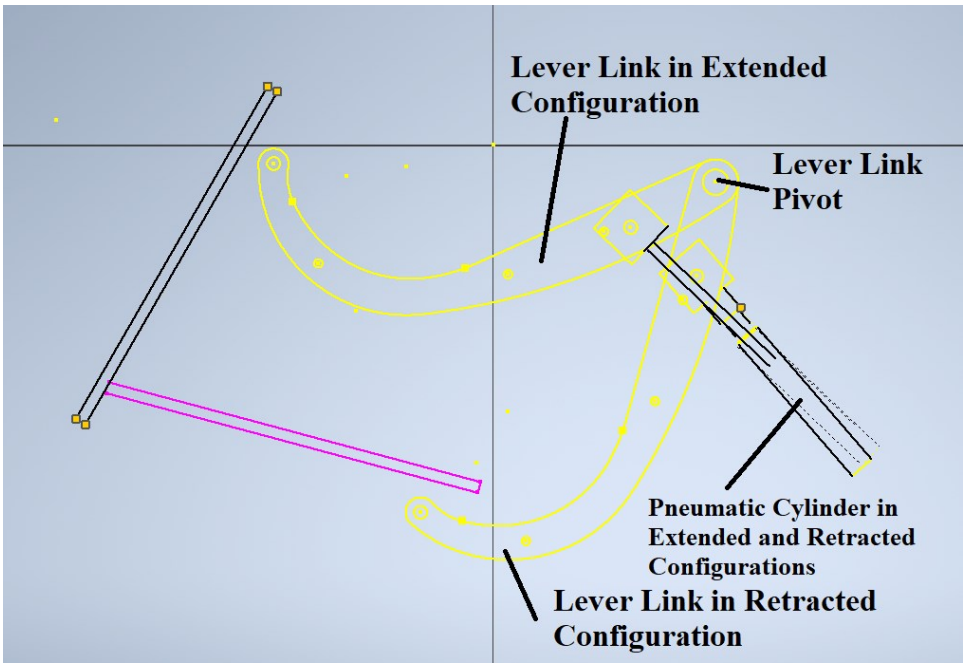

Figure 38: Annotated Adjusted Pivot Holder Actuation Lever Link Geometry Sketch

One can observe above from Figure 38 that the lever link does not contact the bottom panel of the pivot holder in the retracted state. This vertical offset was introduced to prevent collision between the sidewalls of the pivot holder and the ball bearing at the tip of the lever link.

With the actuation geometry finalized, the team proceeded to further develop the design by modeling in structural components. The lever link was initially a single layer of laser cut plywood, a single layer would be lacking in rigidity and maximum load. This was amended by stacking layers to produce a thicker link, the stacked layers were fastened together using #8-32 bolts across the length of the link. At the pivot point of the link was a hole cut to the outer diameter of a .5” nylon spacer which would be used as a friction and wear absorbing bushing, the highly frequent cyclic nature demanded such a wear reducing feature. At the ball bearing mount point at the tip of the link was a hole cut to the diameter of .25” steel shaft to support the bearing. The features described are shown in Figure 39.

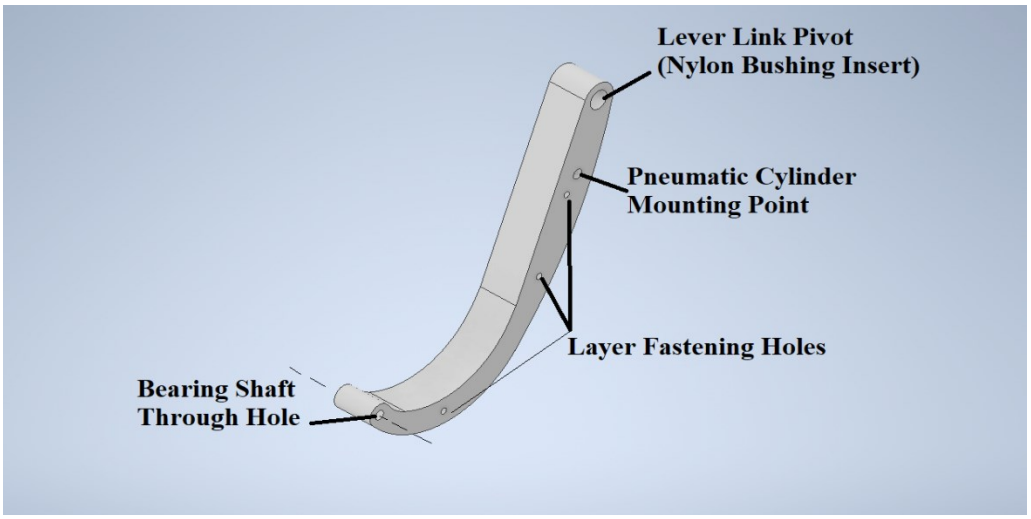

Figure 39: Annotated Actuation Lever Link

The team established that packaging 2 lever links in a single actuation system would improve rigidity and would not increase the actuation system's volume envelope. The connection hardware to the pneumatic cylinder could nest between the 2 lever links. Joining the 2 lever links is a single space block. This spacer block significantly adds to the torsional rigidity and utilizes 2 of the 3 already existing layer fastening holes as through holes for bolts that can be threaded into the spacer. These changes are shown in Figure 40.

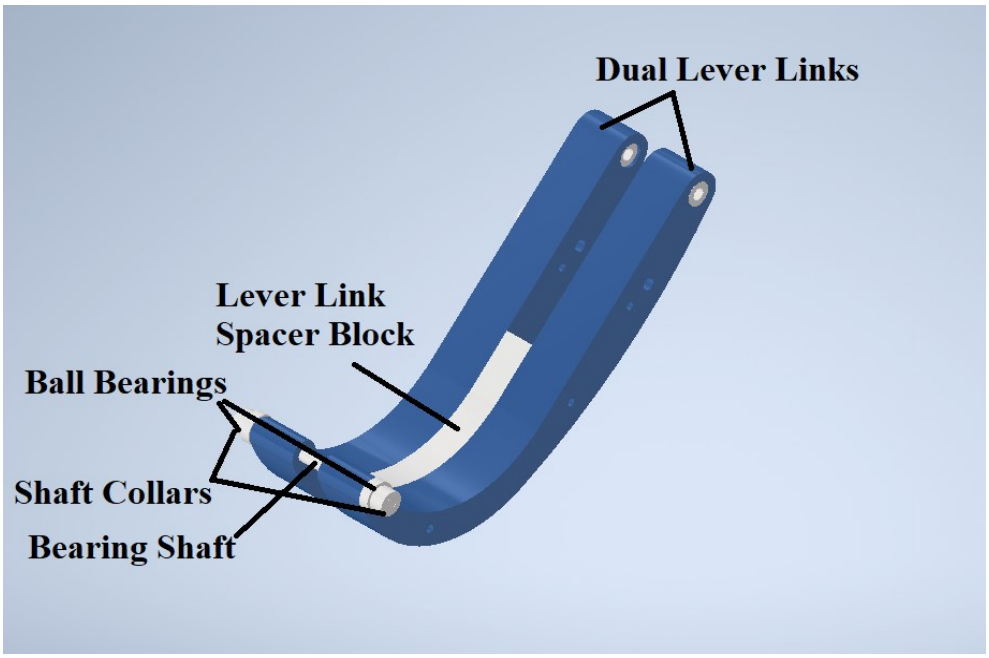

Figure 40: Annotated Dual Actuation Lever Link Assembly

The pneumatic cylinder then needed 2 critical hardware components, hardware to connect the rod to the corresponding pin joint on the lever link and a bracket for the cylinder to pivot on. As previously mentioned, the pneumatic cylinder is nose mounted via a nut and shoulder. The bracket needed pivot holes corresponding to the pivot holes in the previous geometric sketch as well as a hole for the cylinder itself to mount in. At the end of the cylinder's rod, there needed to be hardware to join it to the lever arm. Topologically, this was straightforward, develop a shape that encapsulated a nut that could thread onto the pneumatic cylinder's rod and had a through-hole for a bolt or shaft that would then join it to the lever link. The hardware is outlined in Figure 41.

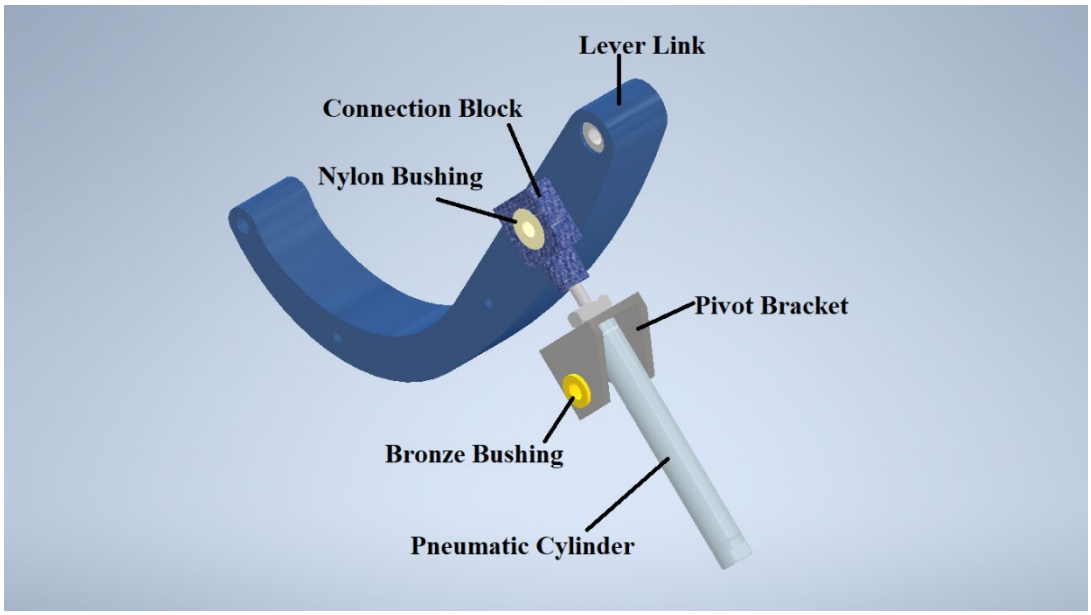

Figure 41: Annotated Dual Actuation Lever Link Hardware Features

The connection block has a hexagonal pocket which a #10-32 nut could press fit in to. The block could then thread onto tip of the rod of the pneumatic cylinder. Above the nut in the connection block is a hole bored out to receive a .25" ID nylon bushing. The bushing would absorb wear from actuation of the system. Passing through the bushing is the shaft that joins the connection block to the lever link and thus joining the pneumatic cylinder to the lever link. The pivot bracket has a hole at its top-most face to receive the treaded nose of the pneumatic cylinder which the nut could thread onto and secure the cylinder to the bracket. On the sides of the pivot bracket are holes which .25" ID bronze bushings could be press fit in to, these bushings absorb the wear from the actuation of the system.

The actuation system at this point, lacked structure for which to exist in. Walls to enclose the system and provide mounting features for the pivoting hardware was necessary. A rectangular plane was extruded and using the established pivot locations, the sidewall for the actuation assembly was generated. The tops of the sidewalls were fastened together using a spacer spanning the internal width of the sidewalls. The bottoms of the sidewalls would be fastened together using a single bracket. The two joining features allowed the assembly to be modular which was ideal given the repetitive application of the actuation system throughout the distribution carousel. The sidewall and its discussed features are shown in Figure 42. The fillets and parallelogram cutouts were later added for aesthetic quality.

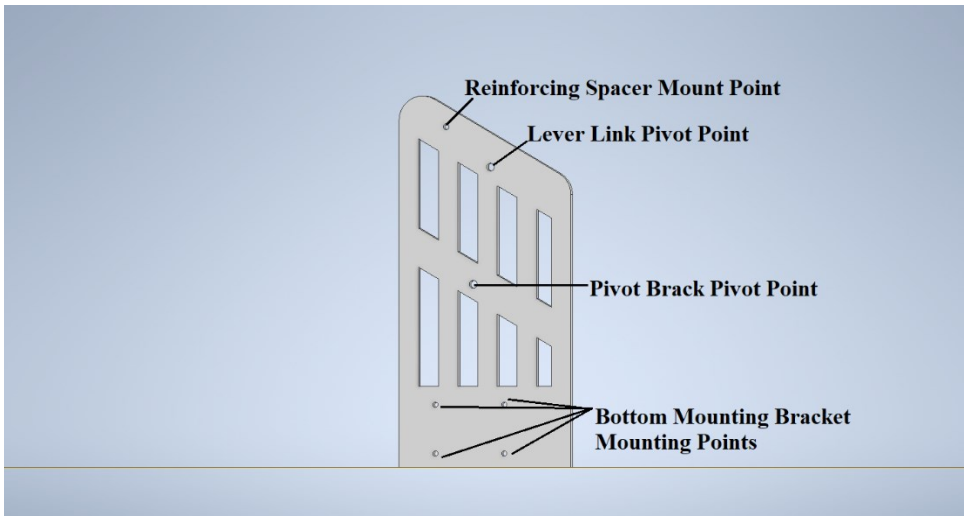

Figure 42: Annotated Pivot Holder Actuation System Support Walls

To join the 2 sidewalls together at the bottom was a bottom mounting bracket. The bracket was designed to be parallel across one of its origin planes to reduce complexity in later assembly. To further reduce complexity, fastening hardware was designed to press fit into the bracket in the form of heat sensitive brass nutserts. Circular cutouts were made to each side of the bracket to reduce material usage. A rectangular mounting holes pattern was added to the bottom face for later mounting to the base plate of the assembly. These described features are highlighted in Figure 43.

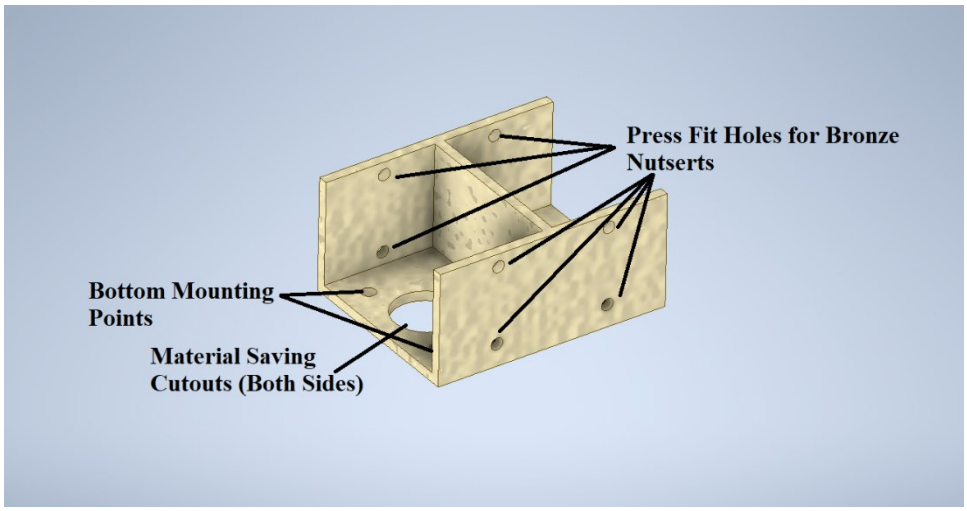

Figure 43: Annotated Pivot Holder Actuation System Bottom Support Bracket Features

At this stage in the design of the actuation system, all that was left was modeling in minor hardware components such as fasteners and spacers. A view of the actuation system and its critical components is seen in Figure 44 where the pneumatic cylinder is in its retracted state, immediately below is Figure 45 where the pneumatic cylinder is in its extended state.

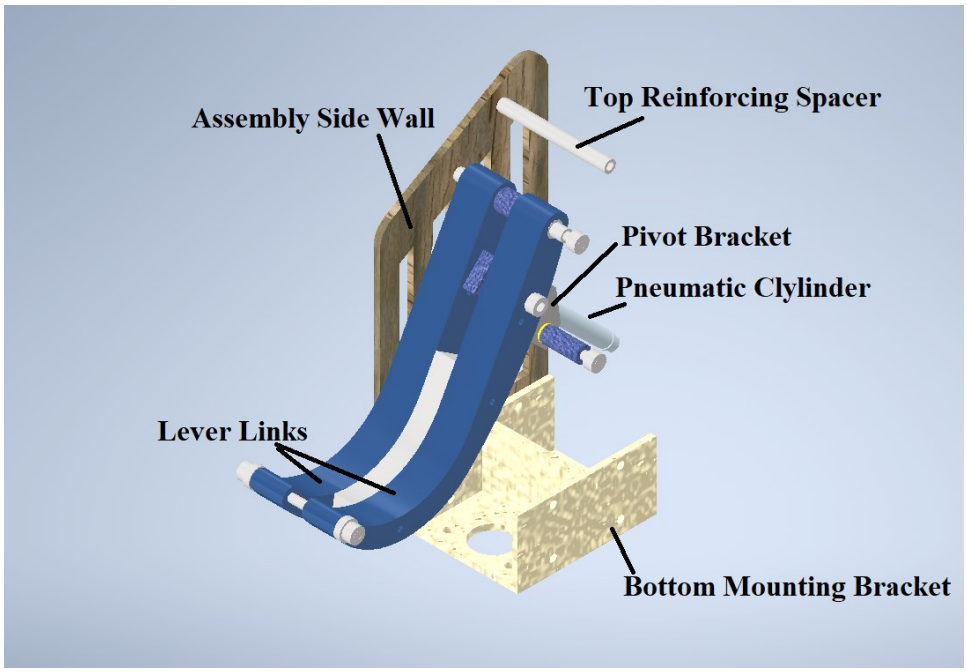

Figure 44: Annotated Pivot Holder Actuation System Components

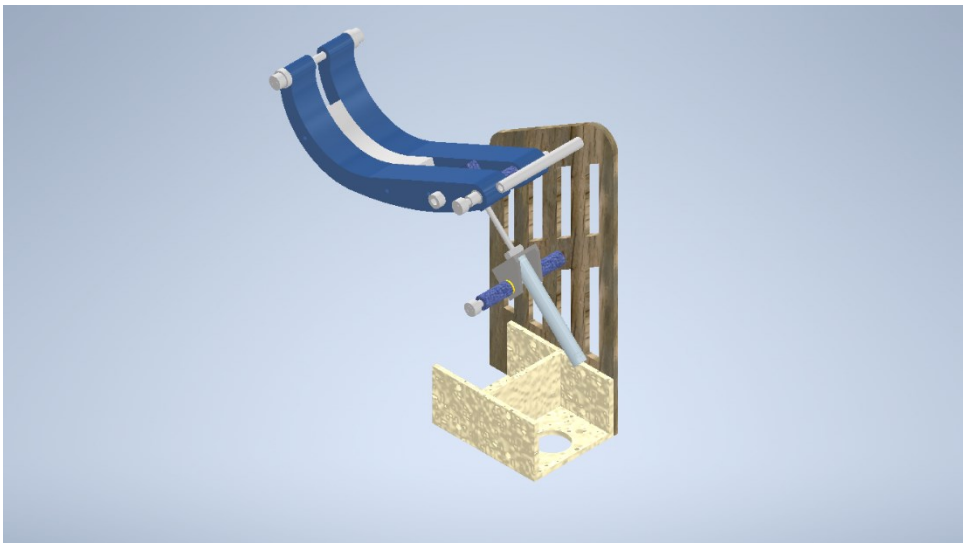

Figure 45: Pivot Holder Actuation System Isometric Rear View

The completion of the actuation system design prompted attention to be brought back to the pivot holders. Mounting of the actuation system being established called the mounting of the supporting hardware for the pivot holders into question. Support brackets for the pivot holders needed to be designed to progress the design of the rest of the subsystem. The bracket would need a through hole on its side for a shaft to pass through on which the pivot holder would pivot. From there, it would need through holes to mounting it to the rotating ring. The team also elected to integrate mechanical stop features for the pivot holder reaching its loading or unloading position. To absorb wear of the pivoting action, bronze bushings were selected, and the side through-holes were bored out to the appropriate diameter to press the bushings. These described features are shown in Figure 46.

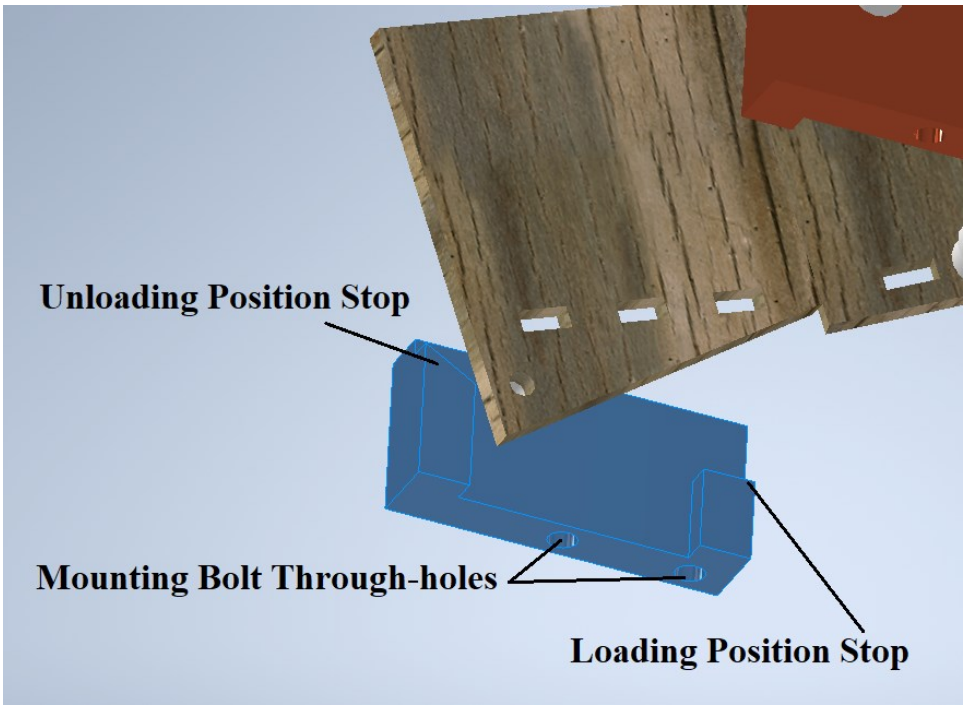

Figure 46: Annotated Pivot Holder Pivot Bracket Mechanical Stop Features

The next step in the design of the distribution carousel was the design of the rotating ring. The rotating ring had to serve as a support platform for the pivot holders and their respective pivot brackets. The rotational nature of the ring required a track and bearings to ride on as well as an actuation mechanism. The team began by creating a rotational pattern of the pivot holders and actuation systems shown in Figure 47. Here, the team adjusted the radial distance of the pattern to tighten the grouping of the pattern, attempting to minimize volume envelope.

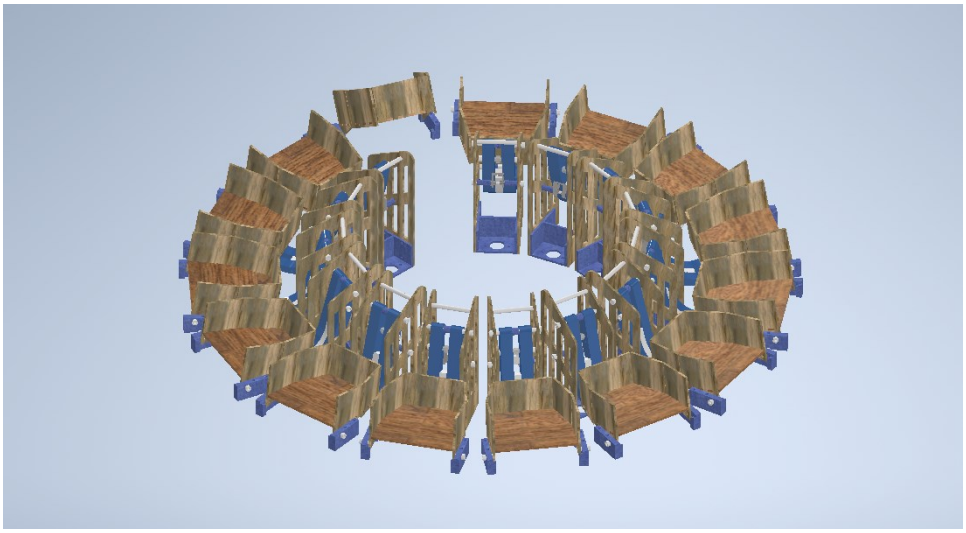

Figure 47: Rotational Pattern of Pivot Holder & Corresponding Actuation Assembly

Using the tightened rotational pattern, a ring made of two concentric circles was drawn and extruded with hole patterns corresponding to the mounting bolt holes of the pivot brackets. These holes were bored out to receive ¼ ”-20 T nuts which would be used to fasten the pivot brackets to the rotating ring. The ring and T nut insert holes are highlighted in Figure 48.

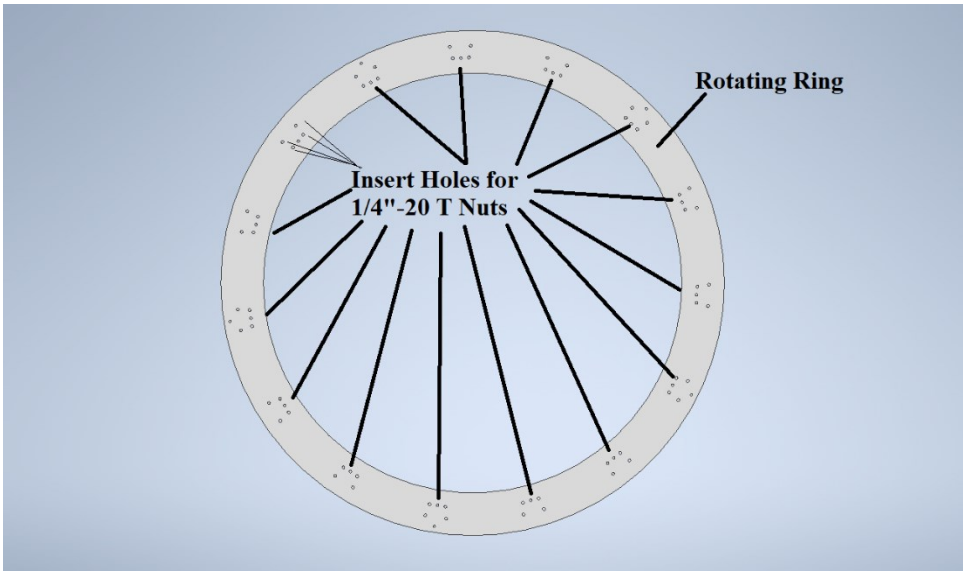

Figure 48: Annotated Rotating Ring Insert Hole Features

Earlier on in the distribution carousel design process, it was established that larger structural components, such as the rotating ring, would be produced from ½” Medium Density Fiberboard via CNC routing. MDF of this size is cheap, widely available, and easy to machine, making it ideal for prototyping, and allows for usage of T nuts which are straightforward to implement in both design and assembly.

The rotating ring then needed a track to ride along which would call for an additional circular structural component and bearings for the component to ride along. The team was faced with the option of placing the bearings and their mounting hardware on the rotating ring or the option of placing the structural component on the rotating ring and leaving the bearings and mounting hardware fixed. Engineering intuition suggested the latter as it would potentially have less mass, reducing the rotational inertia of the rotating ring and corresponding load on the motor actuating the rotating ring.

The track ring would mount to the underside of the rotating ring. Due to the high speeds the distribution carousel would operate at, the team speculated high potential of wear on the sides

of the track ring. The track ring would be produced from layers of ½" MDF which would be highly prone to wear due to the porous, soft nature of MDF. This prompted the team to design in aluminum side walls on the outside and the inside of the track ring, absorbing load and wear from the actuation of the rotating ring. These aluminum sidewalls consisted of 1" wide and 1/8" thick aluminum strips which could be cheaply sourced at a variety of lengths. These aluminum strips could be wrapped around and fastened to the track ring. The sidewalls took care of side loads but the normal force and corresponding frictional force due to the weight of the assembly would also wear the bottom side of the track ring. This resulted in the team designing in a bottom ring made of Delrin, the Delrin would absorb the loads and wear exerted by the bearings on the bottom face of the track ring. The sidewalls, bottom layer, and track ring are shown in Figure 49.

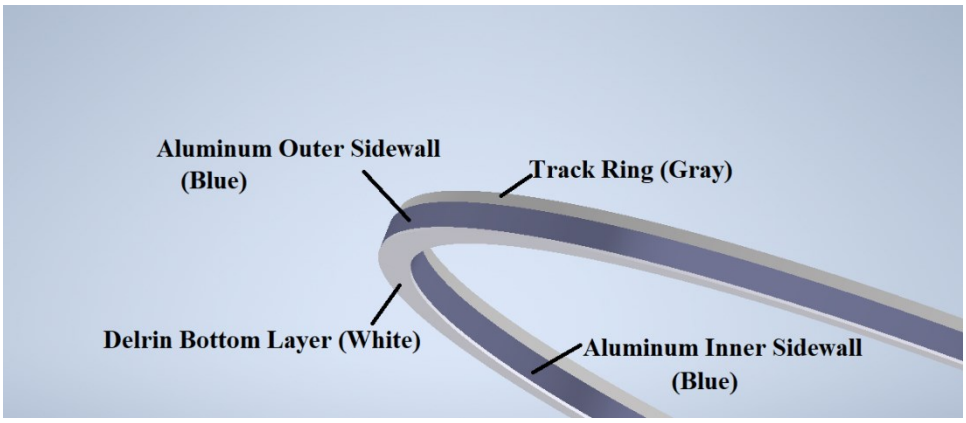

Figure 49: Annotated Track Ring Features

The track ring was then segmented across its circumference, not only did the footprint of the track ring exceed the footprint of the CNC router available to the team but segmenting the design would result in more efficient material usage. The track ring was segmented such that only one segment version would exist per layer and be repeated throughout the segmented track ring. This made the segments of each layer of the track ring reorientable, reducing assembly complexity. The track ring was designed to have 3 layers and they were joined by spring pins hammered into the layers. A hole pattern was generated for the spring pins and the design used a copious amount of spring pins to ensure rigidity and dimensional accuracy of the resulting assembly, deviation from dimensions would result in poor kinematic performance. The middle layer was rotationally offset by 2 spring pin holes to further improve rigidity of the system by providing reaction surfaces to the top and bottom edges of the middle layer segment ends. These features are shown in Figure 50.

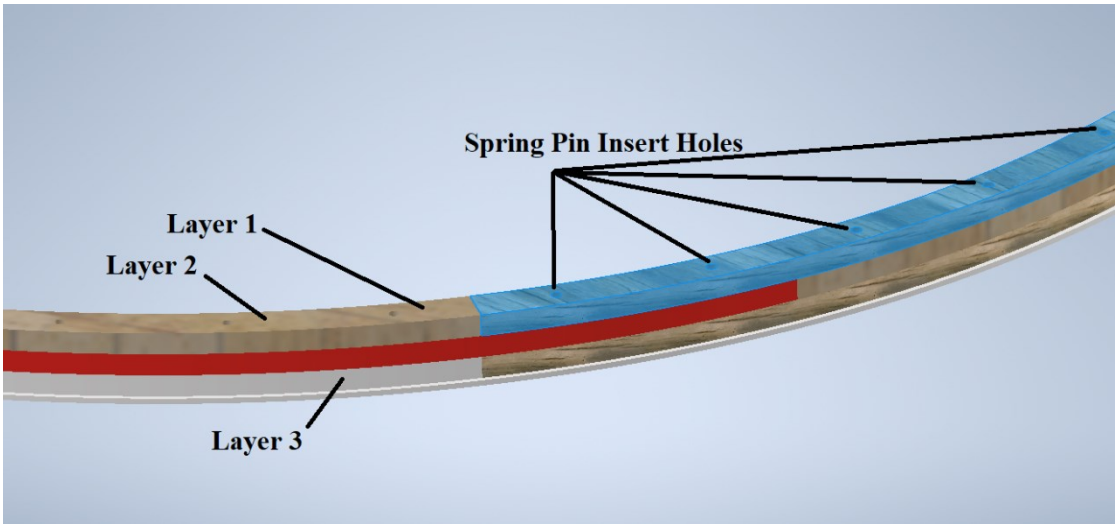

Figure 50: Annotated Track Ring Layers

The bottom layer, shown as layer 3 in Figure 50, required hardware to mount the segmented track ring to the rotating ring. The team elected to use T nuts inserted in the bottom side of layer 3 which bolts running through the rotating ring and layers 1 and 2 of the track ring could thread into. Because the Delrin bottom layer was directly below layer 3 and would ride atop bearings, a pocket feature was necessary to recess the top face of the T nut. In addition, mounting holes for the Delrin bottom layer were also designed into the segments of layer 3. These mounting holes were made tight enough such that #6 wood screws could securely thread into them. These features are annotated in Figure 51.

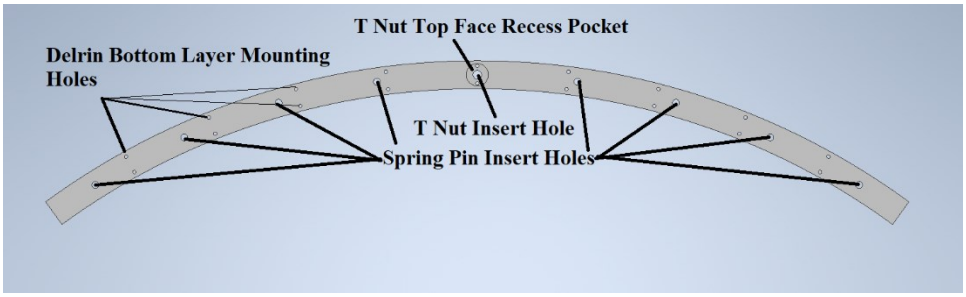

Figure 51: Annotated Track Ring Layer #3 Features

The segmentation of the track ring also resulted in the segmentation of the Delrin bottom layer. The Delrin bottom layer was intended to be produced via laser cutting which the machine did not have a large enough working platform for the full size Delrin bottom layer. Segmenting the design not only made production on the available equipment possible but also resulted in more efficient material usage. The segmented Delrin bottom layer had dovetail features designed into its segments to lock the segments together, dove tail features would later be used in other designs segmented for production. The dovetails are shown in Figure 52.

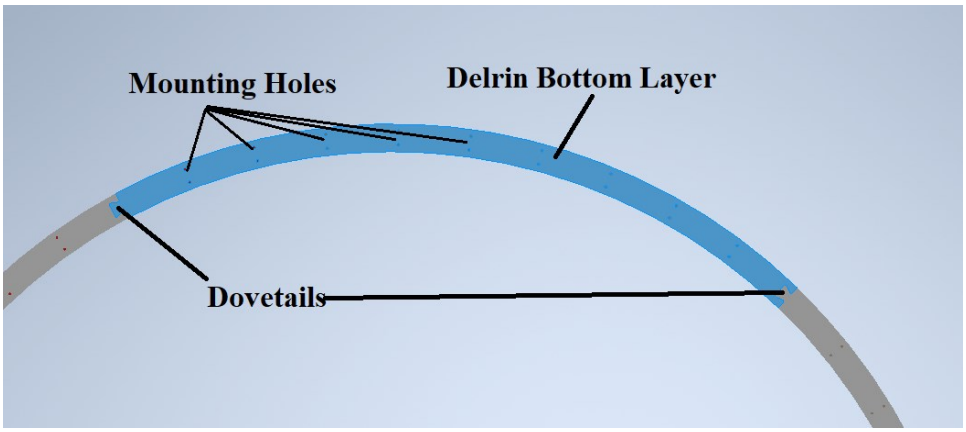

Figure 52: Annotated Track Ring Bottom Delrin Layer Features

The conclusion of the track ring design led to the beginning of the bearing solution design. The track needed bearings to ride in. The team believed it could accomplish this need for bearings through bearing blocks, an array of bearing enclosed in a single unit of hardware which could be repeated when deemed necessary. The bearing blocks were designed with the intent of utilizing 7/8" OD, 3/8" ID sealed ball bearings, the team could source these bearings at relatively low costs. The team began with projecting in a cross-sectional profile of the track ring with its aluminum sidewalls and Delrin bottom layer along with the cross section of the selected ball bearing. The bearing blocks were intended to be produced from PLA extruded via 3D printing. 3D printing introduces dimensional inaccuracies, these inaccuracies were considered in the spacing between the side bearings. Too tight of a spacing would result in binding or excessive friction against the track ring, negatively impacting dynamic performance. To address this potential binding issue, an offset equivalent to the dimensional accuracy of the intended 3D printing platform was introduced, this offset was .2mm. The projections and dimensions were used in guiding the design of the track bearing blocks and can be seen in the geometric sketch in Figure 53.

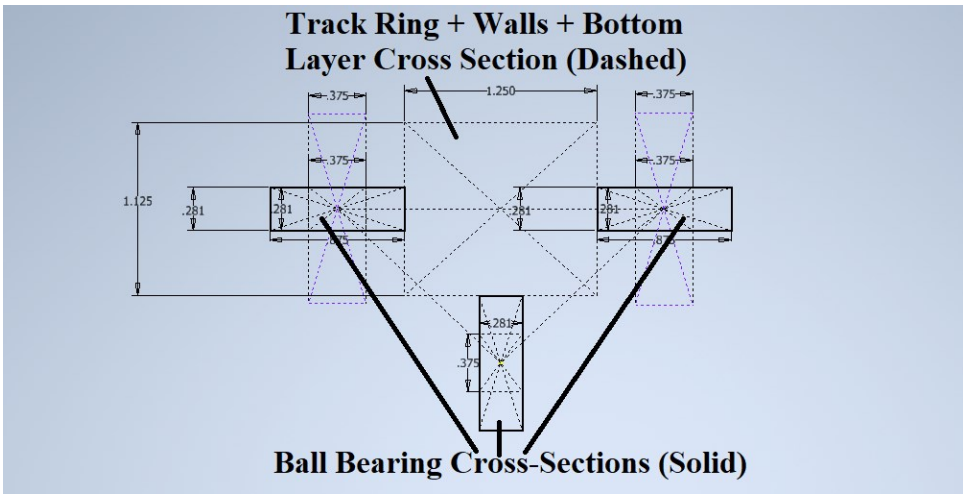

Figure 53: Annotated Track Ring Bearing Block Geometry Sketch

The track ring bearing blocks were then modeled with the intent of producing them from PLA filament via 3D printing. Mounting points were designed such that they could be physically accessed without interference from the rotating ring. The through-hole on the longer side was extended out such that it lied directly underneath the rotating ring. An access hole was designed into the rotating ring to allow a hand tool to pass through it to access the fastener fed through the through-hole on the bearing block. An excess of the access holes was created to increase system serviceability. The blocks were designed to make assembly straightforward, simply insert the bearings and their corresponding shafts, shafts are held in place via epoxy. Support fins were added to the bearing blocks to improve rigidity. The final bearing block design and its mentioned features are annotated in Figure 54.

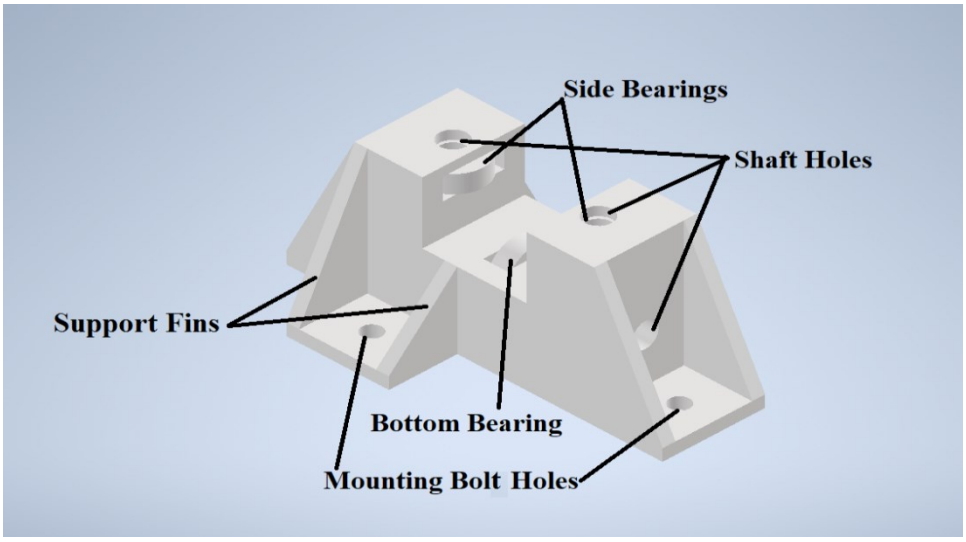

Figure 54: Annotated Track Ring Bearing Block Features

The track ring bearing blocks were then added to the assembly file and appropriately patterned, a view of the track ring sitting in its bearing blocks is shown in Figure 55.

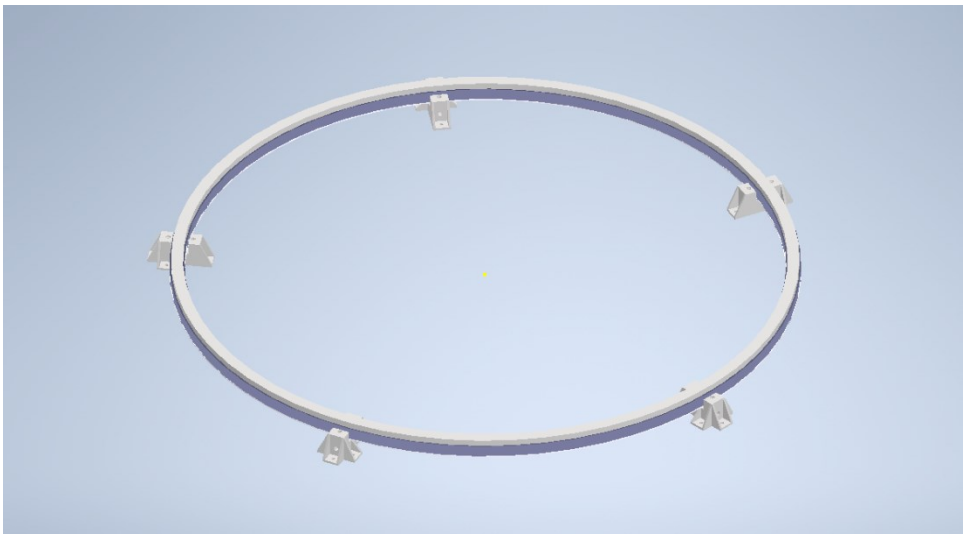

Figure 55: Track Ring & Bearing Block Arrangement

The segmentation of the track ring led to the necessity of segmenting the rotating ring. As seen in Figure 56, dovetail features were added in such that the segments could interlock with one another. The interlocked assembly could then bolt directly onto the track ring which would provide the rigidity needed to keep the assembly true to its dimensions in the CAD assembly.

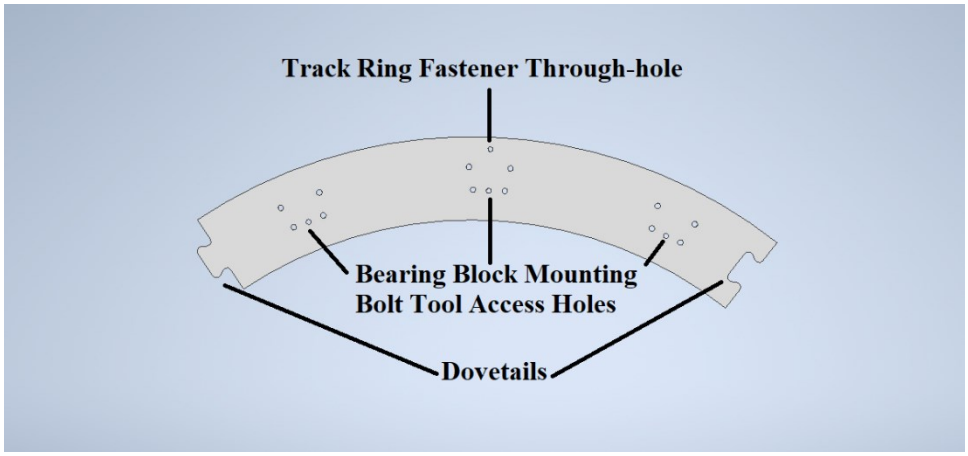

Figure 56: Annotated Rotating Ring Segment Features

The supporting structure of the carousel was next. The team initially envisioned two parallel circular baseplates with supporting fins between them, fastened to the baseplates using tab-slot-fastener features. The space between the baseplates would house pneumatic related hardware and component fed to the pivot holder actuation systems. The track ring and bearing

blocks were projected onto a circle which was then extruded with the appropriate hole patterns for the fasteners going through the bearing blocks. The team intended to produce the baseplates and supporting fins out of .5” MDF via CNC router. Like the track ring and rotating ring, the baseplates had to be segmented to fit on the CNC router bed and conserve raw material. Seen in Figure 57 is the assembled baseplate, directly below in Figure 58 is one of the baseplate segments with its annotated features.

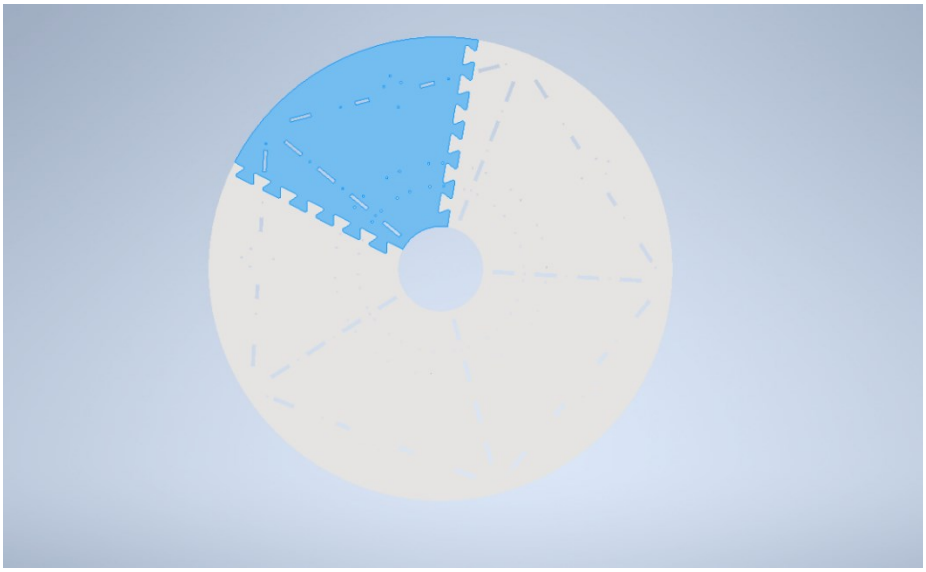

Figure 57: Assembled Distribution Carousel Baseplate

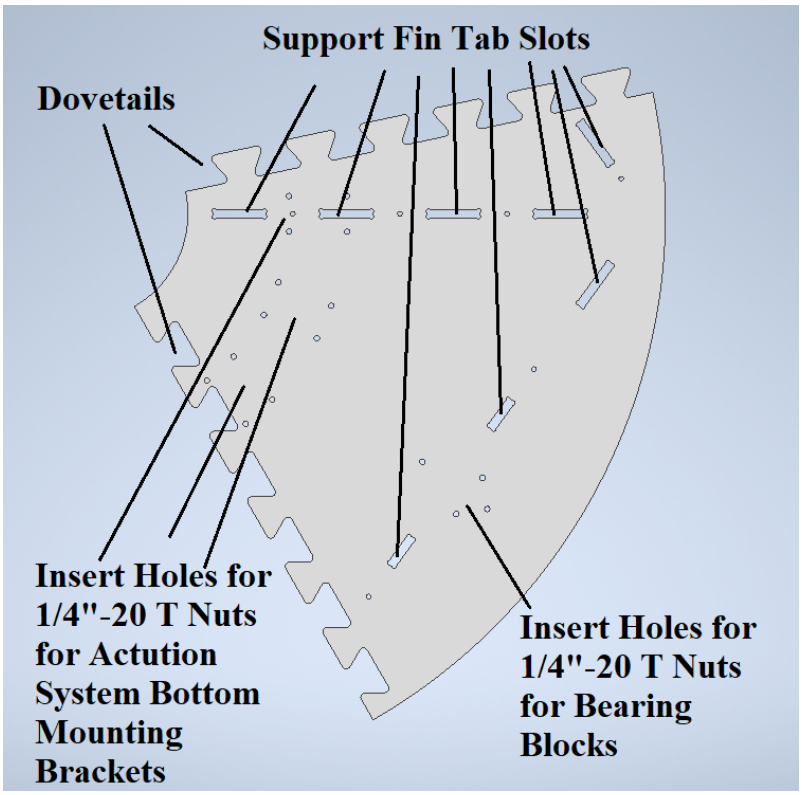

Figure 58: Annotated Distribution Carousel Baseplate Features

A design for manufacturing consideration the team implemented was the necessary dog bone slots to fit the rectangular tabs of the supporting fins. Routing a rectangular pocket will result in a profile seen in Figure 59, the geometry of the routing tool prevents perfectly square corners from being cut.

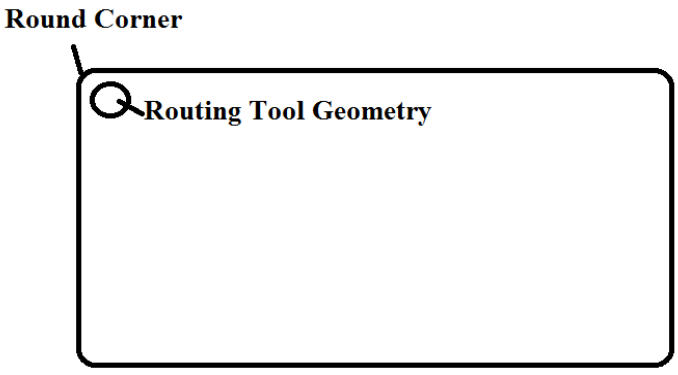

Figure 59: Annotated Routing Tool Path Geometry for Rectangular Pockets

By designing a pocket profile seen in Figure 60, the created extra space in the corners allows for the corners of the inserted tab to fit into place.

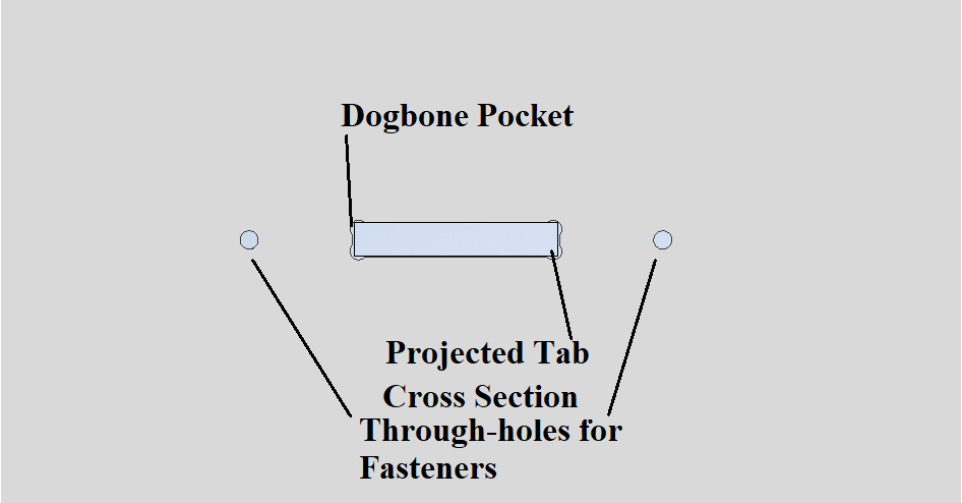

Figure 60: Annotated Distribution Carousel Baseplate Segment Dogbone Pocket and Hole Features

To constrain the top and bottom baseplates to one another, support fins were needed. The team intended to produce 2 sets of fins. One set would extend out from the center to support the weight of the top baseplate and its supported components. The other set would be rotationally patterned around the circumference of the baseplate to keep the baseplate segments parallel to one another and prevent any angular cocking between the segments. The support fins were also intended to be produced from .5" MDF. Similar to the dogbone pocket, the designed tab features on the support fins would need rounded corners to fit the rectangular cross-section of the baseplate segments. To fasten the baseplate segments to the support fins, .25"-20 T nuts and bolts were implemented. The T nuts could fit into their appropriate slots and the bolts could be fed through the through-holes in the baseplate plate and thread into the T-nuts, fastening the components together. For both the radial and tangential support fins, a basic lightening pattern was created to make component handling easier on the team as they transported the components from Technocopia back to 38 Westbrook. The tangential support fin and radial support fin can be seen in Figure 61 and Figure 62, respectively.

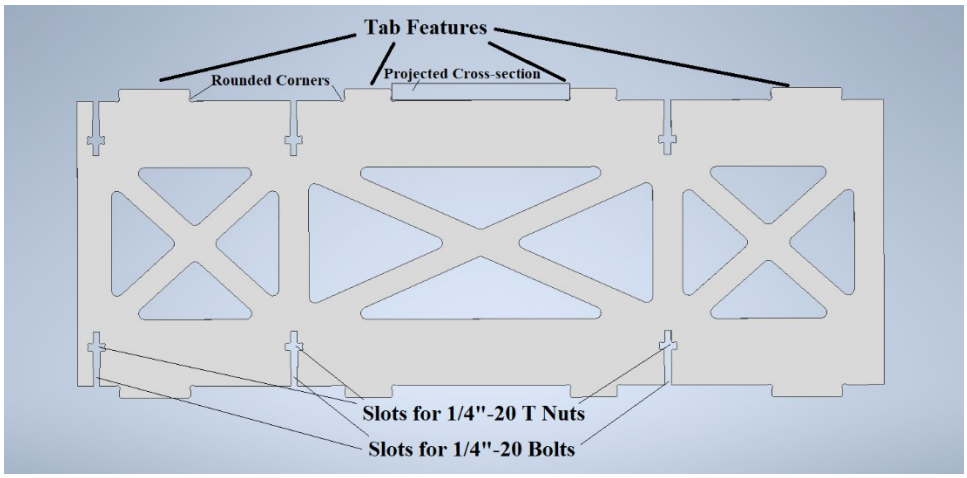

Figure 61: Annotated Distribution Carousel Tangential Support Fin

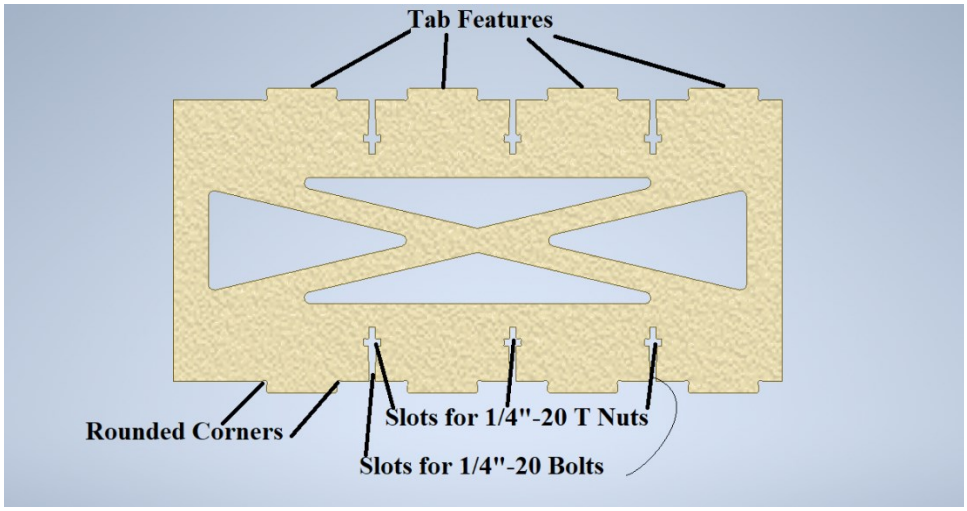

Figure 62: Annotated Distribution Carousel Radial Support Fin

Excluding hardware components and stationary bins, the assembled distribution carousel can be seen below in Figure 63. The stationary bins were intended to be sourced as a common off the shelf part in the later prototyping phase and were not modeled. Note that the pivot holder lacking a corresponding actuation system is the entry point for components entering the distribution carousel. The carousel at this point, still lacked an actuation system to rotate the rotating ring, the space not occupied by a pivot holder actuation system would be allocated towards the rotating ring actuation system.

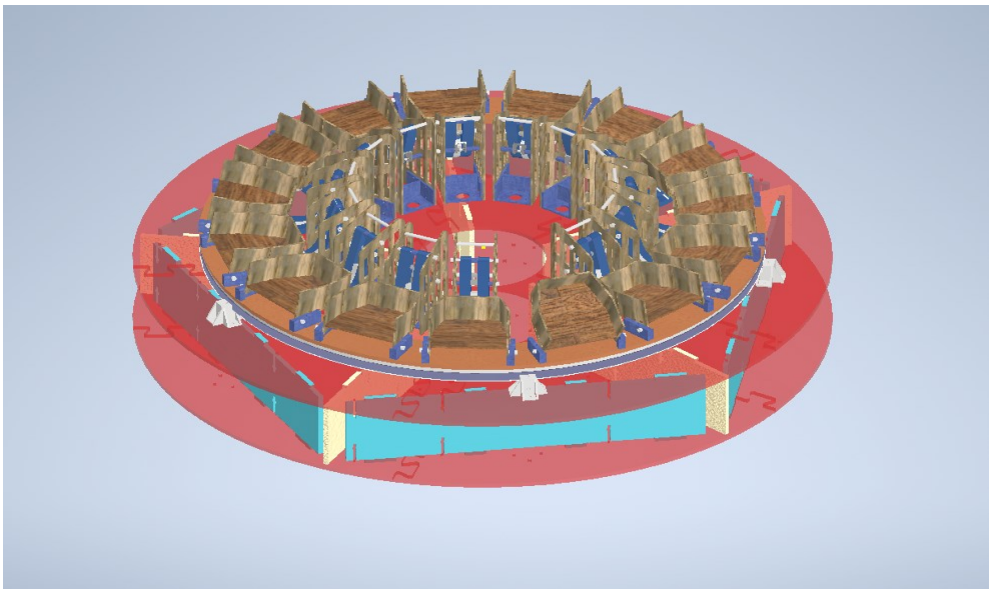

Figure 63: Distribution Carousel Assembly

At this point, lacking an actuation system to rotating the distribution carousel, the team conducted inertial, torque, and power analysis of the system to understand the system needed to actuate the carousel at the intended operational rate.

To establish the mass moment of inertia of the system, a simplified, approximative lumped point mass model is used, shown in Figure 64.

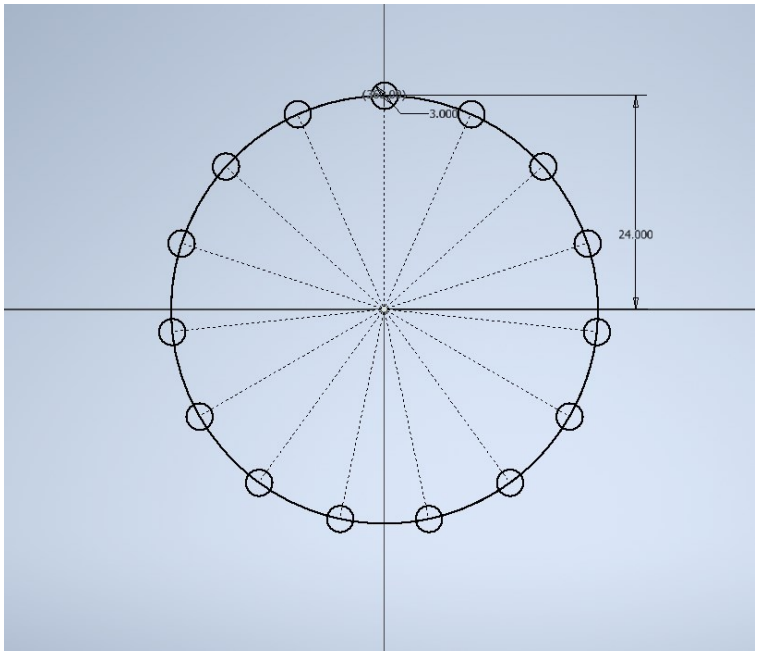

Figure 64: Rotating Ring Lumped Point Masses Model

Each of the 15 point masses represent 1/15th the mass of the rotating ring, the track ring, the mass of a holder and the mass of an extreme case component. Figure 113 shows that the average mass of a component is 1.2 grams, the team established an extreme case would be 10 times that value, 12 grams. The radius of 24" is an approximated distance located on the rotating ring. The expression of mass moment of inertia for a point mass is shown in Figure 65. Computations were performed using python and the numpy python library, the variables and mass moment of inertia calculation are shown in Figure 66.

$$Moment\ of\ Inertia_{point\ mass} = mass * radius^2$$

Figure 65: Expression for Moment of Inertia for a Point Mass

```
import numpy as np

massTrackRing = 12500 ##grams
massRotatingRing = 3000 ##grams
massHolder = 100 ##grams
massComponent = 12 ##grams
radius = .6 ##meters

massPoint = (1/15 * (massTrackRing + massRotatingRing)) + massHolder + massComponent

massMomentofInertiaPointMass = massPoint * np.power(radius,2)
massMomentofInertiaSystem = 15 * massMomentofInertiaPointMass

print("System Mass Moment of Inertia = ",massMomentofInertiaSystem/1000,"kilogram-meters")
```

```
System Mass Moment of Inertia =  6.184799999999999 kilogram-meters
```

Figure 66: Rotating Ring Lumped Point Masses Model Parameters & Mass Moment of Inertia Calculations

The mass moment of inertia is one of the two components needed to derive torque, the expression for torque is seen in Figure 67.

$$Torque = Moment\ of\ Inertia * Angular\ Acceleration$$

Figure 67: Expression for Torque

The team now had to ascertain the angular acceleration based on some angular acceleration profile. At this point, the team assumed a parabolic acceleration profile, the expression for change in angular position is shown in Figure 68.

$$\Delta\theta = \int_0^1 \int_0^1 \alpha t^2 \, dt$$

Figure 68: Expression for Change in Angular Position Given Double Integration of a Parabolic Acceleration Profile

Where Δ Θ is the change in angular position, t is time, and α is angular acceleration. The bounds for the integral are from 0 to 1 as the change must occurs within the takt time of 1 second. The results of the double integration is shown in Figure 69.

$$\Delta\theta = \lim_{t=1} \frac{\alpha t^4}{12}$$

Figure 69: Result of Double Integration of a Parabolic Acceleration Profile

After substitution of variables and simplification, the angular acceleration is calculated below in Figure 70.

$$24\,deg = \lim_{t=1} \frac{\alpha t^4}{12}$$

$$288\,deg = \lim_{t=1} \alpha t^4$$

$$288 \frac{\text{deg}}{\text{sec}^2} = \alpha$$

$$288 \frac{\text{deg}}{\text{sec}^2} * \frac{\pi\, rad}{180\, deg} = 5.027 \frac{rad}{\text{sec}^2} = \alpha$$

Figure 70: Result of Angular Acceleration Analysis for Rotating Ring

The results for angular acceleration and approximated mass moment of inertia can be substituted into the expression for torque, the results are seen in Figure 71.

$$Torque = 6.185\, kg - m * 5.027 \frac{rad}{\text{sec}^2}$$

$$Torque = 31.1 \frac{kg - m}{\text{sec}^2} = 31.1\, N - m$$

Figure 71: Result of Torque Analysis for Rotating Ring

Torque is one of the two components necessary for calculating power, the next step was finding the angular velocity of the system as prescribed in the equation for power shown below in Figure 72.

$$Power = Torque * Angular\ Velocity$$

Figure 72: Expression for Rotational Power

The team proceeded by establishing the degrees per second the carousel needed to operate at given a system takt time of 1 second per component. 15 pivot holders correspond to (360 degrees / 15 pivot holders) = 24 degrees per pivot holder, each pivot holder must actuate once every second to maintain the system takt time of 1 second. This results in a rotational velocity of 24 degrees per second. The expression for angular velocity is shown below in Figure 73, below that is Figure 74, the result of the calculation.

$$Angular\ Velocity = \frac{Change\ in\ Angle}{Time}$$

Figure 73: Expression for Angular Velocity

$$Angular\ Velocity = \frac{24\ deg}{sec} * \frac{\pi\ rad}{180} = .419\ \frac{rad}{sec}$$

Figure 74: Result of Angular Velocity Analysis for Rotating Ring

With angular velocity established, the power was calculated, seen below in Figure 75.

$$Power = 31.1\ N-m * .419\ \frac{rad}{sec} = 13.039\ W$$

Figure 75: Result of Power Analysis for Rotating Ring

The required power fell below the team's expectations. In the initial concept assembly seen in Figure 27, the intended actuation method for rotating the carousel was a ring gear fixed to the rotating ring. This ring gear would be driven by a motor, specifically a worm gear drive motor to prevent inertial over-driving or back-driving of the system. The approximated power revealed that it's possible to go with a less hardware intensive and thus cheaper approach.

A ring gear drive would have been costly to manufacture and carries mechanical risk factors such as variation in tooth dimensions leading to changing pressure and transmission angles, affecting drive performance. The approach the team then decided to take was friction drive.

2nd Stage Sort: Duplication of the 1st Stage

Repeating Hardware

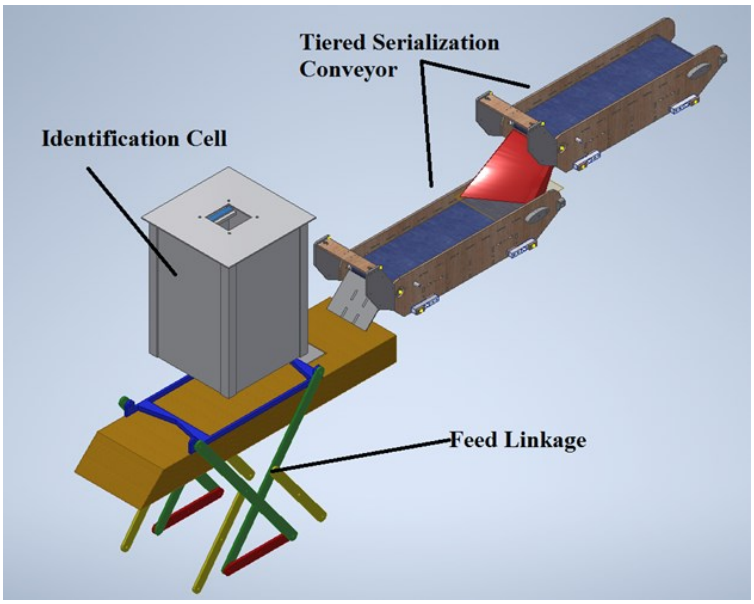

Figure 76: 2nd Stage Sort, Identical to 1st Stage Sort

One of the placing approaches the team considered was placing components in a continuous process which would be the most direct approach to placement. The challenge posed a problem where after a component is identified, it must be placed into its respective drawer, but each drawer has non-trivial volume and mass. The rate at which components are identified far exceeds the rate at which components can be placed into drawers presented to the placement system. While temporary storage locations for individual components are possible, they would take up a considerable amount of space given the volume of the system throughput. Temporary individual storage locations would also add additional manipulation steps and increase cycle time as a function of number of individual storage locations. Temporary storage, however, is unavoidable given the physical constraints in component placement and drawer presentation. The solution was to restrict the number of temporary storage units to the number of drawers in the final storage tower. This was the function of the distribution carousel, to distribute components into temporary storage locations corresponding to final storage tower drawers. The cost of the solution is having to reidentify the components by drawer group, however, the subsystems required to identify the components can be reimplemented to reidentify the components.

In the 2nd stage sort, the same identification hardware is reimplemented to identify components being sorted into their respective XY locations after being sorted into their drawer groups. While the mechanism for manipulating components from their stationary drawer groups to the 2nd stage sort subsystem was viewed out of scope for the purposes of the MQP, the team is certain it can be accomplished by an elementary robotic manipulation system.

Seen in Figure 76 is the duplicated tiered serialization conveyor and identification cell. Although it may be volume prohibitive, the team speculates that it will be possible to sort multiple drawer groups in parallel. Like the end of the 1st stage sort, classified components are pushed out of the identification cell by the feeding linkage. Components then land in the loading area of the manipulation gantry where they await placement into their appropriate drawer compartments.

Granular Jamming Manipulator and Gantry

Once components reach the loading area of the manipulation gantry, they are ready for the final step in the sorting process, storage. The manipulation gantry places components taken from the loading area into their respective compartments in their respective drawer. The drawer itself is manually retrieved from the storage tower. For the scope of the MQP, the mechanism for retrieving drawers from the storage tower was not designed or ideated, however, the team is confident this can be done using an elementary robotic manipulation system.

Precisely manipulating the components into their compartments proved to be a challenge. The variability in component size and geometry is vast across the 70,000 variants. A single rigid manipulator would be insufficient and so the team considered using a series of manipulators as opposed to one. But this approach does not scale well, each additional manipulator has spatial and physical implications, additional actuators, and cost implications. This approach can be seen in Figure 94.

The team elected to not detail the design of this concept, instead, different manipulation methods were considered. The team determined that the method with the highest potential for success would be granular jamming manipulation. This form of manipulation was unfamiliar to the team and its concept had to be proven and understood through prototyping and testing which was done extensively in the later prototyping phase.

The prototyping led to the design shown in Figure 77.

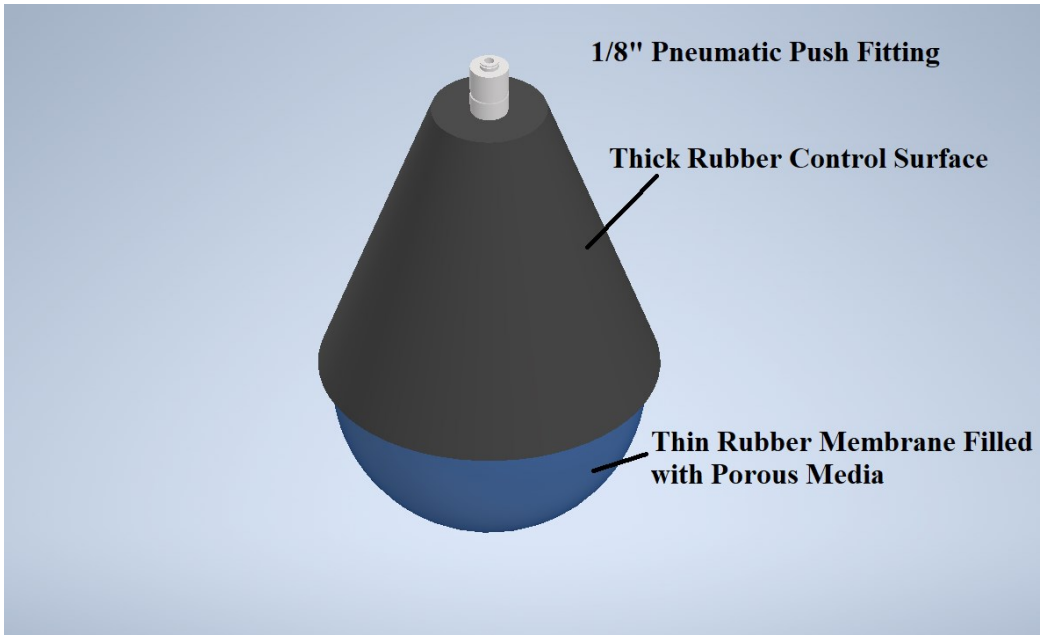

Figure 77: Annotated Granular Jamming Manipulator

The design implements a push fitting for easy splicing into the pneumatic system. The thick rubber control surface helps evenly distribute load across the rubber membrane as it conforms to geometries with tall extremities. The control surface is made of rubber to add lateral compliance as the thin rubber membrane expands outwards.

Prototyping & Testing

Fabrication Capacity

The team was faced with the challenge of realizing their designs and transferring ideas from CAD to real life. This involved understanding the resources the team had available to them and the capacity of these resources. Regarding manufacturing equipment, the team had the following available to its disposal after seeking external equipment support from Technocopia.

-Multiple 100W laser cutters

-Multiple 3D printers outfitted with .2 mm and .4mm diameter extrusion nozzles

-4’x8’ CNC Router

-Power tools and hand tools

Drum Sorter

Prototyping the drum sorter began with laser cutting the fiberboard sheets with the designed hole pattern. From there, the .5” plywood forming rings were also laser cut. The angle aluminum lengths were cut to appropriate length. The sheets were inserted into the rings and manually deformed. Following this was the insertion of the angle aluminum sections to orient each ring. Once the rings were oriented, the sheets were fastened to the inner ring surfaces using wood screws. Once the sheets were fastened, the assembly of the drum was complete.

The first step in producing the drive system was laser cutting its support panels and cross braces. The wheels were then slotted via bandsaw and the hubs and sprockets were fastened to the wheels bolt circle. With all the custom components produced, the drive system was assembled. Running the chain across the sprockets and linking the chain ends with a master link was the final step. The same process was followed for the non-driven support assembly with the exception of all driven elements.

Finally, the drum was placed onto the drive system and the supporting assembly. Tests were conducted using test loads involving all edge-cases, smallest and largest test components. In all, the tests were a success and evidence of this is shown in Appendix 2.

Tiered Serialization Conveyor

The conveyor prototype was left unfinished at a static state due to external constraints. Components were produced such as the supporting walls and the separation wedge, however, with the system left unpowered, almost no testing could be done on the prototype. Separation tests were conducted on the separation wedge where two components residing at the same height were dropped synchronously which was a success. One can see the progress made on the prototype in Figure 78.

Figure 78: Tiered Serialization Prototype

Identification Cell

Similar to the tiered serialization conveyor, the progress on the identification cell was halted by external constraints. The digital scale was not implemented, however, the vision system was successful as seen in the testing conducted in Appendix 8. The constructed identification cell after modification and adjustment can be seen in Figure 79.

Figure 79: Identification Cell Prototype

Carousel

Prototyping the distribution carousel began with producing the components for the pivot holders. To verify the design, only one was initially produced. As mentioned in the design section, the pivot holders were going to be produced from laser cut plywood. After sourcing the plywood, minor dimensional adjustments were made to account for the true thickness of the plywood, measured by calipers, as well as the kerf of the laser beam. The laser cut side panels of the assembly can be seen in Figure 80.

Figure 80: Pivot Holder Actuation System Support Panels

The pivot brackets were 3D printed on the Monoprice Maker Plus. The dimensions of the pivot brackets were also adjusted to account for the nozzle diameter of the 3D printer. The hardware for the pivot holders, as well as the corresponding actuation system, was sourced from Jerry's Hardware. The laser cut panels were assembled, utilizing the tab and slot features, and hot glued together. The pivot holder, brackets, and hardware were assembled to produce the first assembly of the distribution carousel subassembly, shown in Figure 81.

Figure 81: Pivot Holder Assembly Prototype

The actuation assembly then had its components laser cut; dimensions appropriately adjusted. For the purposes of proving the design, only one actuation assembly would be produced. Once the components were 3D printed, hardware such as the nylon bushings were press fit, threaded, and placed into their appropriate locations and the assembly received its first powered test, seen in Appendix 3.

The carousel structure was produced via CNC routing MDF, this process can be seen in Appendix 4. GCode, generated from DXF projections of part geometry, was creating for contouring and pocketing tool paths necessary for producing parts and their geometries. The CNC router, part production, and produced workpieces can be seen, respectively, in Figure 82, Figure 83, and Figure 84.

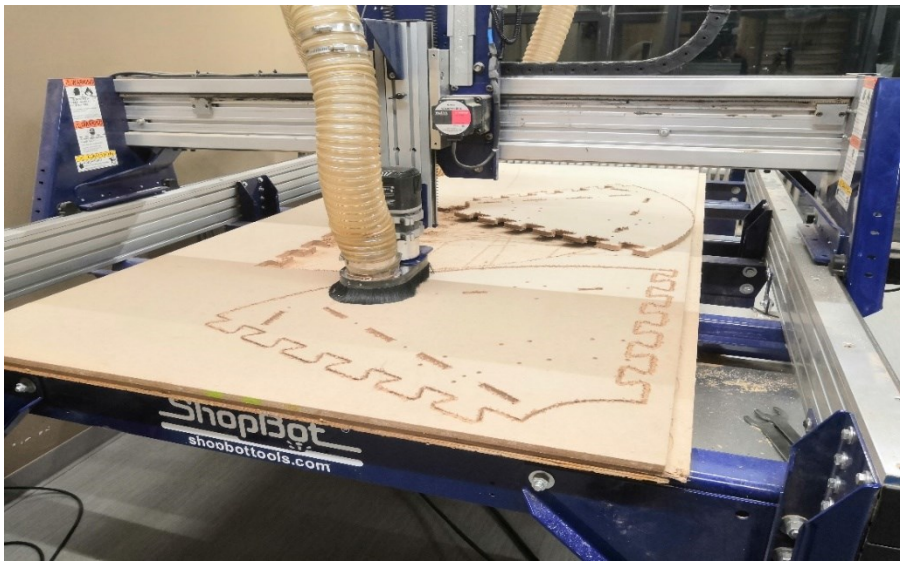

Figure 82: CNC Router

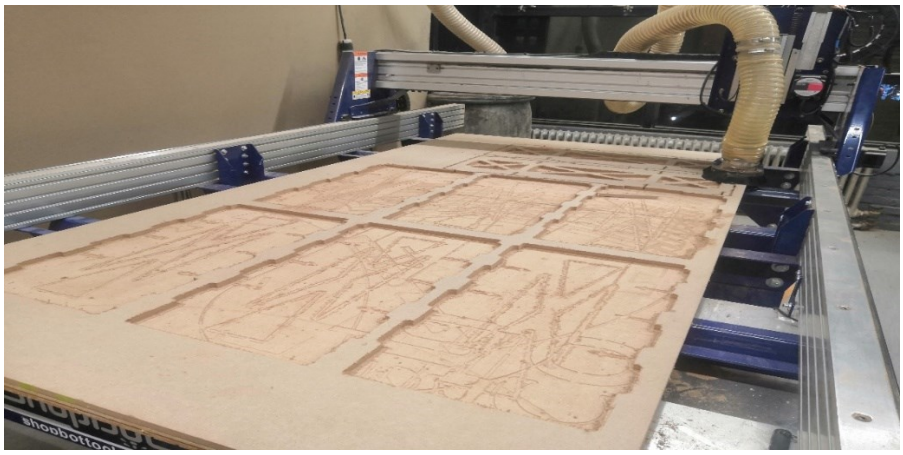

Figure 83: CNC Router Part Production

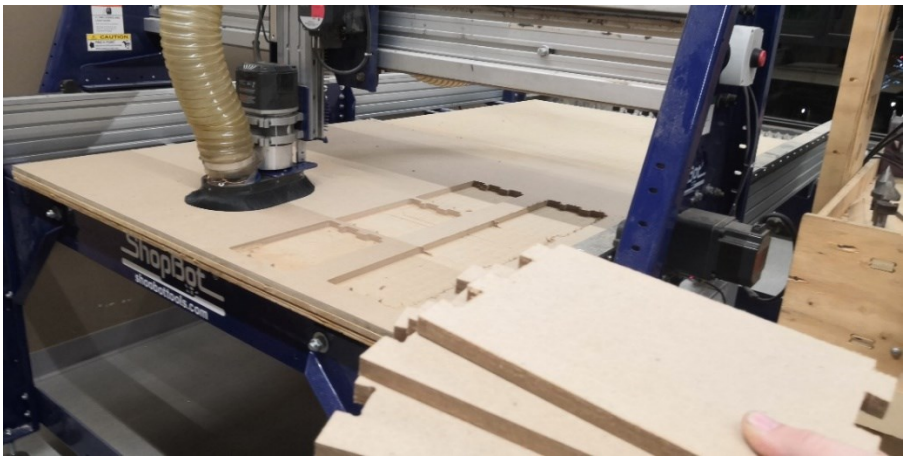

Figure 84: Finished CNC Router Workpieces

Assembly of the carousel structure began with an initial test of the dovetail interlocking feature. Despite the CNC router producing at high precision, the compound dimensional inaccuracies were enough to prevent successful interlocking. The team solved this by using a rotary grinder to machine chamfers across all of the dovetail features, leading to successful interlocking as seen in Figure 85. Mating of all components was done using care and a rubber mallet to prevent deformation of the soft MDF.

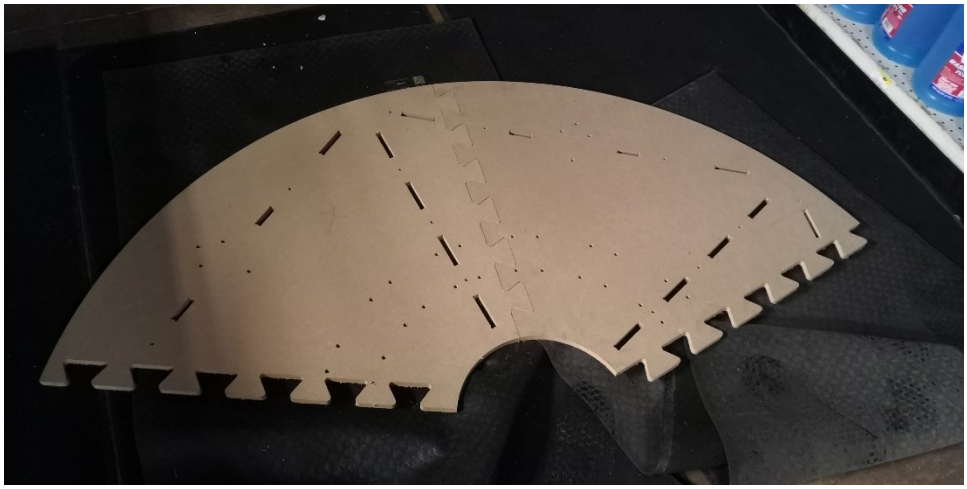

Figure 85: Mating of Carousel Baseplate Segments

Mild post-machining swelling in the machined pocket features in the baseplate prevented tab insertion during mating of the baseplate and support fins. The same approach for dovetail interference was used on the tab interference and was successful as can be seen in Figure 86 and Figure 87.

Figure 86: Mating of Radial Support Fin and Baseplate Assembly

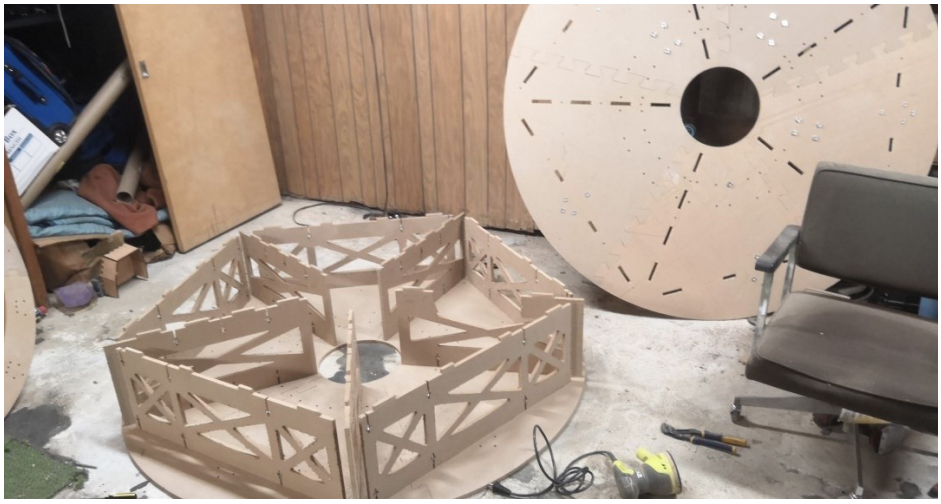

Figure 87: Mated Baseplate and Support Fins

At this point, the structure was assembled, as well as the rotating ring. The track ring and bearing blocks had yet to be produced. While the bearing blocks were still on the 3D printer beds, the track ring was assembled. The greatest challenge in assembling the track ring was fastening the aluminum sidewalls to the assembled MDF ring segments. The aluminum strips had to be plastically deformed into circular segments, this was done using a roll bender as seen in Appendix 5 and Figure 88.

Figure 88: Roll Bending of Track Ring Aluminum Sidewall

The now deformed sidewalls had to be fastened to the MDF ring. The next challenge was in securing the sidewalls to the ring with as close of a tolerance as possible. If there was any gap

between the MDF and aluminum, this would cause binding and excessive friction during rotation. This was accomplished by installing fasteners in pairs, one at the top and one at the bottom, in sections around the circumference of the ring. When a section would be fastened, it would be held in place by clamps as seen in Figure 89. Multiple clamps were used to ensure the tightest possible fit between the two materials. Once one section was fastened, the clamps were strategically repositioned. One set of clamps would maintain tightness as the other set was used to apply pressure in the next section. For each fastener, the aluminum was center-punched, drilled for a pilot hole, and then counter sunk. Wood screws were delicately threaded in to prevent material tear out from excessive torque. Over 200 fasteners were installed in a 6-hour period.

Figure 89: Aluminum Sidewall to Track Ring MDF Fitting Operation

The track ring and rotating ring were mated, the bearing blocks were assembled, and the assembly of the carousel reached the point seen in Figure 90.

Figure 90: Distribution Carousel Assembly

In an initial friction drive test, seen in Appendix 6, the track ring experienced some friction high points, but was a kinematic success. In this friction drive test, the aluminum sidewalls were driven by the rubber wheel fixed to the cordless drill. While initially successful, the team realized that it would be detrimental long term to drive on the aluminum surface as wear and gumming from the driving wheel would affect bearing performance.

This then pushed the team towards driving from rotating ring itself from its inner surface. Two friction drive iterations were attempted but were not successful in driving the rotating ring. Prior to each iteration, the inner surface of the rotating ring was lined with duct tape to improve engagement.

Drive System Iteration 1

The first drive system iteration was produced via laser cut plywood and assembled from COTS parts with the only other custom component being a steel shaft wrapped in a polyurethane rubber as a friction material. The system was retrofitted to the baseplate of the distribution carousel as precisely as possible, the installation can be seen in Figure 91. During testing, the pivoting action caused the driving capstan to deform under its own driving force. The capston would then apply excessive normal force to the point where load on the bearing blocks was high enough to cause complete binding of the rotating ring. Adjustments were attempted but either

excessive normal force was applied or not enough friction would be generated to drive the rotating ring. This led the team to attempting a second drive system iteration.

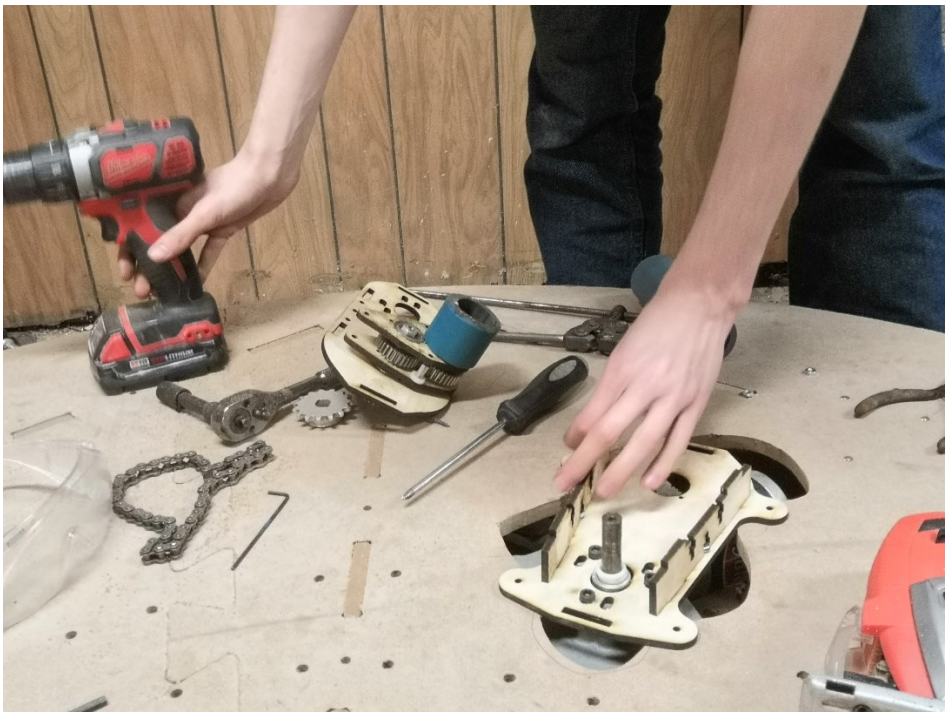

Figure 91: Installation of First Drive System Iteration

Drive System Iteration 2

The second iteration removed the pivoting action and instead used direct normal force to drive the ring. The first drive system iteration was modified to move the driving wheel linearly towards the inner surface of the rotating ring along the ring's radius. This attempt was also unsuccessful, rather than driving the rotating ring, the capstan removed the friction material on the ring's inner surface, seen in Figure 92.

Figure 92: Rotating Ring Friction Material Wearing

At this point, the team believed it was due to high pressures on the driving surface. The rotating ring was constructed from .5” MDF, evidently the ring’s thickness did not provide adequate contact area for the friction needed to drive the ring. The team believed the issue could be addressed by increasing the ring thickness, which poses other implications. Additional weight would lead to more resistance, increasing the driving force needed. Multiple approaches were considered but it was at this point that production and prototyping ceased.

Granular Jamming Manipulator

The Granular Jamming Manipulator began as a potential solution to the end manipulation problem. The variability in sizes and geometries of target components was vast, having a single, rigid manipulator that could handle tiny, cylindrical components and larger, flat components seemed virtually impossible. The initial approach to the variability problem was using multiple manipulators as opposed to one, as seen in Figure 93 and Figure 94.

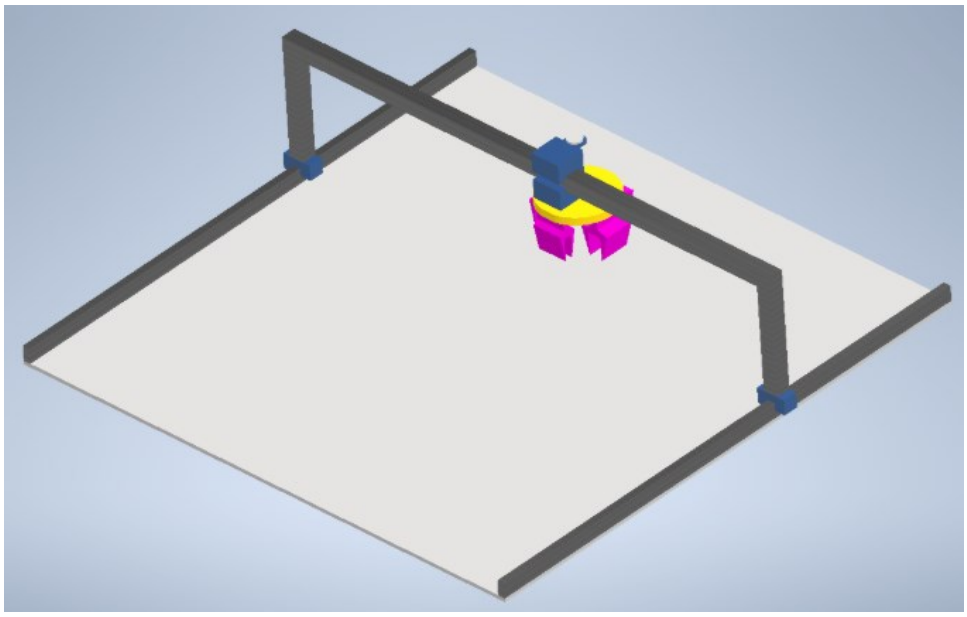

Figure 93: Manipulation Gantry

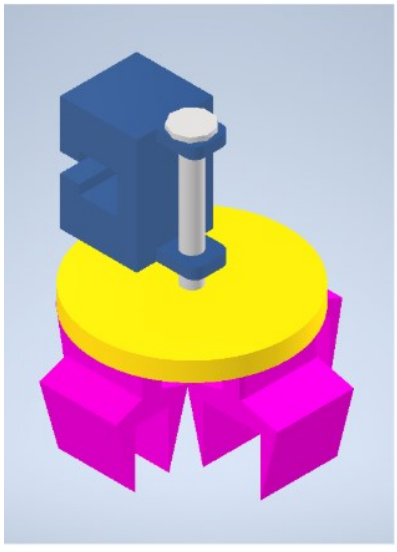

Figure 94: Initial Turret Manipulator Array Concept

Here, the gantry used to pick and place components has an end effector with multiple manipulators on it, capable of handling different size and geometries. Although it's a direct approach to the problem at hand, the scalability and effectiveness was in serious question, as well as other physical considerations such as increasing assembly load on gantry rails as number of manipulators increases. Each manipulator would need its own actuator which conflicts with the minimal actuator count axiom of the system level architecture.

The team at this point had entertained the notion of applying granular jamming manipulation. This notion was reinforced and promoted by the team's advisors and so, prototyping began. The team had no experience with this technology, the prototype itself was a proof of concept to the individual team members.

Granular jamming manipulators utilize three key components, a flexible membrane filled with a porous media, one popular media is coffee grounds, and vented air pressure, vented air pressure refers to air pressure exiting the balloon. The flexible membrane allows the manipulator and its media to conform to a target object. Once the membrane has conformed to the object and the media has settled, vented air pressure is introduced. The vented air pressure causes the membrane to contract and the porous nature of the media allows the particles to tightly pack, making the manipulator rigid. This applies frictional and normal forces against the target object, physically engaging the target object to the manipulator.

With this knowledge, the team constructed the initial prototype, seen in Figure 95. The prototype consisted of a hand powered balloon pump with a plastic funnel acting as a reducing coupling. The plastic funnel is adhered and sealed to the air inlet of the balloon pump via hot glue. A balloon filled with coffee grounds is attached to the spout of the funnel and sealed to the funnel via tie wrap. The prototype operates by placing the balloon on top of the target object, applying slight hand pressure to balloon, and the retracting the pump handle to introduce vented air pressure into the balloon.

Figure 95: Initial Granular Jamming Manipulator Prototype

The first test of the prototype was a success in engaging and manipulating a target component and proved the concept to the team. Further tests were conducted to optimize for the design. Variables such as balloon material, balloon size, inert air-coffee ground ratio, air pressure source, and inlet location relative to media mass were adjusted to observe system performance. Inert air-coffee ground ratio refers to the volumetric ratio of air to coffee grounds with no pressure applied to the balloon. The experiments carried out were primarily based on qualitative observations, little to no quantitative data was collected.

The initial prototype was tested using pearlized and non-pearlized balloons. Pearlized balloons were found to have higher friction against target components. Higher friction results in better engagement. Further prototype iterations then used pearlized balloons.

Balloon size was adjusted from the initial prototype and on, larger balloons are not only capable of engaging larger parts but allowing for more media and thus more innate pressure on target components. Stretching the balloon was also experimented with, an optimally stretched balloon was found to not only engage larger targets, provide space for more media, but also required less applied force in conforming to target geometry extremities.

Inert air-coffee ground ratio was also adjusted in the experiments. If the volume of coffee grounds vastly exceeded the volume of air, the balloon would over-stretch and conforming to target geometry extremities was unsuccessful in testing. Conversely, excessive high air to coffee ground ratios showed that the lack of media resulted in little to no target engagement. The team found a balance of roughly 10% air filling the topside of the balloon and 90% coffee grounds filling the bottom side. This ratio showed success for many edge-case tests, seen in the video in Appendix 7.

The initial prototype showed that the vented air pressure source affected engagement and pressurized manipulator rigidity. The initial prototype used a hand balloon pump whereas the second iteration used a double action manual pump designed for larger inflatables, shown in Figure 96. The larger displacement provided more vented air pressure which further improved target engagement and pressurized manipulator rigidity. These improvements then motivated the team to apply even high pressures via an electric air compressor shown in Figure 97.

Figure 96: Second Air Pressure Source

Figure 97: Final Air Pressure Source

Inlet location also plays a vital role in system performance. If the inlet was too close to the neck of the balloon, then clogging would occur as the suction force would draw the balloon membrane into the inlet opening. If the inlet was too deep into the media, then it would react against the target's geometry and extremities as the manipulator conformed to the target. Minimal submerging of the inlet proved to be effective in edge-case testing, enough media prevented the balloon membrane from clogging the inlet while not interfering with target acquisition. For future iterations, the team established that a flexible inlet with multiple inlet openings would be optimal in that the inlet's compliance wouldn't interfere with target acquisition. Multiple inlet openings provide the advantage of membrane clogs being unlikely as there are multiple points from which air in the balloon is drawn.

The final prototype iteration is shown in Figure 98. The grey 14" pearlized balloon was pre-stretched and filled with the appropriate ratio of coffee grounds relative to volume. The inlet consisted of a $^{1}/_{2}$" diameter aluminum rod, bored out and tapped to accept an **1/8"** pneumatic push fitting. The inlet was submerged into the media, deep enough such that no clogging from the balloon membrane would occur. The vented air pressure source was an electric air compressor with a Venturi device spliced into the pneumatic circuit. As air passed through the venturi device, vented air pressure was generated. The inlet fitting was connected to the rest of the pneumatic circuit with a knife valve used to trigger the vented air pressure. To uniformly distribute applied pressure across manipulator, a control surface was constructed out of two funnels, cut and appended to create a single, larger cone.

Figure 98: Final Prototype Iteration

Further testing was conducted using the final prototype iteration. From this testing, the team gained more knowledge on the application of the manipulator. The higher pressures did in fact vastly improve the manipulator's pressurized rigidity and its target engagement. However, a new phenomenon was observed, shown in Figure 99.

Figure 99: Component Impression on Manipulator Post-Manipulation

After depressurization, an impression of the target component remained on the surface of the manipulator. This impression would then prevent engagements with smaller components. This led to the team realizing the necessity of positive air pressure in the manipulator, to reform the balloon membrane to its initial state. Further testing by the team showed that applying positive air pressure during the conformation stage of manipulator operation helped with stretching the manipulator across the target components, improving engagement. Testing also showed the significance of balloon orientation, a stretched balloon is prone to forming a nipple at the bottom, partially filled with air and media. This nipple affects target engagement, trapped air at the nipple prevents the media from stiffening around targets small enough to submerge into the nipple. Turning the manipulator on its side, however, eliminated that issue.

The final iteration of the prototype, implemented with the optimal conditions discovered in testing, was successful in every test case the team derived for the scope of its application.

Economic Model and Analysis

Motivation

One of the interests in developing the scalable sortation automation framework is its commercial applications. Utilizing the initial application of LEGO, an economic analysis was conducted to evaluate economic performance of a company employing the technology to conduct aftermarket sales. This company, "The Legosortus Company" is the subject for this case. The aforementioned economic analysis includes a model built on demand, cost, and price for LEGO components along with the system's capacity. In industrial engineering, models are constructed to predict the performance of an operation based on assumptions and sampled data, an approximation of how the system will behave in real-world applications (Salvendy, 2007). Analysis can be conducted at many levels at different resolutions, for this application, analysis is conducted on a simplified model to establish whether or not further analysis on a more developed model is worth conducting.

Data for demand and price was derived from samples taken from bricklink.com, the premier aftermarket sales website for LEGO components. Mixed LEGO bulk costs were derived from samples taken from ebay.com, a popular choice for procuring mixed LEGO bulk although many other avenues are available such as direct secondhand sales. Finally, system capacity was established through time trials at the system's perceived bottleneck. Capacity has many metrics associated with it, the observed capacity metric here is throughput, the volume of components the system can handle per unit time (Salvendy, 2007). Capacity is limited by bottlenecks, points in the flow(s) of the system where flow is most restricted relative to the rest of the system (Salvendy, 2007).

A spreadsheet based statistical model, created in Microsoft Excel, can be seen in Appendix 1. In this section, the spreadsheet and model are elaborated on segment by segment.

Assumptions

Assumptions are made to simplify the development of models to prevent calculations from becoming overwhelming (Salvendy, 2007). To conduct this evaluation, the following operating assumptions are made.

1. Strictly conduct sales in the Americas

2. Become one of the top 10 sellers by monthly component volume within 3 years

3. Start with 10% of volume of average top seller sales as a best case scenario and adjust to derive multiple cases

4. Normal distribution assumed when applicable

5. Capacity limited by manipulation system

6. 24/7 Lights out operation

7. Capacity remains fixed across 3 years

8. Cost and price remain fixed, Market is stagnant

9. No human intervention

10. Capital equipment operated at a no-cost lease, fixed operating costs lumped into a single overhead cost.

11. The system never depletes its capacity

12. Largest operating costs are salaries for two employees receiving an annual salary of $85,000 with no benefits.

13. Shipping and handling costs are completely offloaded to the customer and to the bulk suppliers.

14. 2-3 Percent transaction fee.

15. 5% Annual loss from lost, broken, or unsatisfactory components.

Each assumption will now be elaborated on.

1. Strictly conduct sales in the Americas

Many businesses regionally restrict their operations, including sales, to make conducting business more straightforward, having only to consider the political, societal, legal, and economic aspects of one region as opposed to many. To only conduct sales in the Americas is a realistic assumption.

2. Become one of the top 10 sellers by monthly component volume within 3 years

As seen in the technical portion of this paper, this technology is novel and it is unlikely that even the top bricklink.com vendors have been exposed to it. Taking advantage of a cutting edge technology is how many companies outclass the status quo. In addition, while advertising and product promotion are not services offered by bricklink.com, popularity can be established by having lower prices than the rest of the competition as products can be sorted in ascending prices. While this is a bold assumption, it's not unrealistic.

3. Start with 10% of demand volume of average top seller sales as a best case scenario and adjust to derive multiple cases

Despite the technology being potentially revolutionary, the top vendors have already built an extensive customer base. The company can only initially expect a fraction of the demand the top vendors have. To establish a range, this percentage is halved to create a likely case scenario, the percentage of the likely case is then halved to create a worst case scenario. Creating multiples cases adds to validity of the assumption, making it moderately realistic.

4. Normal distribution assumed when applicable

Many systems, be it social, economic, or natural follow a normal distribution and it is one of the most common distributions used in building probabilistic economic models such as this model. Assuming a normal distribution allows for a standardized measurement for variation in a dataset (Salvendy, 2007). Datasets in the analysis, such as the manipulator time trial, may fall under this distribution this is a realistic assumption.

5. Capacity limited by manipulation system

Systems have bottlenecks, in the case of the automated sortation system, it was ascertained that the system bottleneck is at the final stage of the system. The granular jamming manipulator, which places components into their compartments once they've been classified, has

the takes the longest time to complete its task relative to the other subsystems of the overall system and therefore is the system's bottleneck. This is real assumption based on the reality of the system.

6. 24/7 Lights out operation

Automated systems have the advantage of not having to take breaks, go home, or go to lunch and don't require lights to function. Companies are already taking advantage of automation in this manner (Essentracomponents). Downtime and maintenance are unavoidable in any automated process, but to reduce the model's complexity they will be neglected. This is a moderately realistic assumption to make for such an automated process.

7. Capacity remains fixed across 3 years

No changes, upgrades, or improvements will be made to the system once it's implemented. While it would be operationally disadvantageous to The Legosortus Company to not improve, this is a realistic assumption.

8. Cost and price remain fixed, Market is stagnant

Markets are dynamic on even a second by second basis and so to assume the market remains stagnant over the course of 3 years is highly unrealistic. As previously mentioned, however, assumptions are made to simplify the development of the model. Constructing a model that would reflect bricklink.com's market dynamics would be difficult, has its own problems with being reflective of the reality of the situation, and is not necessary at this level of analysis. This is a highly idealized assumption.

9. No human intervention

For a system to be truly automated, humans need not apply. However, there is yet to be an automated system that experiences no human interaction. This is an ideal assumption to reduce model complexity instead of considering factors such as machine downtime.

10. Capital equipment acquired at a 3 year, no-cost lease, fixed operating costs lumped into a single overhead cost.

While many technology companies offer trials of new products at reduced prices to clients. The Legosortus Company receiving the automated sortation system at a no-cost lease for 3 years is ideal and unrealistic. To add validity to the assumption, a single lumped overhead cost is derived considering employee salaries, facility, etc.

11. The system never depletes its capacity

The system operating at full capacity is bound to deplete its components, this would result in machine downtime. This ideal assumption is made to reduce model complexity.

12. Largest operating costs are salaries for two employees receiving an annual salary of $85,000 with no benefits.

Typically, the only operational costs associated with an automated system are electricity, maintenance, downtime, insurance, and leasing fees. All of these are neglected either to reduce model complexity or because they are intrinsically negligible. The Legosortus Company, however, does have owners that would like to make a livelihood in working for the company and will receive salaries as such. The engineers owning The Legosortus Company will collect a salary at the median level of $85,000. This is a partially realistic assumption.

13. Shipping and handling costs are completely offloaded to the customer and to the bulk suppliers.

Customers on bricklink.com pay for shipping in every transaction, this is uniform across all transactions carried out through bricklink.com. The majority of the bulk suppliers on ebay.com offer free shipping. As a result, the Legosortus company ends up paying nothing in shipping and handling, only paying for shipping material which will encompass a percentage of the individual sale cost. This is a realistic assumption based on the reality of the sales and supplier channels.

14. 2-3 Percent transaction fee.

Every transaction carried out through bricklink.com imposes a 2-3% transaction fee on the vendor. This is a realistic assumption based on the reality of the sales channel.

15. 5% Annual loss from lost, broken, or unsatisfactory components.

Defects arise in all systems as no system is ideal. Defects in this application consist of broken, tarnished, or unsatisfactory components or components lost in shipping. Factoring an annual loss percentage does not significantly increase model complexity and therefore it can and should be considered. The percentage value itself may or may not be realistic, however, it is realistic to lose some annual revenue due to defects (Salvendy, 2007).

To summarize, some of these assumptions make the operation highly ideal, in that the operations is solely conducted using no cost equipment that does not require human intervention, a 24/7 "turn-key" operation where the only cost involved is the cost of the product and only the product. In addition, the market which the company serves remains stagnant, no changes to costs, demands, or prices. The only limiting parameter in operational capacity is in the final stage manipulation of components which was estimated through timed trials of a prototype. Furthermore, additional costs only consist of transaction fees, an annual loss percentage, and owner salary.

Parameter Definition and Analysis

In conducting an operation, many parameters can be considered. For this model, price, cost, and demand for LEGO components, as well as system capacity. These parameters or variables are significant in understanding the company's potential economic performance.

Deriving values for demand.

In the stated assumptions, the company will begin with 10% of volume of the average top sellers as published by bricklink.com. The current top 10 sellers in the last 3 months are taken from bricklink.com as seen in Figure 100. Leading to an average monthly component demand volume of 2.3 million across a 3 month cycle, shown in Figure 100 is the equation for average. This volume is multiplied by 10% and propagated out from a monthly demand to an annual demand for the initial year, the expression for which is in Figure 103. A probability distribution for best, likely, and worst case demand scenarios was then established for the first, second, and third year. The best case assumes 10% of top demand in the first year, 50% in the second, and 100% in the third. For each year, the likely case assumes 50% of the best case demand and the worst case assumes 50% of the likely case demand. Probability distributions can be thought of the set of likelihoods for a set of outcomes (Salvendy, 2007). These probability distributions and

demand quantities are respectively multiplied and then added to produce an expected value for each year. Expected value is the sum of the product of outcomes and their probabilities and is used as an approximation for an outcome (Salvendy, 2007). This is seen in Figure 102.

DEMAND (Monthly)	
Most recent component volumes.	
Brickfans.com	4,710,222
Heart Bricker	4,687,853
ToyBurg	4,134,221
Brock's Bricks	2,653,133
Big As Bricks	1,202,820
Little Phoenix	1,048,107
Pinball Surplus	877,601
Everything StarWars & More	862,714
TheBrickDude	807,000
ACE of BRICKS	732,835
Average	2,331,519

Figure 100: Sample for Demand

$$\bar{x} = \frac{\sum_{i=0}^{n} x_i}{n}$$

$$Where\ \bar{x}\ is\ the\ average\ of\ a\ dataset, x_i\ is\ a\ dataset\ entry\ value,$$

$$and\ n\ is\ the\ number\ of\ entries\ in\ a\ dataset.$$

Figure 101: Expression for Average

DEMAND (Annual)				
Year 1 (10% of average annual volume)				
Case	P(x)	Demand		Expected Value
Best	0.25	2797823		1573775
Likely	0.5	1398911		
Worst	0.25	699456		
Year 2 (50% of average annual volume)				
Case	P(x)	Demand		Expected Value
Best	0.25	1.4E+07		7868877
Likely	0.5	6994557		
Worst	0.25	3497279		
Year 3 (100% of average annual volume)				
Case	P(x)	Demand		Expected Value
Best	0.25	2.8E+07		1.6E+07
Likely	0.5	1.4E+07		
Worst	0.25	6994557		

Figure 102: Annual Demand Scenarios, Probability Distributions, & Expected Value

$$Annual\ Demand = Monthly\ Demand * 12 * p,$$

$$Where\ p\ is\ the\ percentage\ of\ sales\ conducted\ by\ the\ Legosortus\ Company.$$

Figure 103: Expression for Annual Demand

$$E(x) = \sum_{i=0}^{n} x_i * P(x_i)$$

$$Where\ E(x) is\ the\ expected\ value\ of\ the\ outcome, x_i\ is\ a\ potential\ value\ of\ an\ outcome,$$

$$and\ P(x_i) is\ the\ probability\ of\ x\ as\ an\ outcome.$$

Figure 104: Expression for Expected Value

Deriving values for capacity.

As stated in the assumptions, the limiting operational parameter is in component manipulation at the end sorting stage via the granular jamming manipulator. 20 time trials were conducted where the time it takes for the manipulator to fully engage the component, raise it, and move it by some distance (2ft) was observed. The time trials provides the system cycle time, the time in between each component exiting the system (Salvendy, 2007). The timed trials are shown

in Figure 105, the average of which was roughly 4.5 seconds. From there, expected values of annual capacity are calculated based on established probability distributions for best, likely, and worst case scenarios where each scenario is a different manipulation time which is seen in Figure 106. The calculation for annual component capacity based on time trial average is seen in Figure 107. One can observe that the expected capacity exceeds the expected demands for the 1st and 2nd year, indicating that the system operates at overcapacity, demand will be met with capacity to spare.

Manipulation trials				
3.7				
4.2				
3.2				
5.8				
5.2				
8.3				
7.6		Average seconds per part		
5.4		4.515		
2.5				
3.5				
3.6				
5.3				
6.5				
7.6				
2.8				
3.2				
4				
3.1				
3.3				
1.5				

Figure 105: Manipulator Time Trials

CAPACITY (Annual)		
Potentially limited by robotic manipulation system venturi pneumatic		
	SECONDS PER PART	
Best case (P(x)=.2)	Likely case (P(x)=.6)	Worst case (P(x)=.2)
1	4.5	8
	PARTS PER YEAR	
31536000	7008000	3942000
	Expected value for Capacity Given the Case Likelihoods	
	11300400	

Figure 106: Manipulator Cycle Times, Probability Distribution, & Expected Value

$$Annual\ Throughput = \frac{365\ Days * 24\frac{Hours}{Day} * 60\frac{Minutes}{Hour} * 60\frac{Seconds}{Minute}}{t\frac{Seconds}{Component}}$$

Figure 107: Expression for Annual Throughput

Deriving values for price.

The sheer varieties in component class and quantities by vendor are vast. Average prices for individual components in the LEGO catalog can be found on bricklink.com. The provided average prices of a sample of 30 components, randomly selected by category, color, and part number was taken to calculate an average price. The sample is shown in Figure 108. The random selection was done using the rand() function in Microsoft Excel, which will generate random numbers in a specified range. The randomly generated numbers established which components were selected by category, variant, and color. These figures are based on the last 6 months.

Note while many other sampling approaches can be taken based on class variables, this approach was chosen for simplicity. In addition, rarer components are considered as statistical outliers, that is, data points that vary from the trend of the dataset (Watkins, 2016). In other words, for rarer components, their average price provided by bricklink.com is vastly different than the average price for most of the components on bricklink.com. These outliers were not considered. A histogram of the sample, shown in Figure 109, was constructed. A histogram is a visual representation of the frequencies of values in a dataset (Watkins, 2016). Stochastic, meaning random, distribution parameters, such as mean and standard deviation, expressions for which are respectively seen in Figure 101 and Figure 110, were then generated based on the sample dataset and are also shown in Figure 109. Standard deviation is a measure of variance, how much the data varies (Watkins, 2016) and its expression can be found in Figure 110. Here the mean price was found to be $0.49.

PRICE		Average
https://www.bricklink.com/catalogPG.asp?P=35646&colorID=115		0.28
https://www.bricklink.com/catalogPG.asp?P=822b&colorID=5		1.29
https://www.bricklink.com/catalogPG.asp?P=71184&colorID=22		1.93
https://www.bricklink.com/catalogPG.asp?P=3010&colorID=34		0.04
https://www.bricklink.com/catalogPG.asp?P=85975&colorID=7		0.38
https://www.bricklink.com/catalogPG.asp?P=60614&colorID=85		0.06
https://www.bricklink.com/catalogPG.asp?P=4495a&colorID=11		0.3
https://www.bricklink.com/catalogPG.asp?P=30134&colorID=11		0.56
https://www.bricklink.com/catalogPG.asp?P=2489&colorID=8		0.12
https://www.bricklink.com/catalogPG.asp?P=37775&colorID=98		0.13
https://www.bricklink.com/catalogPG.asp?P=60477&colorID=11		0.06
https://www.bricklink.com/catalogPG.asp?P=89079&colorID=105		0.56
https://www.bricklink.com/catalogPG.asp?P=30103&colorID=11		0.14
https://www.bricklink.com/catalogPG.asp?P=87796&colorID=110		0.09
https://www.bricklink.com/catalogPG.asp?P=93082i&colorID=5		0.07
https://www.bricklink.com/catalogPG.asp?P=3137c02&colorID=11		0.05
https://www.bricklink.com/catalogPG.asp?P=3070px8&colorID=1		0.08
https://www.bricklink.com/catalogPG.asp?P=3070bpb078&colorID=104		0.38
https://www.bricklink.com/catalogPG.asp?P=30395&colorID=85		0.04
https://www.bricklink.com/catalogPG.asp?P=4865&colorID=85		0.17
https://www.bricklink.com/catalogPG.asp?P=archmiA&colorID=5		1.66
https://www.bricklink.com/catalogPG.asp?P=bslot01a&colorID=5		0.74
https://www.bricklink.com/catalogPG.asp?P=29120&colorID=7		0.19
https://www.bricklink.com/catalogPG.asp?P=4073&colorID=94		0.17
https://www.bricklink.com/catalogPG.asp?P=93168&colorID=85		0.43
https://www.bricklink.com/catalogPG.asp?P=4613&colorID=7		0.88
https://www.bricklink.com/catalogPG.asp?P=23325&colorID=11		0.39
https://www.bricklink.com/catalogPG.asp?P=53588pb01&colorID=85		1.77
https://www.bricklink.com/catalogPG.asp?P=65217c01&colorID=86		1.92
https://www.bricklink.com/catalogPG.asp?P=2958&colorID=11		0.05

Figure 108: Price Sample

Frequency Table	
Class	*Count*
0-0.39	20
0.4-0.79	4
0.8-1.19	1
1.2-1.59	1
1.6-1.99	4

Your Histogram	
Mean	0.49767
Standard Deviation (s)	0.60048
Skewness	1.53311
Kurtosis	1.09684
Lowest Score	0.04
Highest Score	1.93
Distribution Range	1.89
Total Number of Scores	30
Number of Distinct Scores	24
Lowest Class Value	0
Highest Class Value	1.99
Number of Classes	5
Class Range	0.4

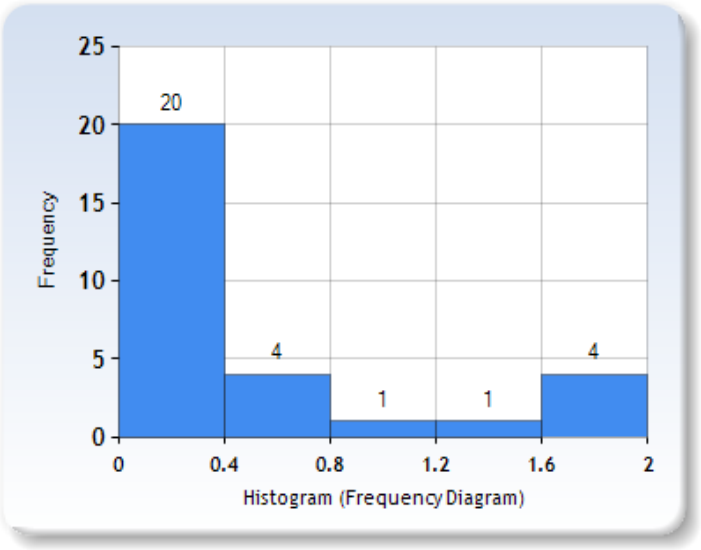

Figure 109: Price Histogram & Stochastic Parameters

$$\sigma = \sqrt{\frac{\sum_{i=0}^{n}(x_i - \overline{x})^2}{n-1}}$$

$$Where\ \sigma\ is\ the\ standard\ deviation\ of\ the\ dataset, x_i\ is\ a\ data\ set\ entry\ value,$$

$$and\ P(x) is\ the\ probability\ of\ x\ as\ an\ outcome.$$

Figure 110: Expression for Standard Deviation

Deriving values for cost.

The figures for cost were estimated based on average individual component costs from LEGO bulk suppliers. A random sample of 30 bulk offerings from eBay.com was taken where cost per pound was calculated for each entry in the sample by taking the cost of the bulk deal and dividing it by the pounds in the deal, the sample and costs per pound are seen in Figure 111. A histogram was constructed from cost data, stochastic parameters was calculated as well, this is seen in Figure 112. From there, using the mass distribution of LEGO components provided by bricklink.com seen in Figure 113, the average mass per component, excluding outliers for model simplicity, was found. Using that value, average number of components per pound was calculated. Using the average number of components per pound, average cost per component was then calculated from average cost per pound. The tabulated values for average component mass, average number of components per pound, and average cost per component is seen in Figure 114. The expression for calculating number of components per pound is seen in Figure 115 and the expression for calculating average cost per component is seen in Figure 116. Here, the average cost per component was found to be $0.037.

COST	
Cost per pound (eBay listings)	
https://www.ebay.com/itm/Bulk-Lego-Lot-1-Pound-Bricks-Tiles-Blocks-BUY-3-get-1-FREE-Star-Wars-city-etc/273888559483	$13.98
https://www.ebay.com/itm/Bulk-LEGO-LOT-5-pound-box-of-Bricks-parts-Pieces-Tires-accessories-5-pounds/274039699789	$9.60
https://www.ebay.com/itm/Lego-Lot-of-100-Pieces-Parts-Bricks-Random-From-Huge-Bulk-Assorted-Clean/183129340934?	$7.99
https://www.ebay.com/itm/LEGO-2-5-Lb-Bulk-lot-Random-Pull-2-Minifigures-Authentic-Educational-Parts-Mix/233375010	$11.98
https://www.ebay.com/itm/U-1-to-1000-POUNDS-LB-of-LEGO-LEGOS-PIECES-FROM-HUGE-BULK-LOT-PARTS-RANDOM/3625	$19.99
https://www.ebay.com/itm/LEGO-100-PIECES-FROM-BULK-SORTED-LOT-RANDOM-SELECTION-CHOICE-OF-COLOR-QTY/2332	$9.50
https://www.ebay.com/itm/Clean-100-Genuine-LEGO-5-LB-Lots-pounds-Bulk-Lot-Cleaned-Sanitized/182096835254?epid=1	$9.35
https://www.ebay.com/itm/LEGO-Bulk-lot-WHEELS-1-2-lb-pound-Tires-Axles-Car-Vehicle-Lots-of-Parts/191754848717?has	$25.68
https://www.ebay.com/itm/Lego-Lot-of-3-lbs-Pieces-Parts-Bricks-Random-From-Huge-Bulk-Assorted-Free-Ship/18387096	$9.99
https://www.ebay.com/itm/BULK-LEGO-LOTS-100-200-500-YOU-CHOOSE-COLOR-RANDOM-PIECE-SELECTION/333393697365	$9.49
https://www.ebay.com/itm/2-POUND-Of-LEGOS-Bricks-part-pieces-Lot-Star-Wars-City-Etc-Bulk-100/272399360766?hash=it	$10.20
https://www.ebay.com/itm/NEW-Lego-100-Bulk-ALL-BRICKS-BLOCKS-LOT-Mixed-Sizes-Basic-Building-Pieces-Mix/3623266	$12.99
https://www.ebay.com/itm/LEGO-BIONICLE-Hero-Factory-Bulk-Lot-1-lb-Pound-of-RANDOM-parts-Pieces-for-MOCs/20251	$24.55
https://www.ebay.com/itm/Lego-dark-grey-bulk-lot-5lbs/264649499431?hash=item3d9e56e327:g:rhcAAOSwjFpeWBmv	$26.53
https://www.ebay.com/itm/LEGO-Bulk-Lot-of-2-Pounds-Bricks-Parts-and-Pieces-Clean-Genuine-2-Lbs-Grab-Bag/27290327	$10.00
https://www.ebay.com/itm/Lego-100-Bulk-ALL-BRICKS-BLOCKS-LOT-Mixed-Sizes-Basic-Building-Pieces-Mix-1/18314248353	$11.99
https://www.ebay.com/itm/Lego-lot-Bulk-Minifigures-parts-pieces-100-Lego-Star-Wars-City-Etc/322425716846?_trkparms=	$27.95
https://www.ebay.com/itm/BULK-LEGO-LOT-2-POUNDS-2-MINIFIGURES-Bricks-Building-Toy-Lbs-Star-Wars-City/223588754	$12.50
https://www.ebay.com/itm/Lego-friends-bulk-lot-5lbs/264649525819?hash=item3d9e574a3b:g:hQ4AAOSwOQNeWCCW	$6.20
https://www.ebay.com/itm/1-to-1000-POUNDS-LB-of-LEGO-LEGOS-PIECES-FROM-HUGE-BULK-LOT-PARTS-RANDOM/351920	$24.99
https://www.ebay.com/itm/LEGO-Bulk-Lot-1-lb-Pound/153854540304?hash=item23d271fa10:g:s5EAAOSwRWdeMMwT	$10.00
https://www.ebay.com/itm/Clean-100-Genuine-LEGO-by-the-Pound-1-100-pounds-Bulk-LOT-Large-Order-Bonus/18140377	$15.75
https://www.ebay.com/itm/LEGO-BIONICLE-Hero-Factory-Bulk-Lot-1-lb-Pound-of-RANDOM-Parts-Pieces-MOCs/233457978	$27.95
https://www.ebay.com/itm/LEGO-BULK-LOT-OF-100-NEW-MINIFIGURE-ACCESSORIES-TOOLS-UTENSILS-FIGURE-PIECES/3235	$17.95
https://www.ebay.com/itm/Lego-Bulk-lot-7-Lbs/324082375209?hash=item4b74d09a29:g:oRsAAOSw4PBeDRtm	$8.00
https://www.ebay.com/itm/8-Lbs-Bulk-Lot-of-LEGO-and-Compatible-Bricks-and-Pieces-LOT/372975359115?hash=item56d7	$6.00
https://www.ebay.com/itm/1-Pound-of-real-lego-Parts-Pieces-HUGE-BULK-LOT-bricks-blocks-etc/333246478884?hash=iter	$9.98
https://www.ebay.com/itm/LEGO-Bulk-Lot-1-lb-of-RANDOM-Parts-Pieces-Free-Shipping/153854539405?hash=item23d271	$10.00
https://www.ebay.com/itm/NEW-100-LIGHT-GREY-GRAY-LEGO-PIECES-FROM-HUGE-BULK-LOT-BRICKS-PARTS-RANDOM/351	$14.99
https://www.ebay.com/itm/8-Lbs-Bulk-Lot-Of-LEGO-and-Compatible-Bricks-and-Pieces-LOT/372975324425?hash=item56d	$5.00

Figure 111: Cost Sample

Frequency Table	
Class	*Count*
5-9.99	11
10-14.99	10
15-19.99	3
20-24.99	2
25-29.99	4

Your Histogram	
Mean	14.03567
Standard Deviation (s)	7.03636
Skewness	0.92336
Kurtosis	-0.45732
Lowest Score	5
Highest Score	27.95
Distribution Range	22.95
Total Number of Scores	30
Number of Distinct Scores	27
Lowest Class Value	5
Highest Class Value	29.99
Number of Classes	5
Class Range	5

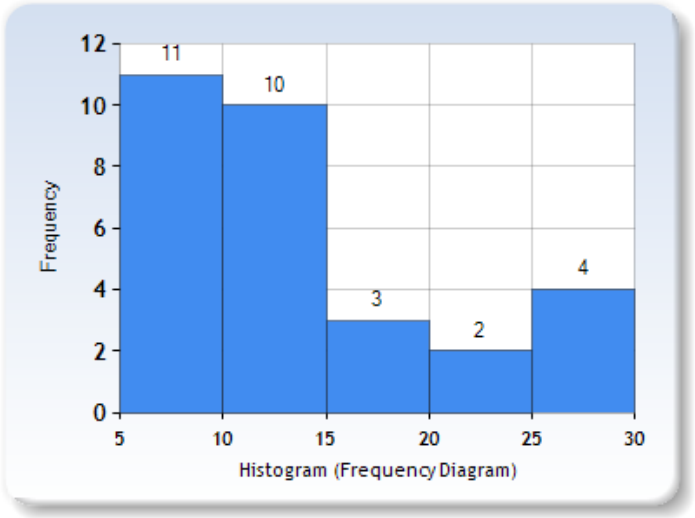

Figure 112: Cost Histogram & Stochastic Parameters

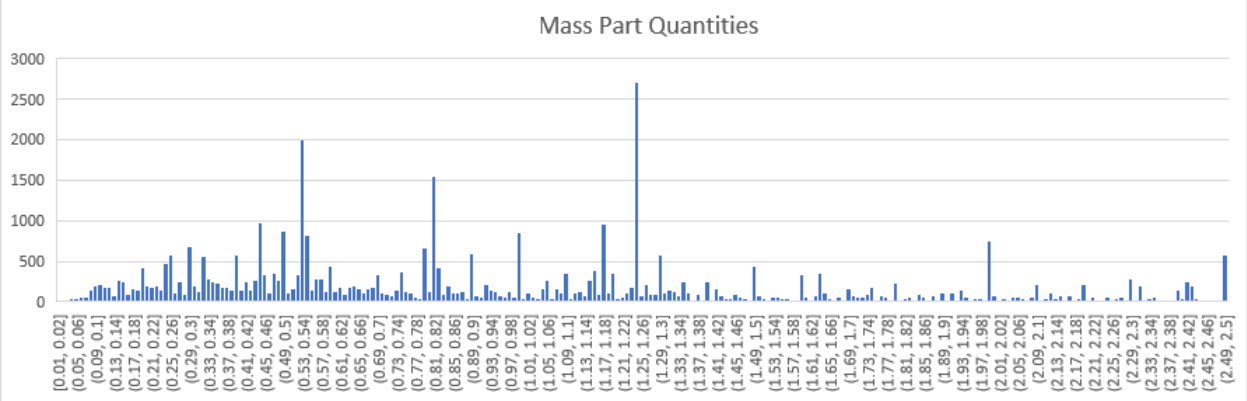

Figure 113: Mass Distribution of Components

Average mass	1.2	grams	
Grams in a pound	454		
Average number of components per pound			378.3333
Cost per component		0.037096916	

Figure 114: Average Number of Components Per Pound as a Function of Average Component Mass Values

$$Average\ number\ of\ components\ per\ pound = \frac{454\frac{Grams}{Pound}}{1.2\frac{Grams}{Component}}$$

Figure 115: Expression for Average Number of Components per Pound

$$Average\ component\ cost = \frac{\frac{Average\ Cost}{Pound}}{\frac{Average\ Number\ of Components}{Pound}}$$

Figure 116: Expression for Average Component Cost

Conclusion

Based on the economic model, one can infer that the Legosortus company, operating under the stated assumptions, although idealized, will be economically functional. Looking at the demand and capacity, one can see that the company is expected to be at overcapacity in the 1st and 2nd year and just slightly at undercapacity, meeting close to 80% of expected demand, in the 3rd year.

Looking at the component cost and price, one can observe a high return on each component, the average component price is $0.46, after adjusting from $0.49 for transaction and packaging costs. While the average component cost is just $0.04, rounded, there is over a tenfold return on each component.

Considering performance on an annual basis, taking the adjusted average component price and subtracting the cost, the company will revenue $0.42 per transaction. Multiplying my demands for years 1,2, and 3, the revenues are $723,936.50, $3,619,683.42, $7,360,000.00 respectively. After adjusting 5% to account for annual defect losses, the annual revenues then adjust down to $687,739.68, $3,438,699.25, $6,992,000.00. Overhead costs total to roughly $200,000. These costs and revenues considered, the expected annual profits for years 1,2, and 3 are respectively, $487,739.68, $3,238,699.25, and $6,792,000.00.

The profits are substantial and at this level of analysis, one can infer that it is well worth conducting further analysis and begin developing the company's framework. Under the stated assumptions and at this level of analysis, the results are favorable and the company seems viable as a commercial pursuit.

Recommendations

Due to both the scope of fabrication and testing involved in this project, compounded by the ongoing global COVID-19 situation which prevented access to key fabrication facilities in the closing months of the project, there remains much to be done to achieve our stated goals of testing the system from start to finish. Most subsystems have work to be done, but also clear next steps forwards.

- The drum sort mechanism needs to be more elegantly integrated with the conveyor feeds to ensure seamless transfer of parts
- The conveyor system needs further testing with different belt surfaces, and for variants optimized for different overall part sizes
- The vision cell needs a more refined structural build complete with weight measurement fully integrated instead of separate, to hold up to the loads passing parts through it will subject it to
- The classification software needs to be tested with the expanded datasets that automatic feeding of parts will enable us to use
- The 1st stage sort needs iteration made to the overall drive system based on initial testing, and additional repeated fabrication of actuated components.
- The jamming gripper requires integration with a gantry mechanism.

Two major system elements were considered from the beginning of the MQP project to be beyond the project's scope, for the purposes of demonstrating the feasibility of our overall scalable system architecture. These are the transfer mechanism, which would empty a single collection bin from the first stage sort, and transfer it to the inlet of the second stage sort. The proposed method for accomplishing this would be a constrained track-based system, which would run in a circle beneath the bin storage on the first stage sort, with the capability of stopping and retrieving any bin as easily as any other. It would then be carted to the entry point of the second stage sort. Our flow analysis shows that speedy operation of this system is crucial, as any dead time introduced into the sort operation causes a ripple effect which dramatically increases the capacity required of the first stage storage system.

The second major subsystem which would need to be designed and created to allow the system to operate without any human intervention is a storage and retrieval system for the drawers used to contain the parts. In our initial design, we planned to test the system using a fixed grid underneath the jamming gripper gantry. In reality, the system would need to be able to sequentially swap out and stack a series of drawers, forming a three dimensional storage system made up of 2d grids, each corresponding to a bin on the first stage sort.

From a project planning perspective, our biggest recommendation would be to go into a project of this scope and complexity with a much clearer vision of how different system elements depend on one another in the developmental process. We spent lots of time early focusing on overall architecture and planning for the details of the classification and vision system, adding lots of details such as component choice, only to find that further progress required effective completion of the serialization and feed mechanisms, to accrue the data required to test and drive our classification algorithm concepts. Most progress was made on the 1st stage carousel, largely because its design and fabrication did not explicitly depend on other mechanisms being realized, not because it was what made the most sense for progression of the project. Exploring and identifying these dependencies to create a more organized path forward would be recommended to any team working on this project or another complex, multi-module system design.

References

Salvendy, Gavriel. *Handbook of Industrial Engineering, Third Edition (3 Volume Set)*. 3rd ed., Wiley, 2007.

Watkins, Joseph. *An Introduction to the Science of Statistics: From Theory to Implementation*. Preliminary Edition, N/A, 2016, www.math.arizona.edu/~jwatkins/statbook.pdf.

"What Exactly Is Lights-out Manufacturing? | Global Manufacturer & Distributor of Component Solutions — Essentra Components." *Essentra Components*, www.essentracomponents.com/en-gb/news/product-resources/what-exactly-is-lights-out-manufacturing.

Mattheij, Jacques. "Sorting 2 Metric Tons of Lego · Jacques Mattheij." *Jacquesmattheij.Com*, 29 Apr. 2017, jacquesmattheij.com/sorting-two-metric-tons-of-lego.

"LEGO Automatic Liftarm Sorter LS-L407." *YouTube*, uploaded by Akiyugi, 30 June 2013, www.youtube.com/watch?v=nlCSlJuD65A.

"LEGO Mindstorms NXT Vision Guided Brick Sorter Ver1." *YouTube*, uploaded by Akiyugi, 25 Mar. 2011, www.youtube.com/watch?v=6lZ9rSZwDzE.

UGCS. "LEGO Sorter [Prototype] by SPH Engineering." YouTube, uploaded by ugcstv, 21 Dec. 2017, www.youtube.com/watch?v=CnIWzBSVEWM.

"The WORLD'S FIRST Universal LEGO Sorting Machine." YouTube, uploaded by Daniel West, 3 Dec. 2019, www.youtube.com/watch?v=04JkdHEX3Yk.

Appendix

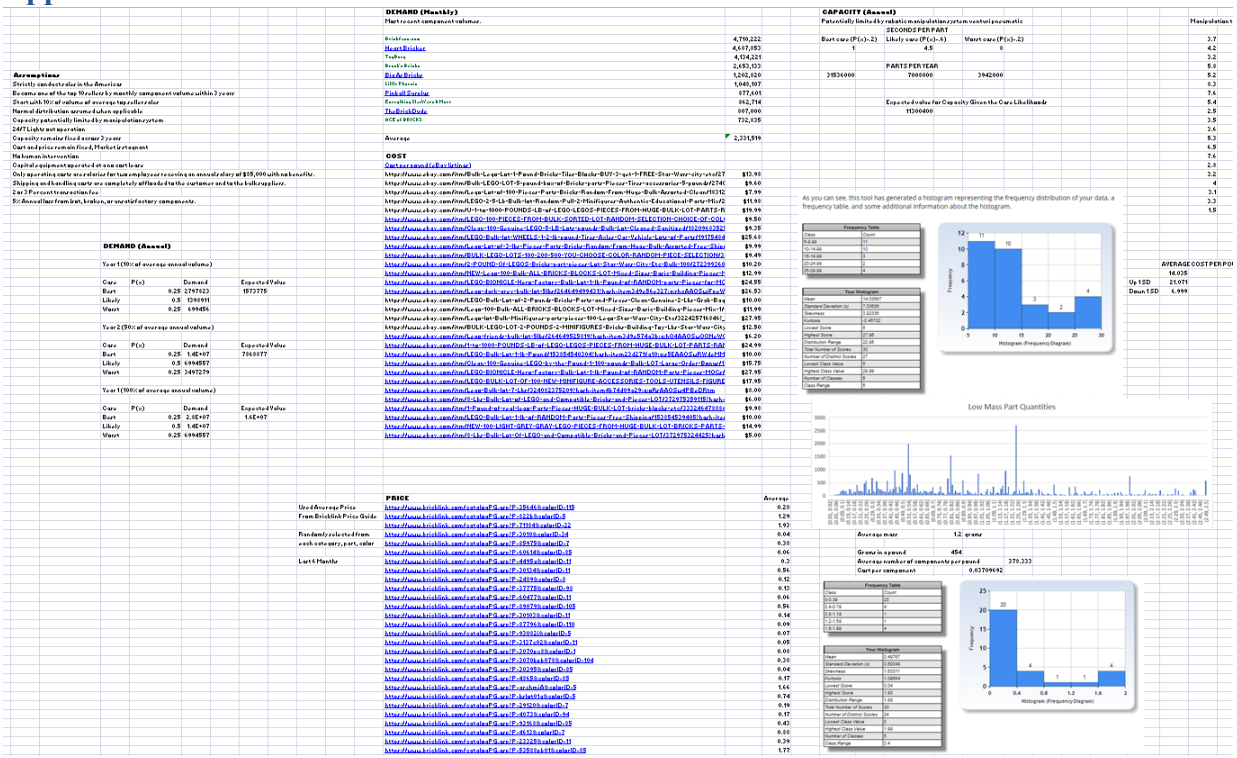

Appendix 1: Economic Model Spreadsheet

https://www.youtube.com/watch?v=9LhfnqwXvWg&fbclid=IwAR0MaaXVW-6VYyHGuBtd-xPMOX_KiSffhoEXSrGji520WDoIHjt7ET1bxBc

Appendix 2: Drum Sorter Test

https://youtu.be/62t4v3Q7Zjs

Appendix 3: Pivot Holder Actuation Test

https://youtu.be/1KBPeXarFy0

Appendix 4: CNC Routing Distribution Carousel Components

https://youtu.be/9RmahIOUQdU

Appendix 5: Roll Bending Aluminum Strips

https://youtu.be/IxDP7bqtKUo

Appendix 6: Friction Drive on Track Ring Test

https://youtu.be/7Fybrf_u808

Appendix 7: Granular Jamming Manipulator Tests

https://youtu.be/i8sHgAOODMw

Appendix 8: Identification Cell Test